

X-ray Photoelectron Spectroscopy (XPS) and Magnetism

- Part I
Introduction
Experimental
Principles of XPS and SRPES
Selected results (intermetallic, organometallic,
spinels)
- Part II
Investigation of oxidic CMR compounds by XPS
and complementary techniques

Introduction

Abbreviations:

PES	Photoelectron Spectroscopy
XPS	X-ray (excited) PES
ESCA	Electron Spectroscopy for Chemical Analysis
SRPES	Spin-resolved Photoelectron Spectroscopy
<i>UPS</i>	<i>Ultraviolet (excited) PES</i>
<i>ARUPS</i>	<i>Angle Resolved UPS</i>
XES	X-ray (Photon) Emission Spectroscopy
<i>XAS</i>	<i>X-ray Absorption Spectroscopy</i>
<i>XMCD</i>	<i>X-ray magnetic circular dichroism</i>
<i>XMLD</i>	<i>X-ray magnetic linear dichroism</i>

Investigation of all kind of materials:

metals, oxides, organo-metallic systems

(not shown: thin films, polymers, adsorbates,,)

surface sensitive technique (electron escape depth)

XPS

- XPS is a very universal useful technique:
 - detection of almost all elements
 - core levels and valence bands are detected
 - determination of absolute atomic concentrations
 - valence state of ions deduced from chemical shifts (ESCA),
 - exchange interaction of the core hole with valence band
 - total DOS by XPS (and partial DOS by XES)
 - Spin resolved PES using circular polarized light or spin detectors

ANNALEN
DER
PHYSIK.
Band 17, 132 (1905)

6. Über einen
die Erzeugung und Verwandlung des Lichtes
betrreffenden heuristischen Gesichtspunkt;
von A. Einstein.

§ 8. Über die Erzeugung von Kathodenstrahlen durch Belichtung
fester Körper.

Die übliche Auffassung, daß die Energie des Lichtes kontinuierlich über den durchstrahlten Raum verteilt sei, findet bei dem Versuch, die lichtelektrischen Erscheinungen zu erklären, besonders große Schwierigkeiten, welche in einer bahnbrechenden Arbeit von Hrn. Lenard dargelegt sind.¹⁾

Nach der Auffassung, daß das erregende Licht aus Energiequanten von der Energie $(R/\Lambda)\beta n$ bestehet, läßt sich die Erzeugung von Kathodenstrahlen durch Licht folgendermaßen auffassen. In die oberflächliche Schicht des Körpers dringen Energiequanten ein, und deren Energie verwandelt sich wenigstens zum Teil in kinetische Energie von Elektronen. Die einfachste Vorstellung ist die, daß ein Lichtquant seine ganze Energie an ein einziges Elektron abgibt; wir wollen annehmen, daß dies vorkomme. Es soll jedoch nicht ausgeschlossen sein, daß Elektronen die Energie von Lichtquanten nur teilweise aufnehmen. Ein im Innern des Körpers mit kinetischer Energie

Photo effect

$$h\nu = E_{\text{kin}} - E_{\text{bin}}$$

$$E_{\text{vac}} = 0$$

one electron type picture

electron mean free path

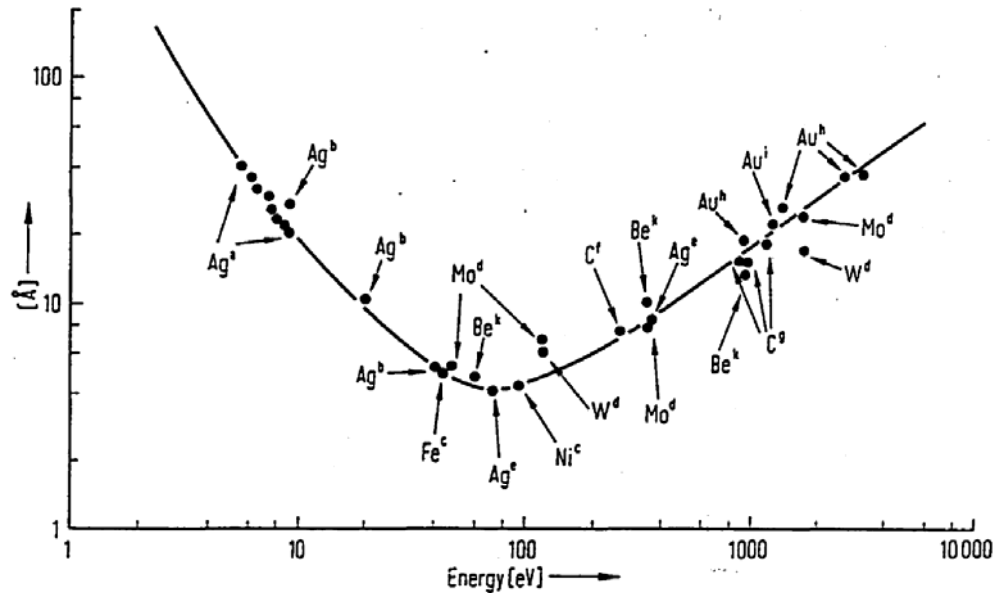


Fig. 1.2. Mean free path of electrons in metallic solids as a function of their energy.

a: H. Kanter, Phys. Rev. B1, 522 (1970) (Electron transmission). b: D. E. Eastman, 32nd Physical Electronics Conference, Albuquerque, N. Mex. 1972 (UPS). c: J. W. T. Ridgeway and D. Haneman, Surface Sci. 24, 451 (1971); 26, 683 (1971) (AES). d: M. L. Tarn and G. K. Wehner, J. appl. Phys. 43, 2268 (1972) (AES). e: P. W. Palmberg and T. N. Rhodin, J. appl. Phys. 39, 2425 (1968) (AES). f: K. Jacobi and J. Hözl, Surface Sci. 26, 54 (1971). g: R. G. Steinhardt, J. Hudis and M. L. Perlman, in: Electron Spectroscopy (D. A. Shirley, ed.) North Holland, Amsterdam (1972), p. 557 (XPS). h: M. Klasson, J. Hedman, A. Berndtson, R. Nilsson and C. Nordling, Physica Scripta 5, 93 (1972) (XPS). i: Y. Baer, P. F. Heden, J. Hedman, M. Klasson and C. Nordling, Solid State Comm. 8, 1479 (1970) (XPS). k: M. P. Seah, Surface Sci. 32, 703 (1972) (AES).

Experimental

Light sources:

XPS: Al K α radiation (1486.7 eV), also monochromatised
Synchrotron radiation with tunable energy

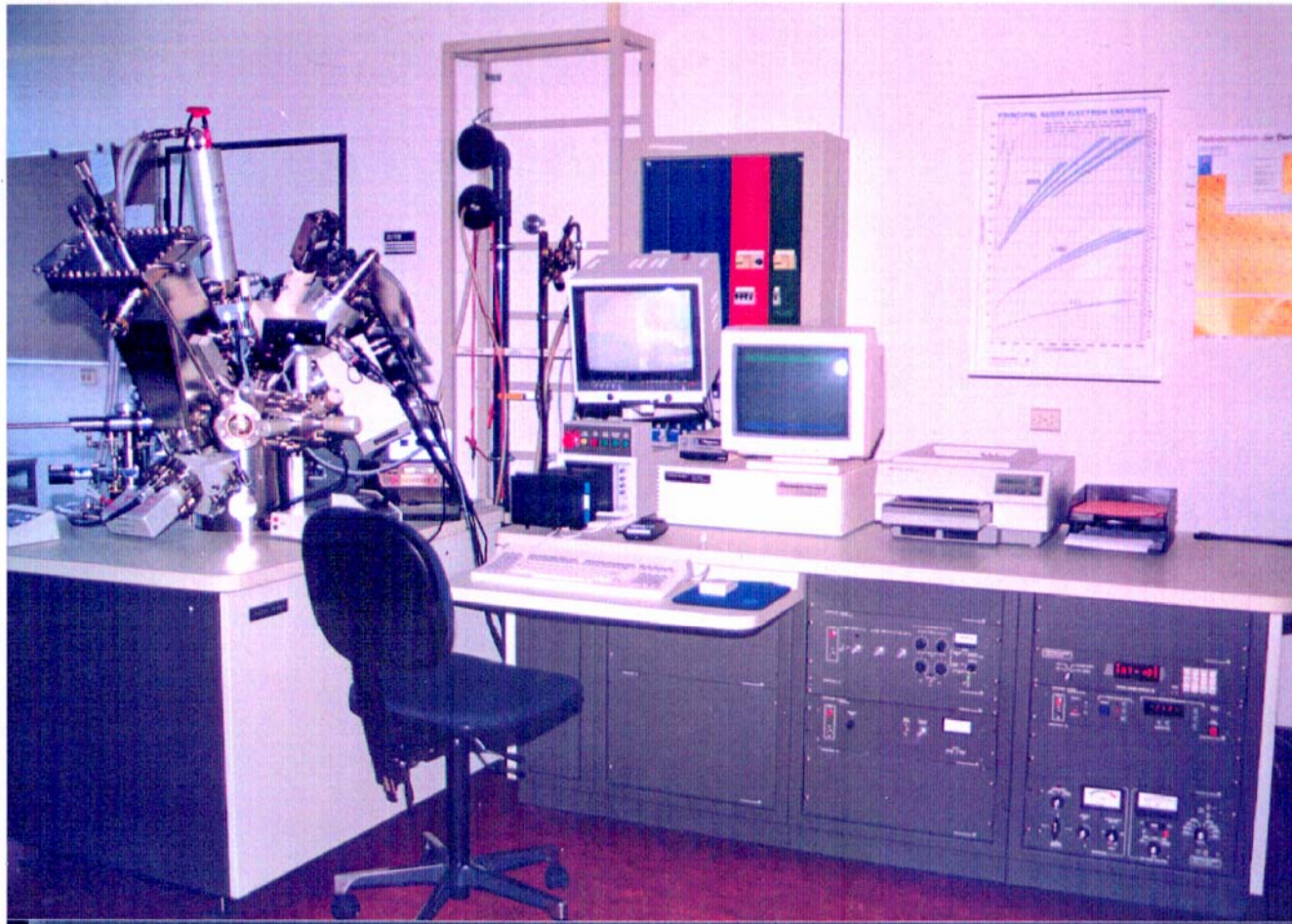
Electron detector:

High energy resolution, multi-channel,
spin resolving

Sample preparation:

in situ (UHV)
fracturing, evaporation,,, no sputtering!

XPS



XPS



XPS

ESCA

Focusing
Monochromator
Crystal

X-rays

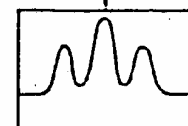
Focusing Electron Gun

X-ray Anode

Electron Lens
Photoelectrons
Sample

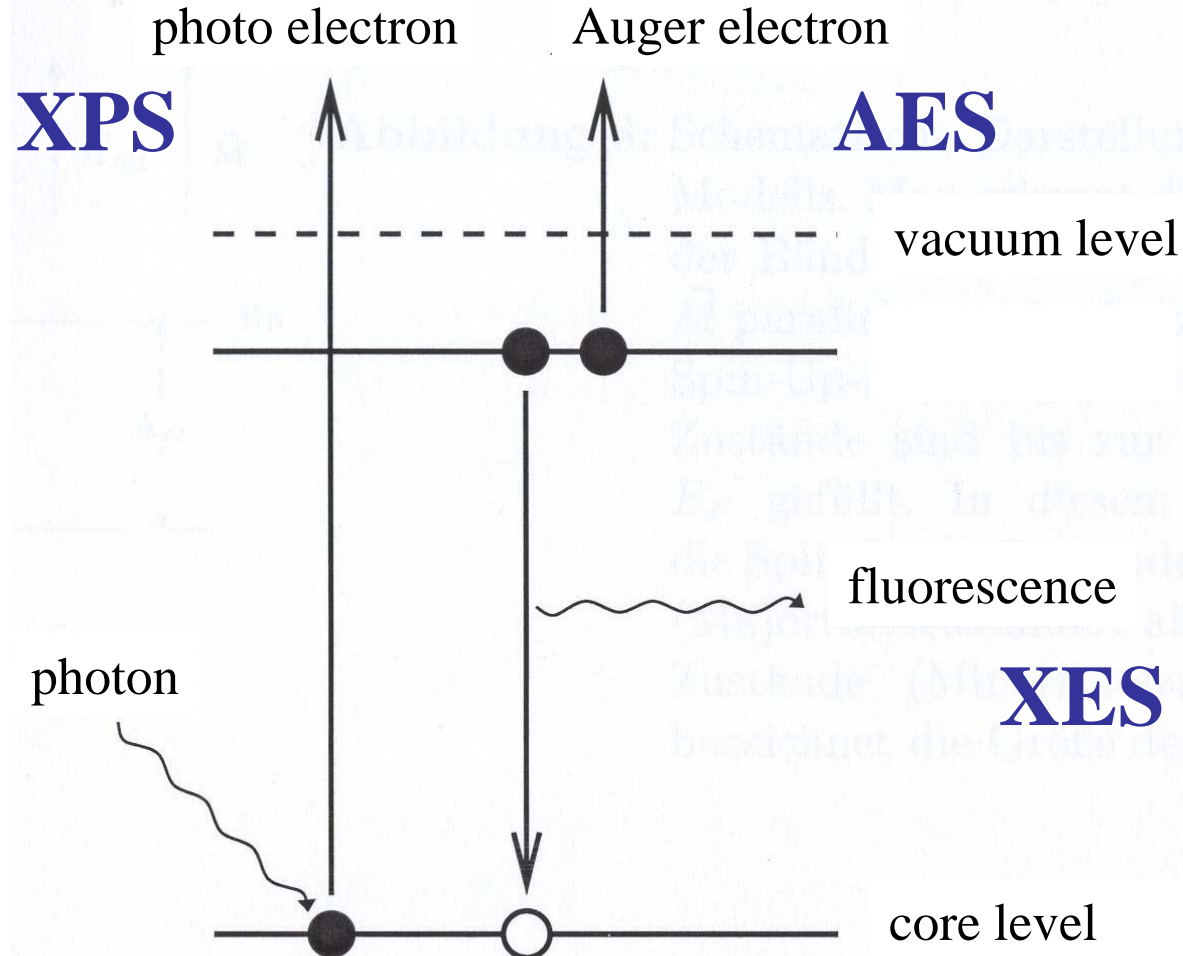
Hemispherical Electron
Energy Analyzer

Fast
Multichannel
Detector



small spot analysis

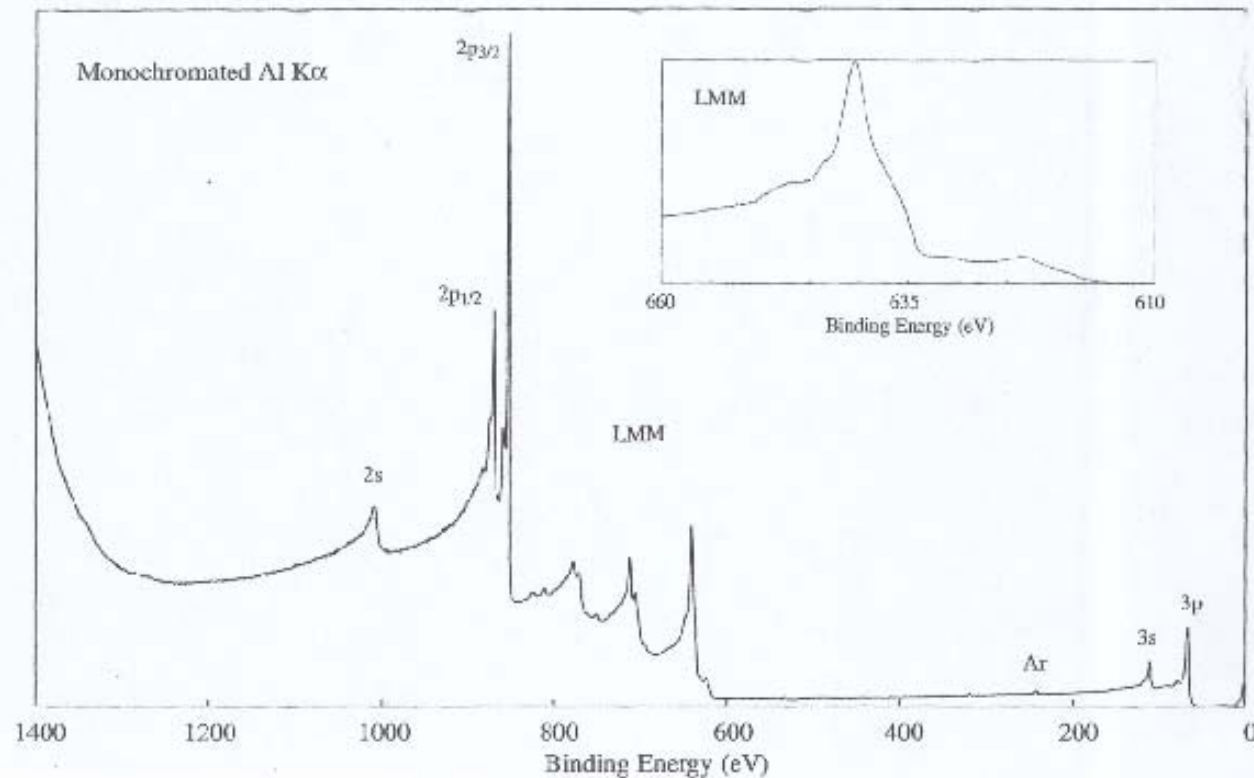
Excitation process



XPS analysis

Nickel Ni
Atomic Number 28

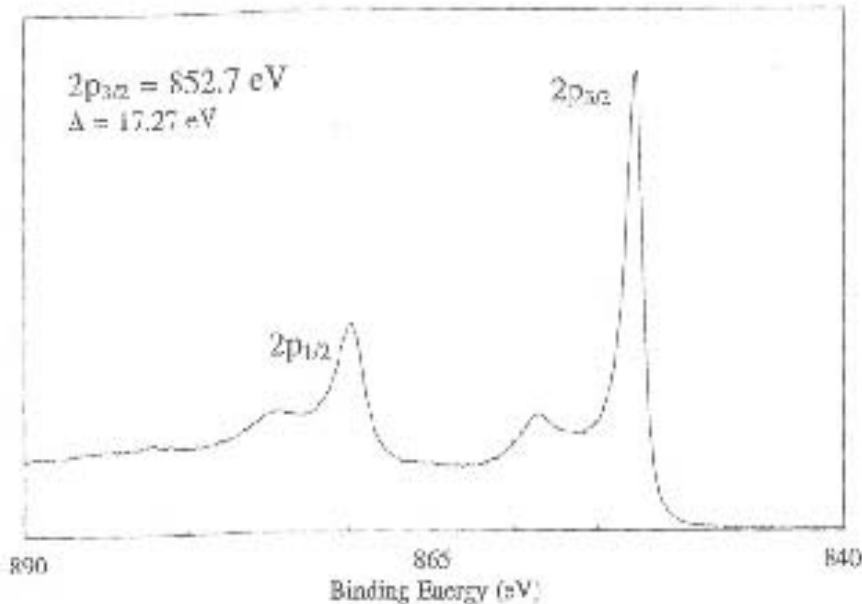
Handbook of X-ray Photoelectron Spectroscopy



$$E_{\text{bin}} = h\nu - E_{\text{kin}}$$

XPS and AES lines can be identified by varying the excitation energy

XPS analysis

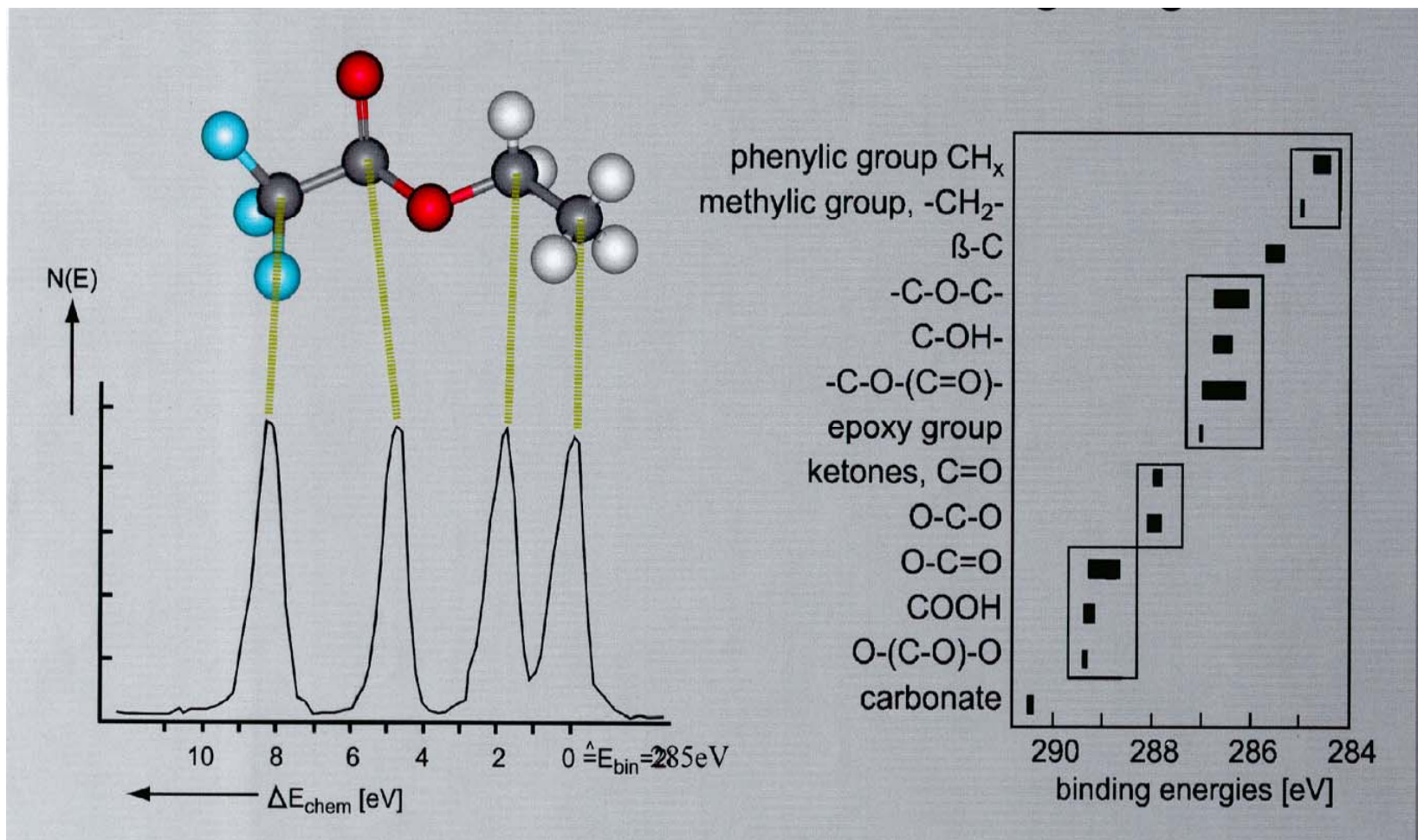


Line Positions (eV)				
Photoelectron Lines				
2s	$2p_{3/2}$	$2p_{1/2}$	3s	3p
1009	870	853	111	67
Auger Lines				
$L_3M_{23}M_{23}$		$L_2M_{23}M_{21}$	$L_3M_{23}M_{45}$ (1P)	
778	545	539	712	479
$L_3M_{23}M_{45}$ (3P)		$L_2M_{23}M_{45}$ (1P)	$L_3M_{45}M_{45}$	(Al)
706	473	408	624	391 (Mg)

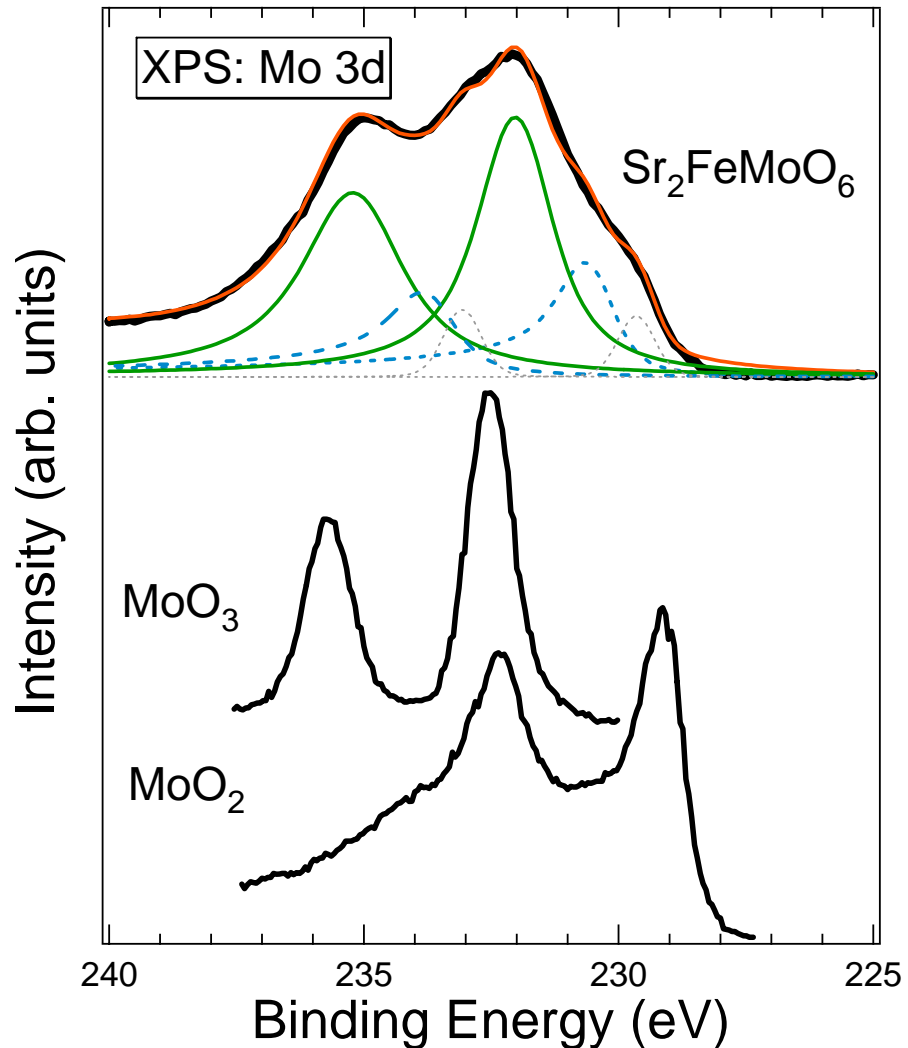


almost all elements are detectable, also quantitatively (sensitivity factors), determination of absolute atomic concentrations, and stoichiometries, $2p_{1/2}$ and $2p_{3/2}$ (LS coupling), 6eV satellite

chemical shift



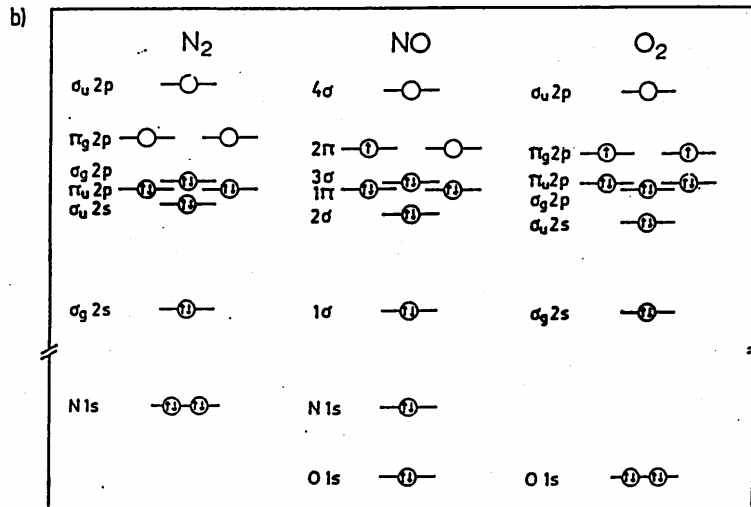
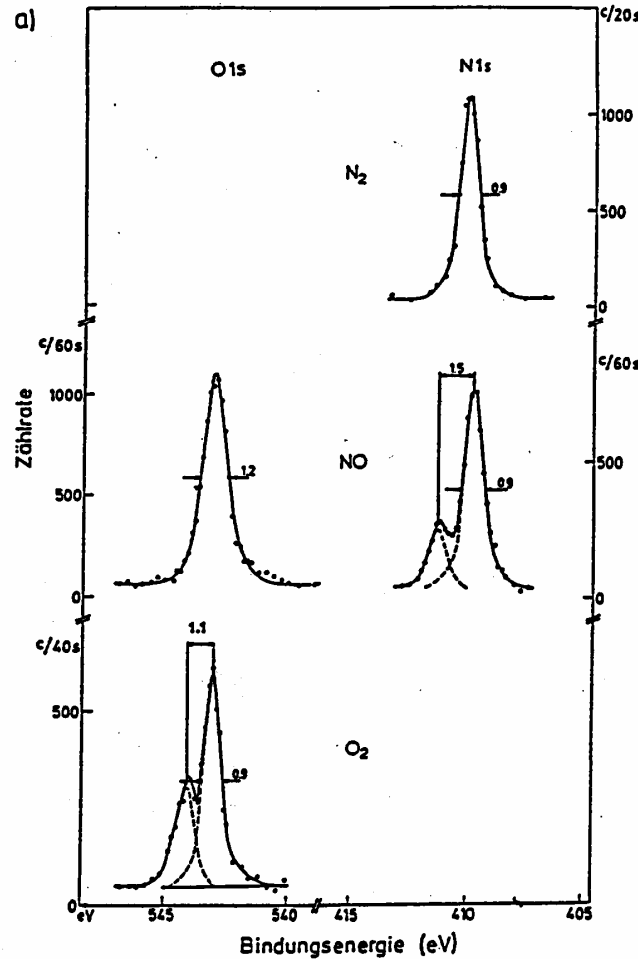
chemical shift



Mo^{6+} and Mo^{5+} ions
in $\text{Sr}_2\text{FeMoO}_6$

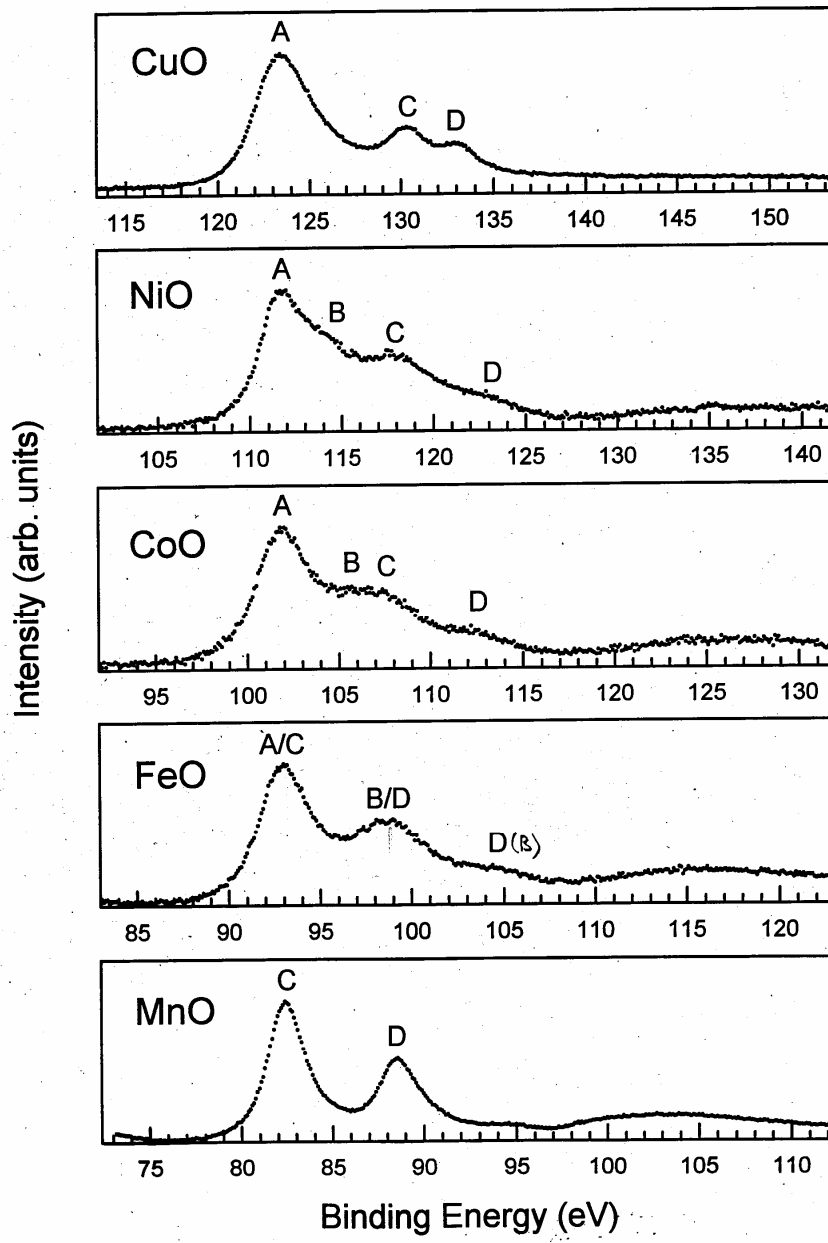
reference compounds
 Mo^{6+} in MoO_3
 Mo^{4+} in MoO_2
the Mo 3d states are split
due to LS-coupling

exchange splitting



1s XPS spectra of paramagnetic molecules show a splitting due to the interaction of the 1s hole with the spin S of the „valence band“

XPS probes the final states with $S \pm 1/2$



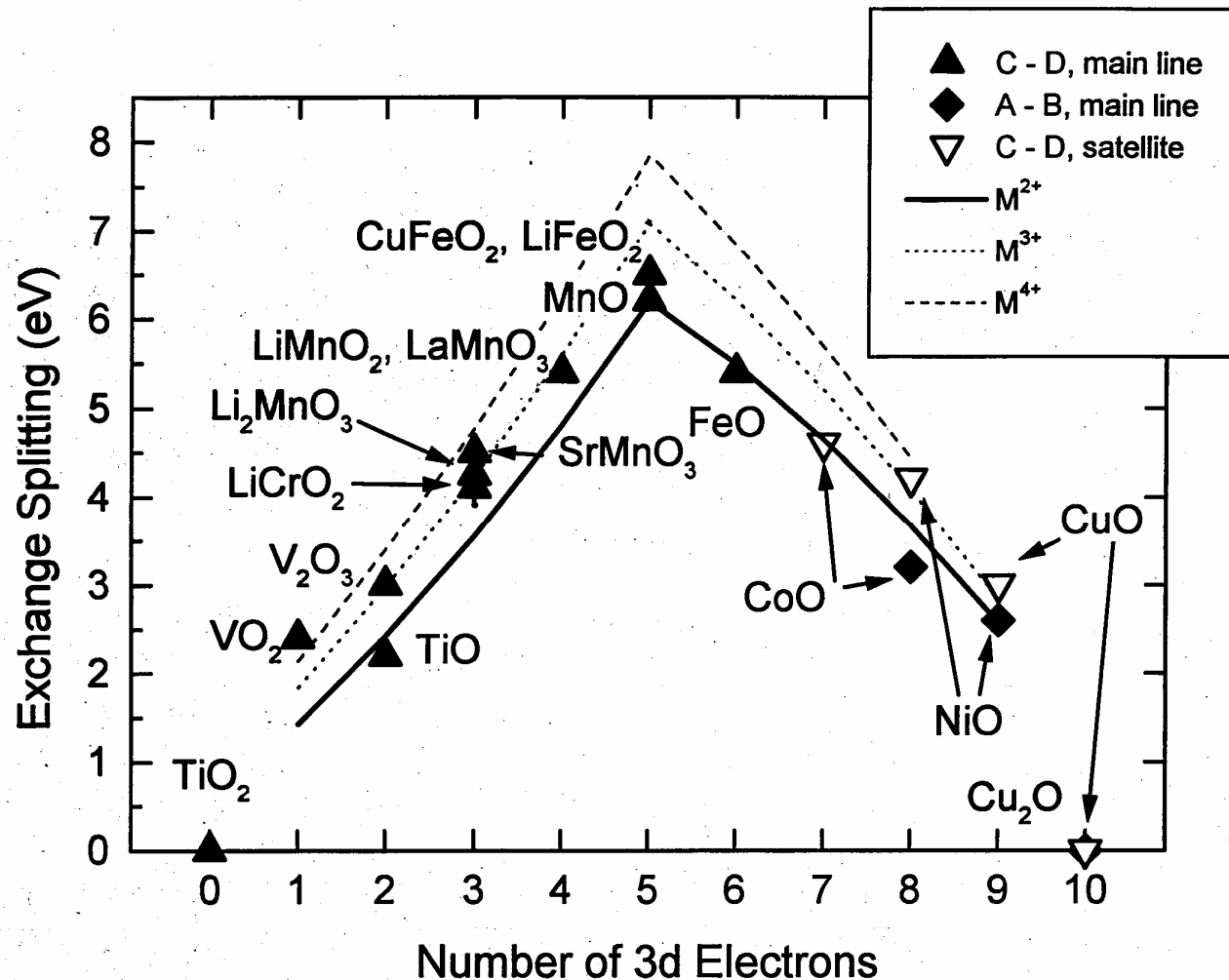
3s splitting and charge transfer (CT) in 3d transition metal oxides

Interaction of the 3s hole with the 3d electrons with spin S

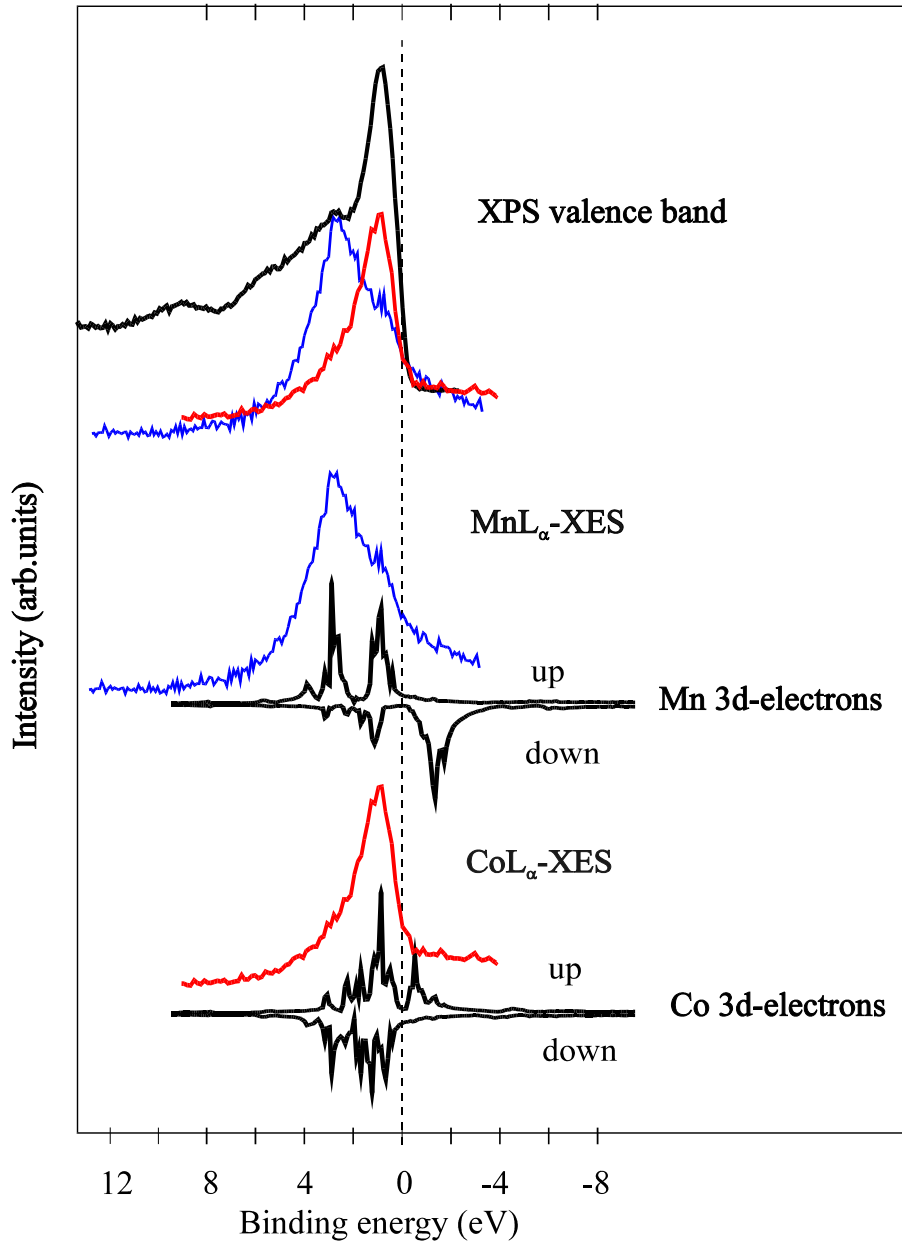
XPS probes the final state $S \pm \frac{1}{2}$ in well screened systems charge is transferred from O2p to 3d states plus spin-spin interactions

A, B with charge transfer (CT)
C, D without CT (less screening)

3s splitting in TM oxides



valence band tDos and pDos

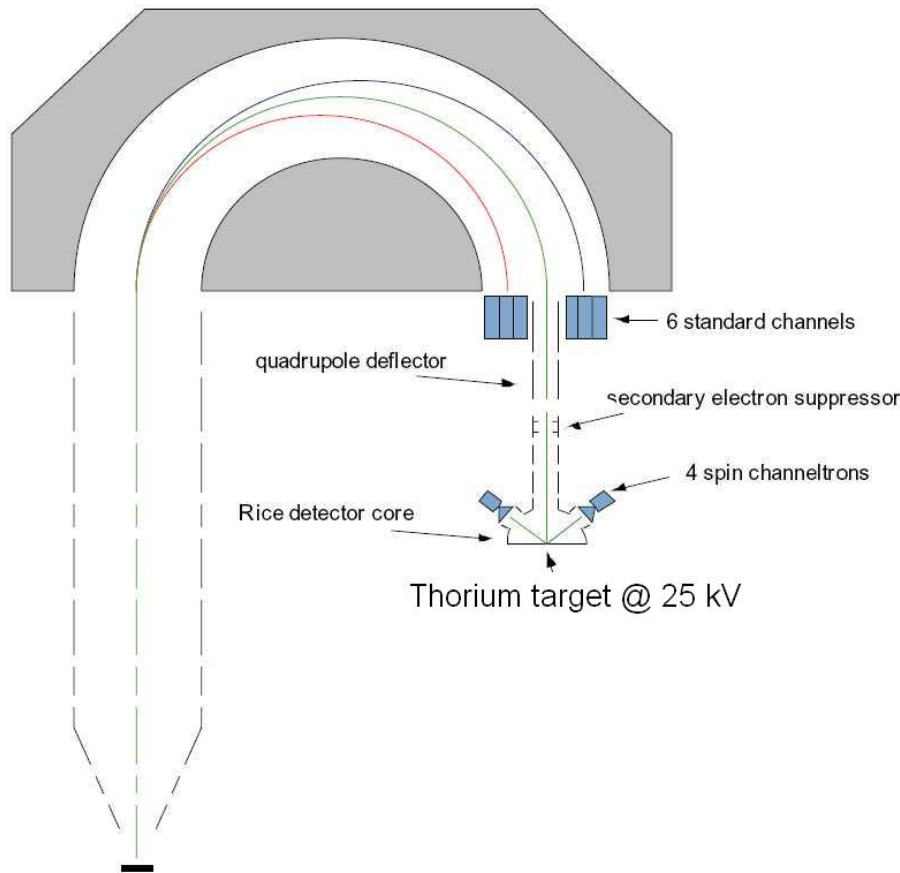


Co_2MnSn
(Heusler alloy)

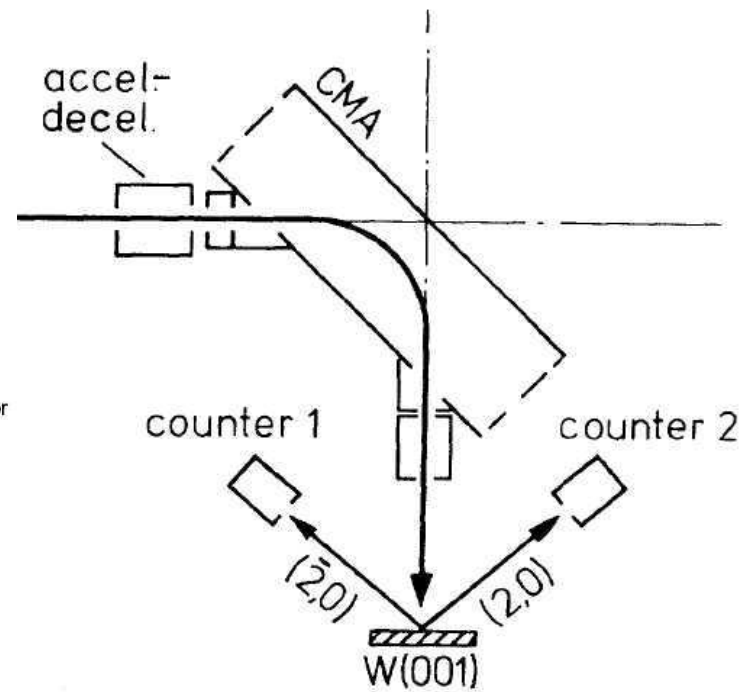
tDos (total densities of states)
probed by **XPS**
pDos (partial densities of states)
probed by XES
comparison with theory
spin resolved
small gap?

Detection of Spin Polarization

Mini Mottdetector (SPECS)

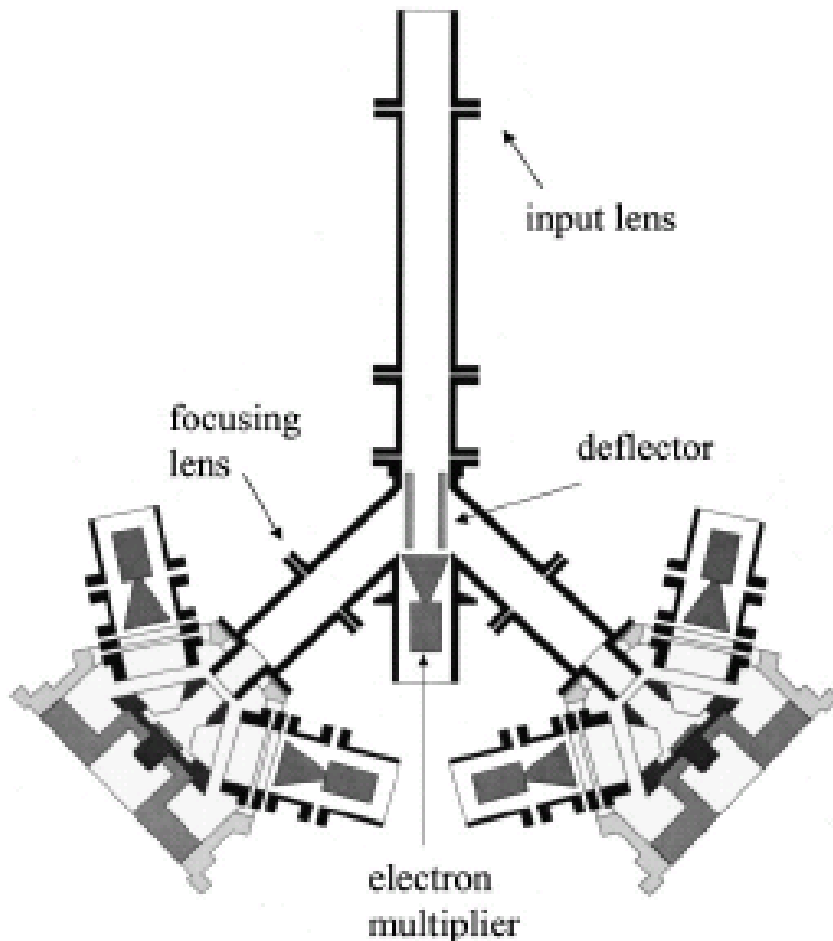


SPLEED detector (Omkron)
Kirschner *et al.*



LEED ANALYZER

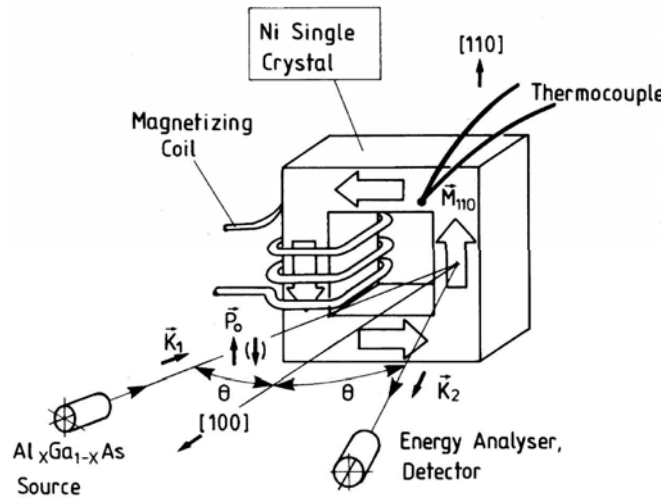
Detection of Spin Polarization



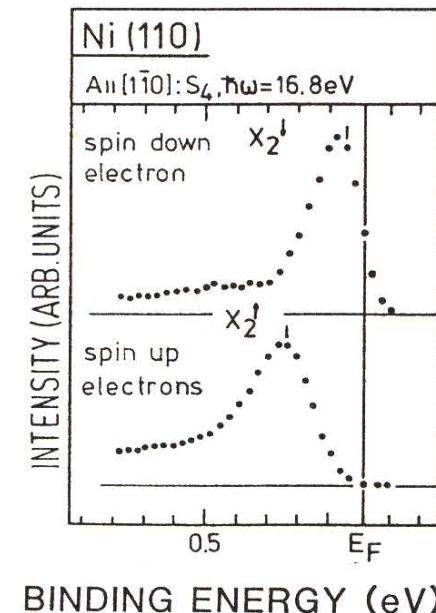
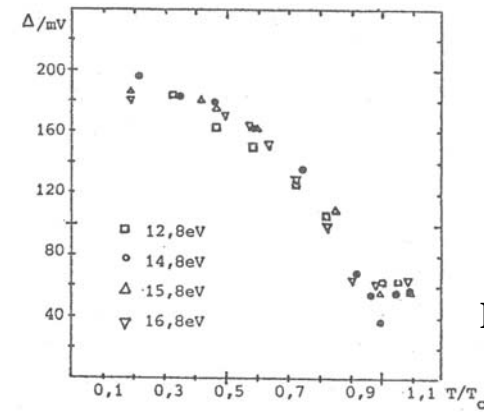
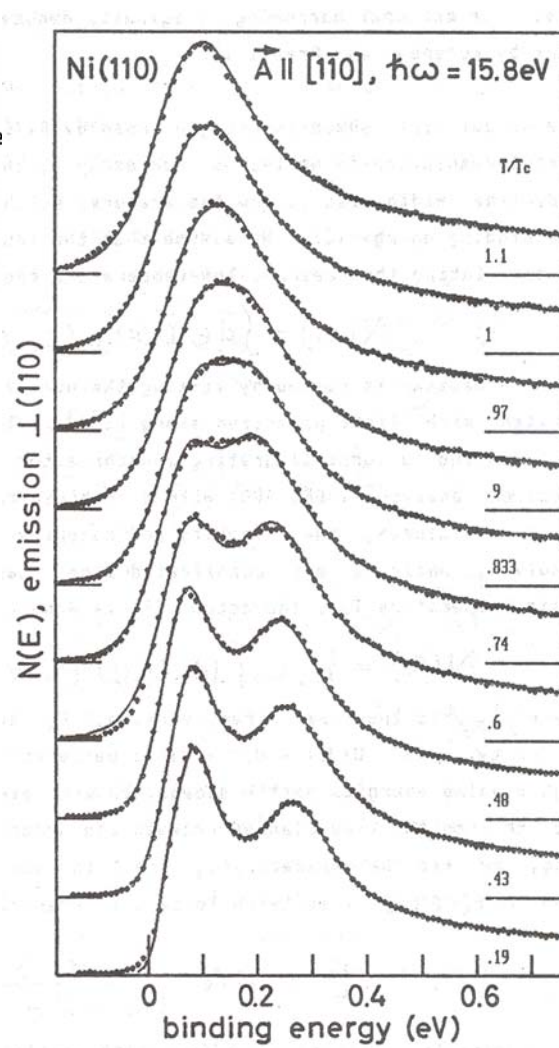
A design to detect all three spin components together with the unpolarised signal.

D.J.Huang, P.D. Johnson, et al.
Rev.Sci.Instr. 73, 3778 (2002)

Spin resolved Photoelectronspectroscopy



Alvarado, Campagna and Hopster



Dietz and Kuhlenbeck (1984)

Campagna 1985

SRPES from Fe 3s

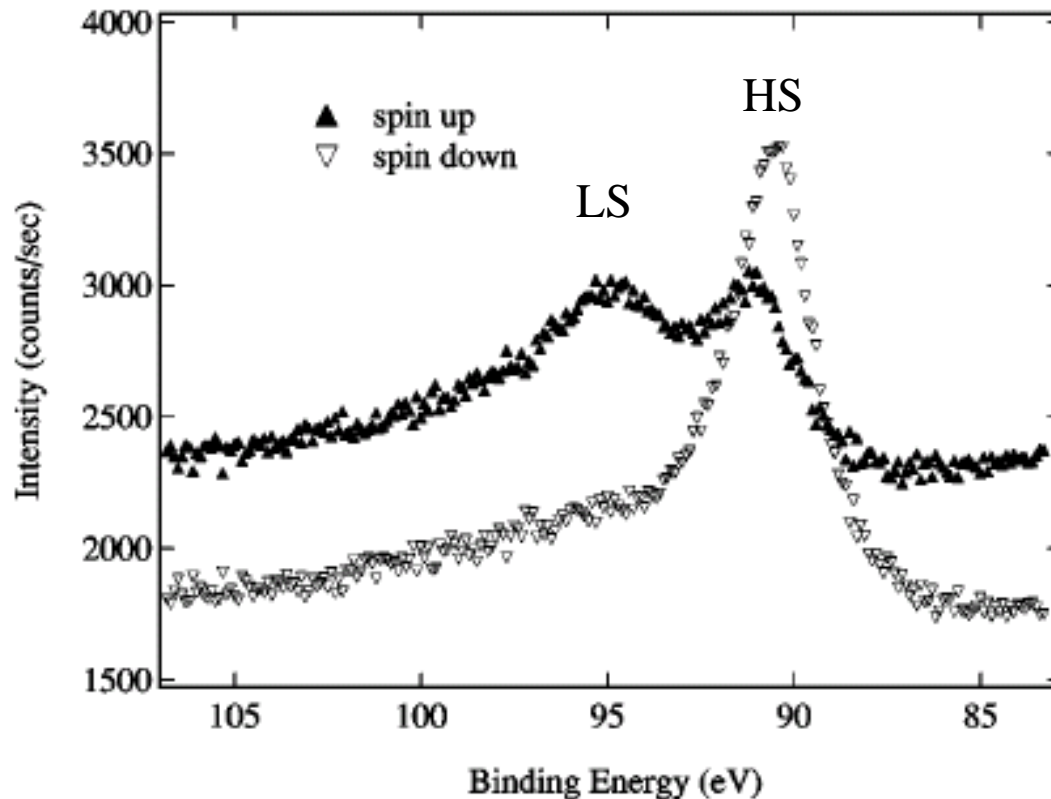


FIG. 3. Spin-resolved $3s$ photoemission of Fe thin films epitaxially grown on W(110) substrates. Linearly polarized synchrotron radiation with an energy 265 eV was used to excite the photoelectrons. The total energy resolution was 0.35 eV.

HS: 2 S_z components
LS: 1 S_z component

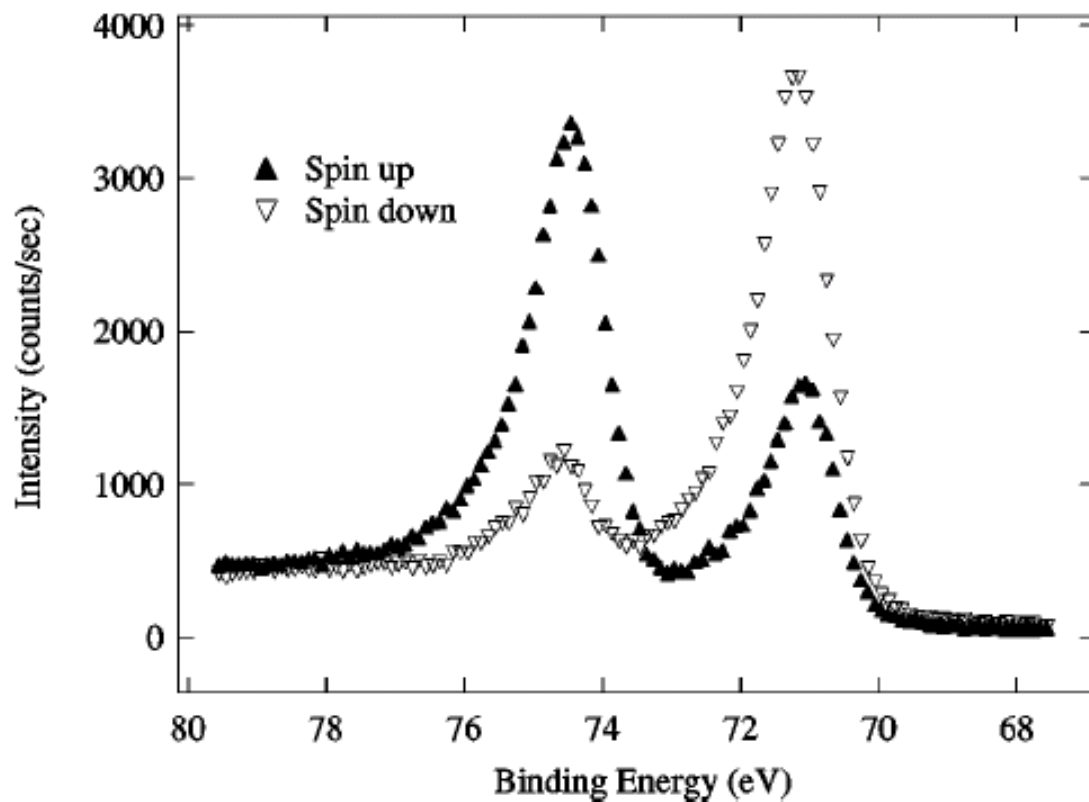
D.J. Huang et al. Rev.Sci.Instr.73, 3778 (2002)

Earlier work by:

F.U. Hillebrecht, et al.
PRL65, 2450 (1990)

Z. Xu, et al. PRB51, 7912 (1995)

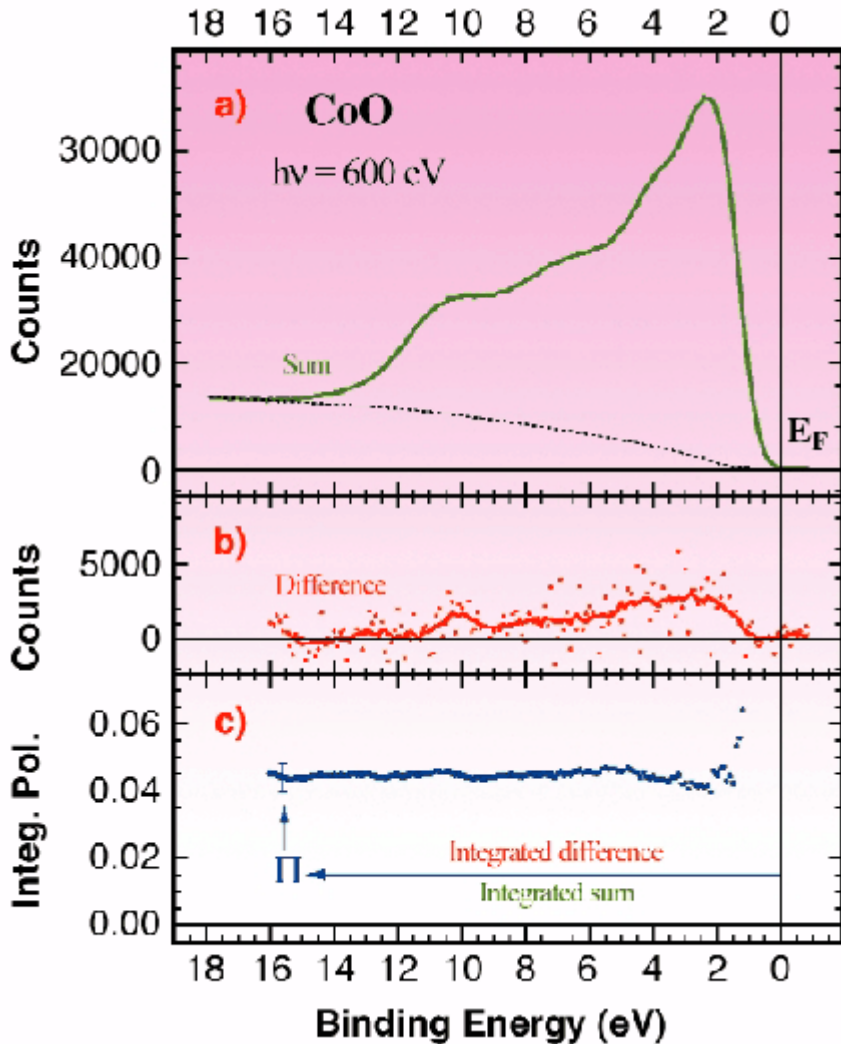
SRPES with circularly polarized light from nonmagnetic metals



total intensities:
 $I(f_{5/2}) : I(f_{7/2}) = 3 : 4$
highly spinpolarized

FIG. 4. Spin-resolved Pt 4f photoemission excited circularly polarized from the EPU beamline. The degree of the light circular polarization is better than 90%. The total energy resolution was 0.35 eV.

SRPES with circularly polarized light



Determination of the orbital moment
of CoO using spin-resolved photoemission

Highlights ESRF 2000
G. Ghiringhelli et al.

The orbital moment is quenched
also **above T_N** !

Selected materials investigated by XPS

all kind of materials have been investigated by XPS,
only a few examples will be shown in the following:

intermetallic compounds (Heusler alloys)

chalcogenide spinels (partly semiconducting)

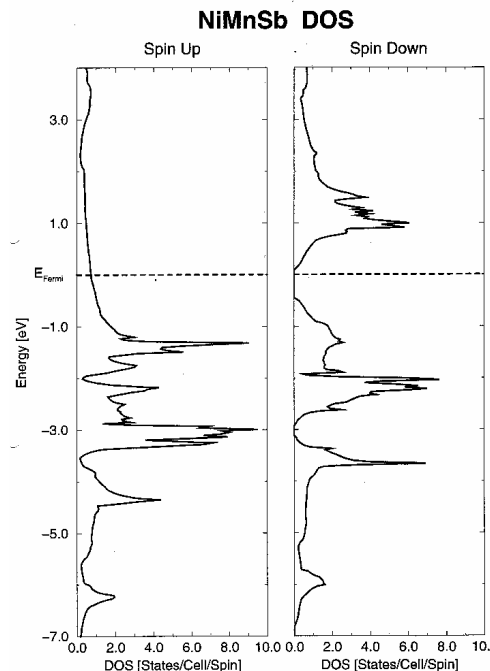
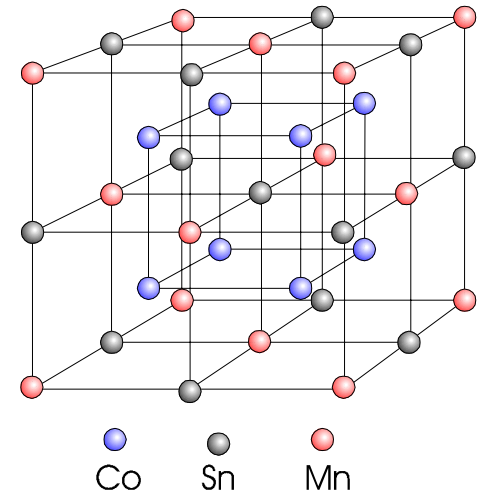
organometallic compounds

(molecule based solids and magnetic molecules)

oxides (CMR compounds: manganites, double perovskites)

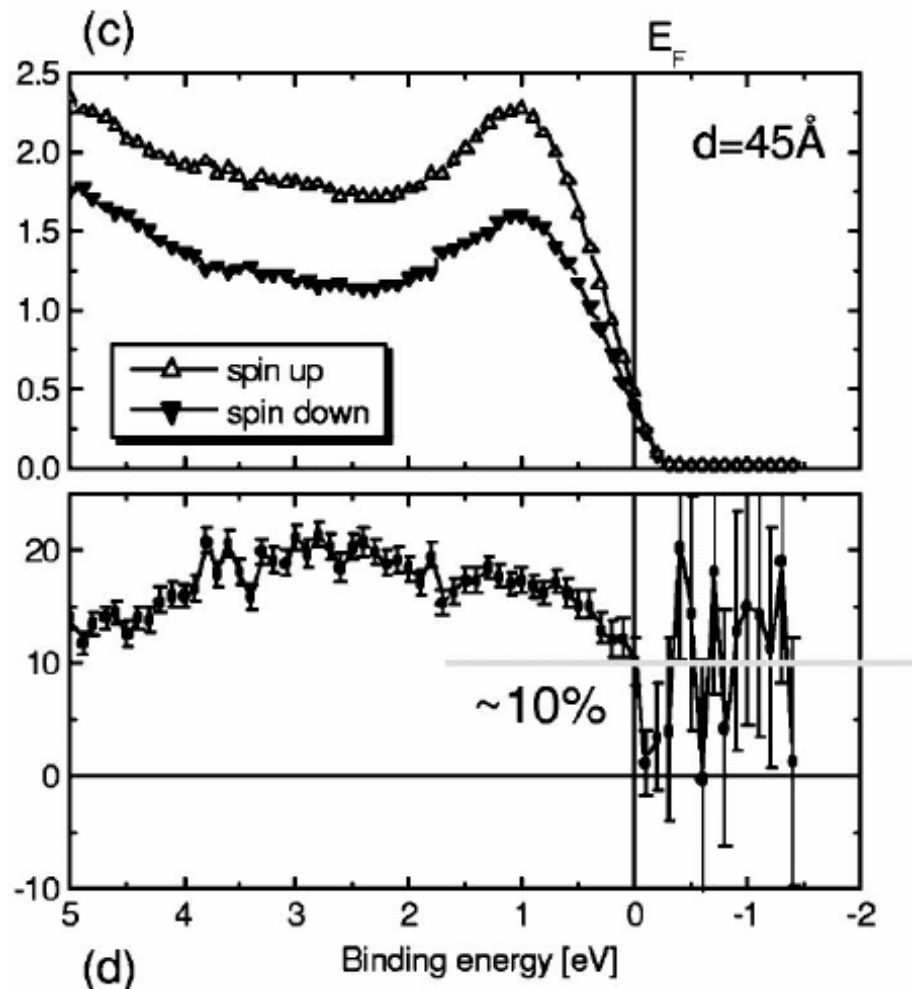
Heusler-Alloys

- discovered 1903 by F. Heusler
- ternary intermetallic alloy:
 X_2YZ
- $L2_1$ structure
- 4 interpenetrating fcc-lattices
- here investigated: X_2MnZ
 - $X = Fe, Co, Ni, Cu$
 - $Z = Al, Si, Ga, In, Sn, Sb$
- partly HMF-behavior
 - spin up: metal
 - spin down: insulator / semiconductor



Magnetic properties and spin polarization of Co₂MnSi Heusler alloy thin films epitaxially grown on GaAs(001)

W. H. Wang,^{1,2} M. Przybylski,^{1,3,*} W. Kuch,^{1,4} L. I. Chelaru,^{1,5} J. Wang,^{1,6} Y. F. Lu,¹ J. Barthel,¹ H. L. Meyerheim,¹ and J. Kirschner¹

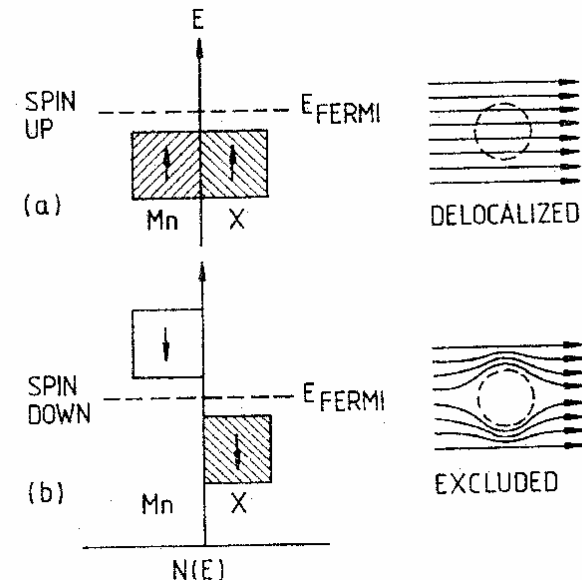


Disorder in the Co/Mn sites can close the gap and also reduce the spin polarization.

Heusler-Alloys

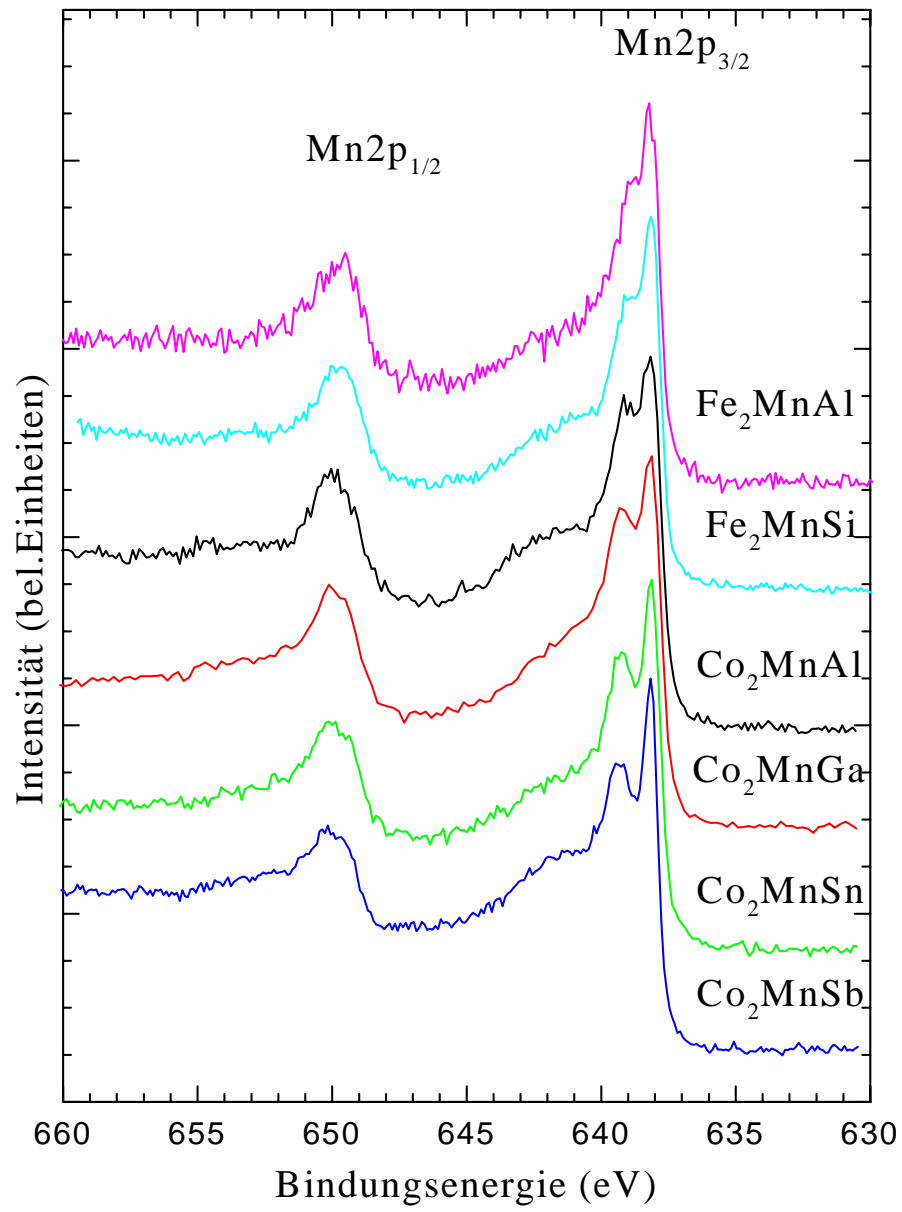
X_2MnZ

- **local magnetic** moment at the Mn-atom $2,3\mu_B - 4,4 \mu_B$
- Mn3d \uparrow : delocalised band; hybridisation with the X 3d electrons
- Mn3d \downarrow : localised unoccupied states
- magnetic coupling by the Z element



L₂₁ Heusler-Alloys with Mn or Cr

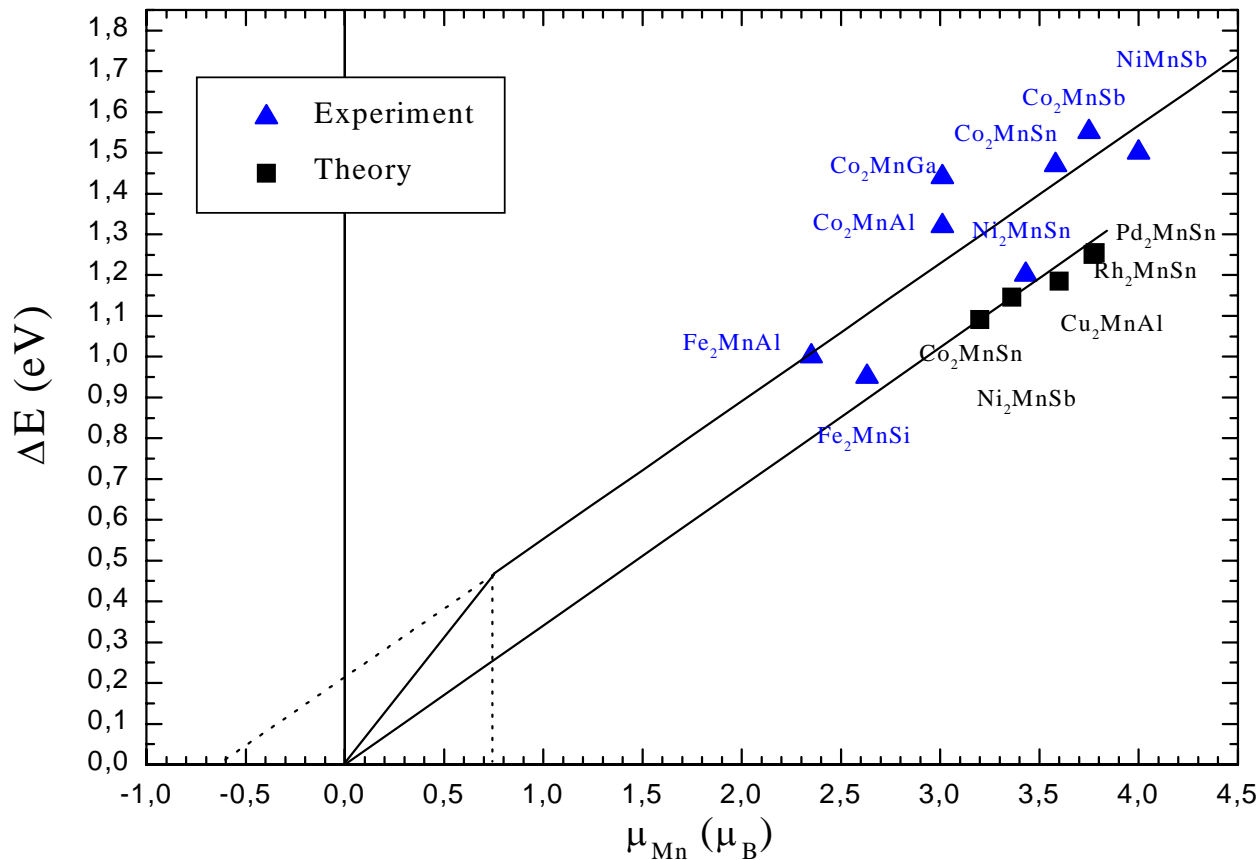
	Material	Struktur	<i>a</i> in nm	μ_{Mn} in μ_B	μ_X in μ_B	μ_{eff} in μ_B	<i>T_c</i> in K
Fe ₂ MnZ	Fe ₂ MnAl ^a	<i>L</i> 2 ₁	0.567	2.35	0.16		
	Fe ₂ MnSi ^a	<i>L</i> 2 ₁	0.559	2.63	0.20		214
Co ₂ MnZ	Co ₂ MnAl	<i>B</i> 2/ <i>L</i> 2 ₁	0.5756	3.01	0.5	4.01	693
	Co ₂ MnGa	<i>L</i> 2 ₁	0.577	3.01	0.5	4.05	694
semi-Heusler	Co ₂ MnSn	<i>L</i> 2 ₁	0.6	3.58	0.75	5.08	829
	Co _{1.5} MnSb	<i>L</i> 2 ₁	0.5929	3.75	0.75	4.9	600
A ₂ CrAl	Ni ₂ MnIn	<i>L</i> 2 ₁	0.6069	3.43 ^b	< 0.3	4.40 ^b	314
	Ni ₂ MnSn	<i>L</i> 2 ₁	0.6053	3.43 ^b	< 0.3	4.05 ^b	360
	Ni ₂ MnSb	<i>L</i> 2 ₁	0.6004	3.13 ^b	< 0.3	3.27 ^b	365
	Cu ₂ MnAl	<i>L</i> 2 ₁	0.5949	3.49	< 0.1	3.73	603
	Rh ₂ MnSn ^c	<i>L</i> 2 ₁	0.6252	3.77/(3.65) ^d	0.38(0.24) ^d	3.1/(4.51/4.09) ^d	412
	Rh ₂ MnGe ^d	<i>L</i> 2 ₁	0.5993	3.61 (3.40)	0.37 (0.23)	4.36 (3.81)	450
	Pd ₂ MnAl	<i>B</i> 2	0.6165	4.4	< 0.1	4.4	<i>T_N</i> = 240
	Pd ₂ MnSn	<i>L</i> 2 ₁	0.638	4.14 / 3.78 ^e	< 0.1	4.26	189
	Pd ₂ MnSb	<i>L</i> 2 ₁	0.6419	4.4 / 3.83 ^e	< 0.02	4.4	247
	NiMnSb ^f	C1 _b	0.5913	4.0	<0.01	4.08	756
	Fe ₂ CrAl ^g	<i>L</i> 2 ₁	0.5805			1.67	246
	Co ₂ CrAl ^g	<i>L</i> 2 ₁	0.5887			1.55	334



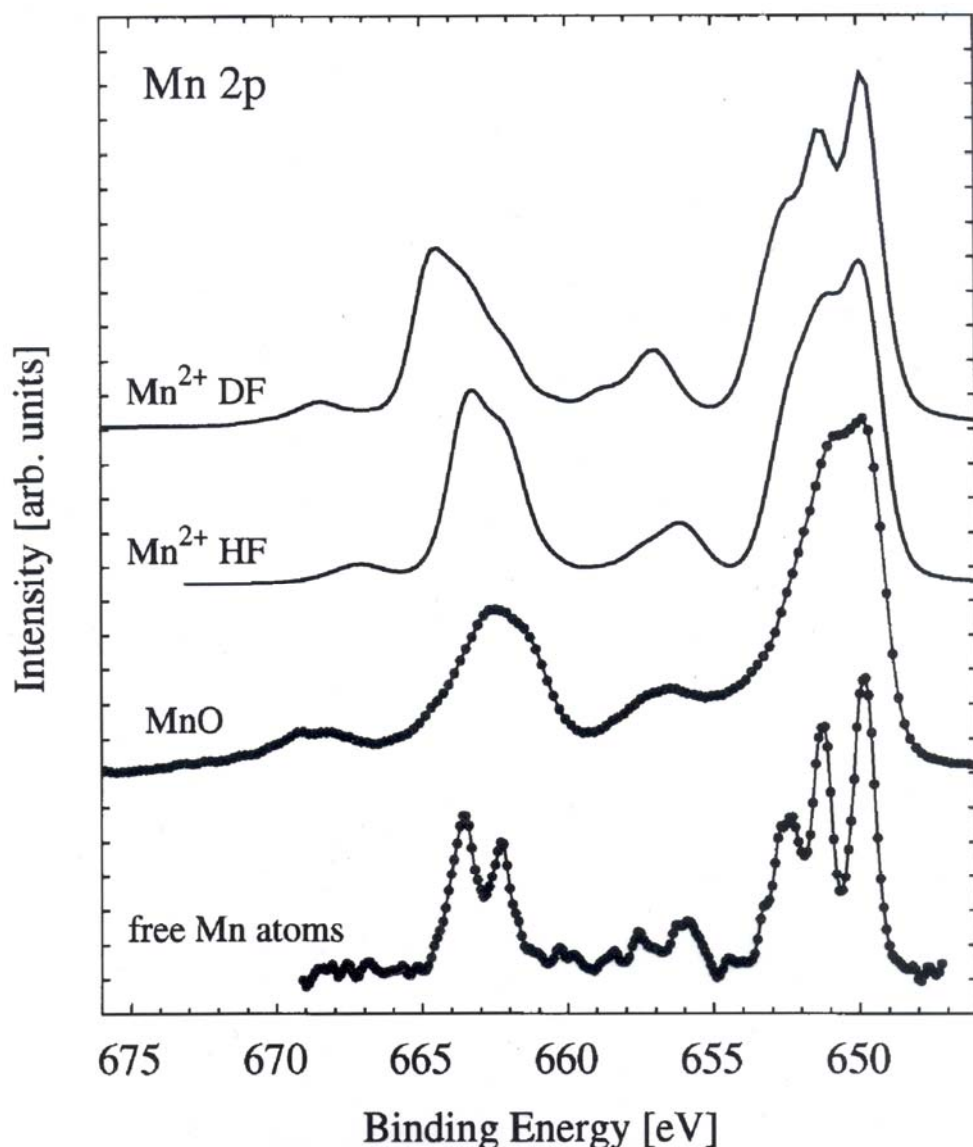
Mn2p core levels

Material	Struktur	a in nm	μ_{Mn} in μ_B
Fe ₂ MnAl ^a	<i>L</i> 2 ₁	0.567	2.35
Fe ₂ MnSi ^a	<i>L</i> 2 ₁	0.559	2.63
Co ₂ MnAl	<i>B</i> 2/ <i>L</i> 2 ₁	0.5756	3.01
Co ₂ MnGa	<i>L</i> 2 ₁	0.577	3.01
Co ₂ MnSn	<i>L</i> 2 ₁	0.6	3.58
Co _{1.5} MnSb	<i>L</i> 2 ₁	0.5929	3.75

Mn2p_{3/2} splitting vs. μ_{Mn}



Mn 2p photoelectron spectra



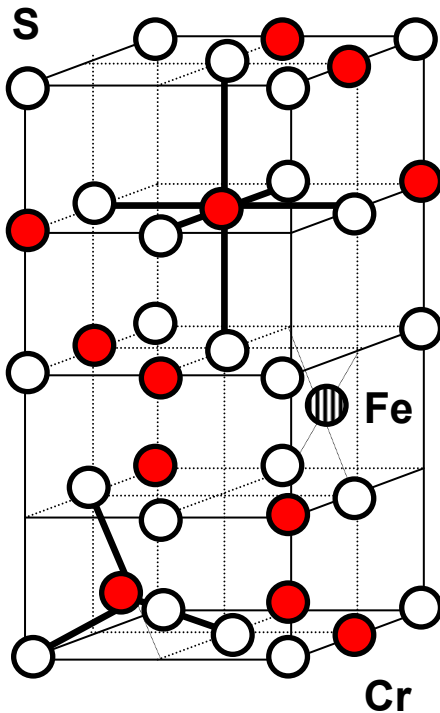
A comparison with atomic spectra demonstrates the localized nature of the Mn 2p states in MnO multiplet effects need to be included in calculations

Local moments also in Heuslers!

Ph. Wernet et. al.
Phys. Rev. B (2001)

chalkogenide spinels

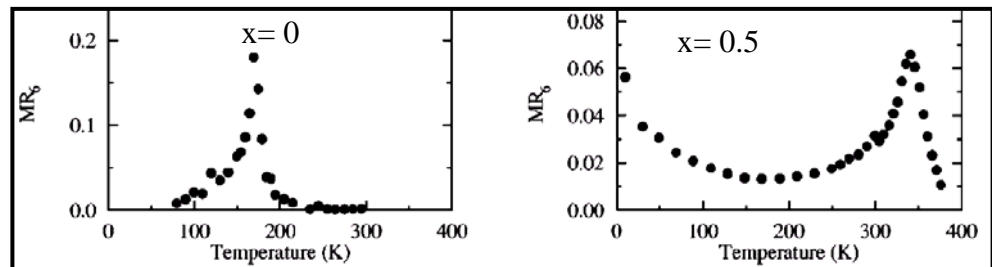
$\text{Fe}_{1-x}\text{Cu}_x\text{Cr}_2\text{S}_4$



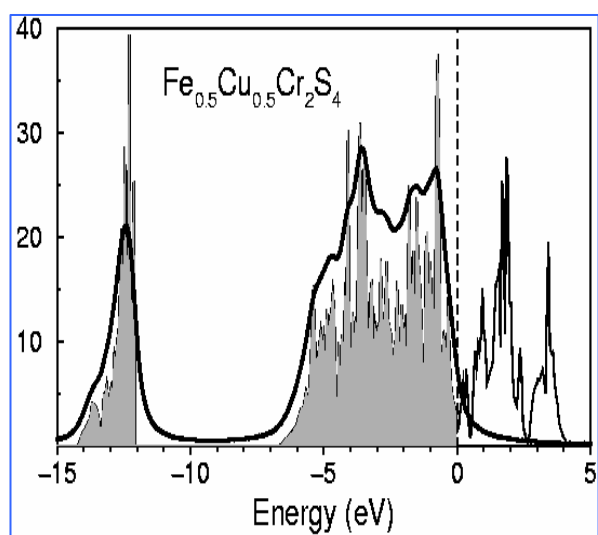
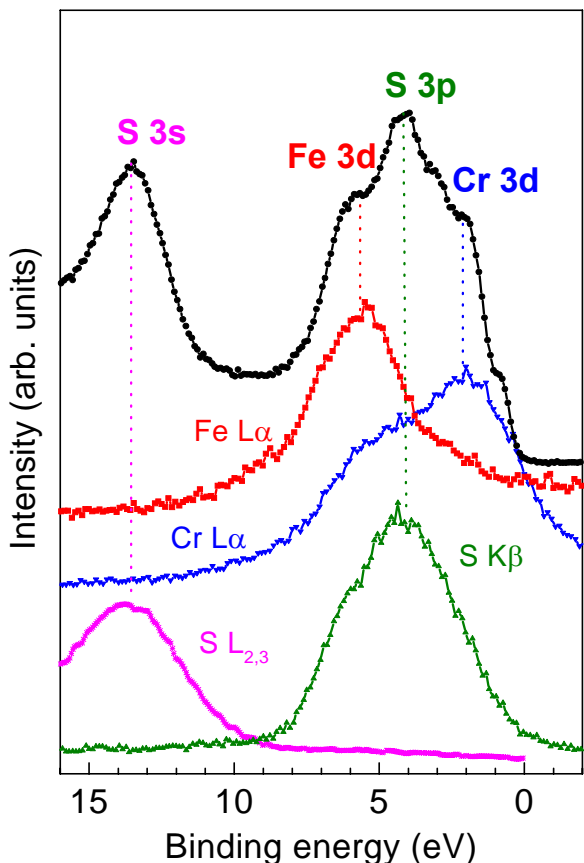
- $\text{Fe}^{2+}\text{Cr}^{3+}_2\text{S}^{2-}_4$
- CuCr_2S_4 : Lotgering : Cu^{1+} (Cr^{3+} , Cr^{4+})
Goodenough : Cu^{2+} (Cr^{3+})
- $\text{Fe}_{0.5}\text{Cu}_{0.5}\text{Cr}_2\text{S}_4$: Cu^{1+} $\text{Fe}^{3+}/\text{Cr}^{4+}$ / S^-

Chalkogenide spinels
prepared by
V. Tsurkan (Kishinau)

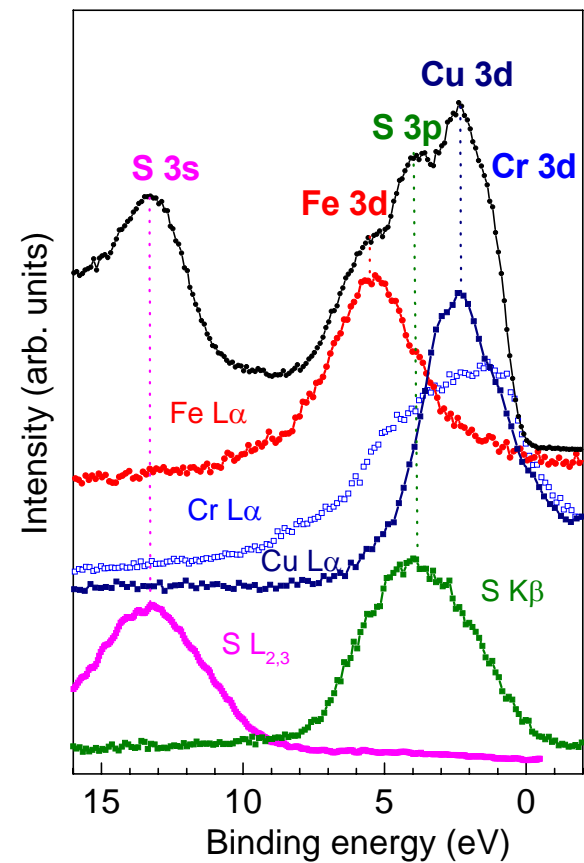
Ramirez et al., Nature, 386, 156 (1997)



FeCr₂S₄



Fe_{0.5}Cu_{0.5}Cr₂S₄

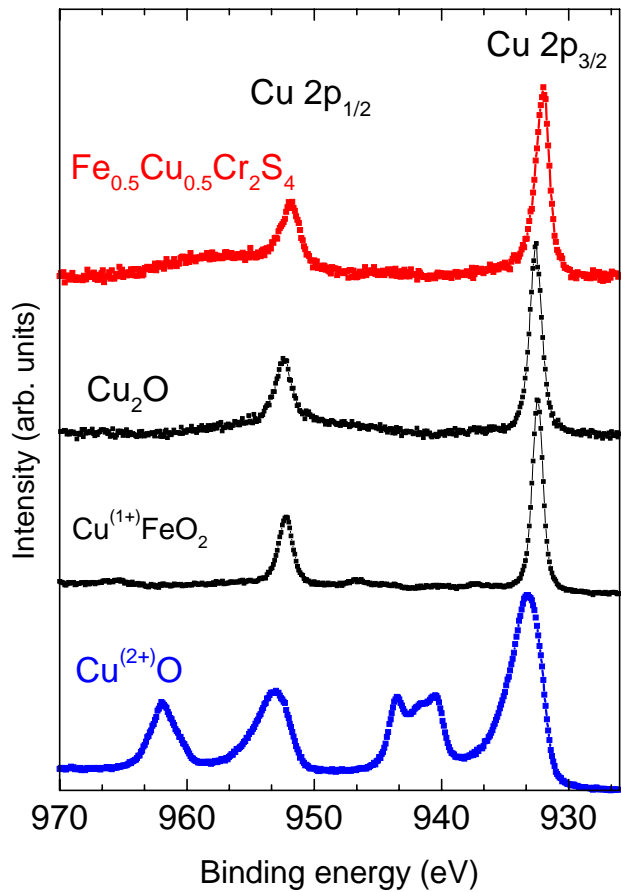


J. Phys.: Condens. Matter **12**,
5411 – 5421 (2000)

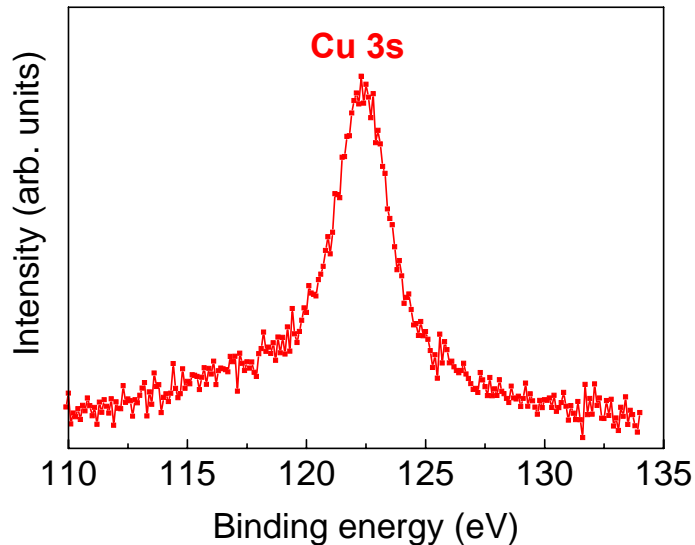
- the VB states below E_F are dominated by ***Cr 3d***;
- minority-spin ***Fe 3d*** states produce a clear Fermi step in spectrum;
- the ***Fe 3d*** states are more localized than ***Cr 3d*** states;
- the ***Fe 3d*** and ***S 3p*** states are represented at slightly higher E_B.

- contribution from the ***Cu 3d*** states just below ***Cr 3d***.

Cu 2p & 3s XPS spectra

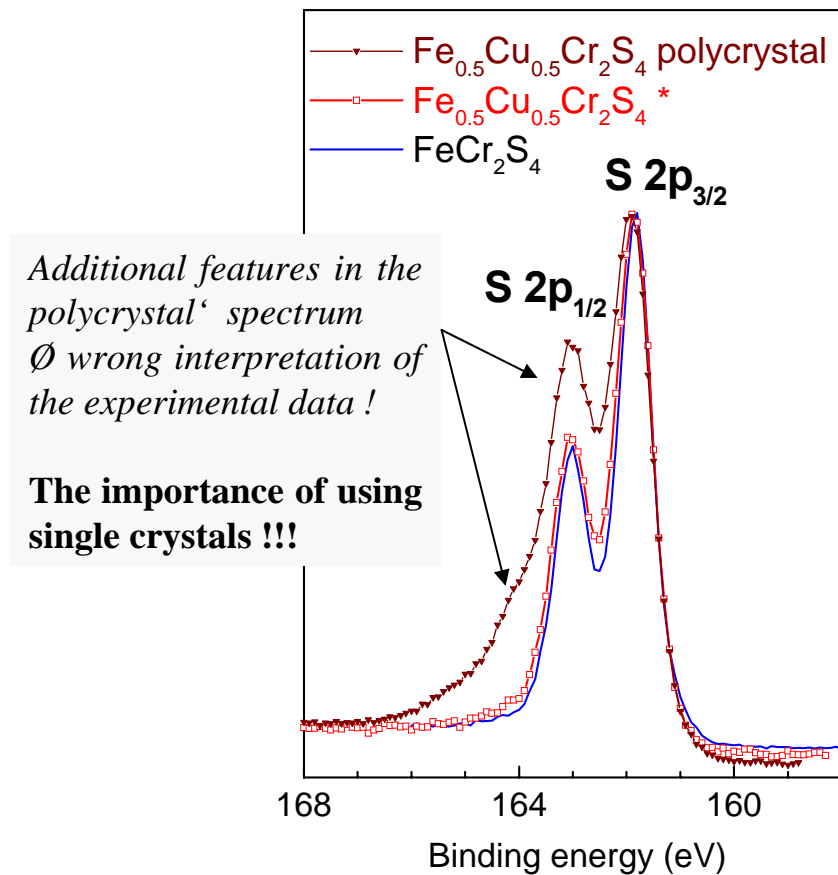
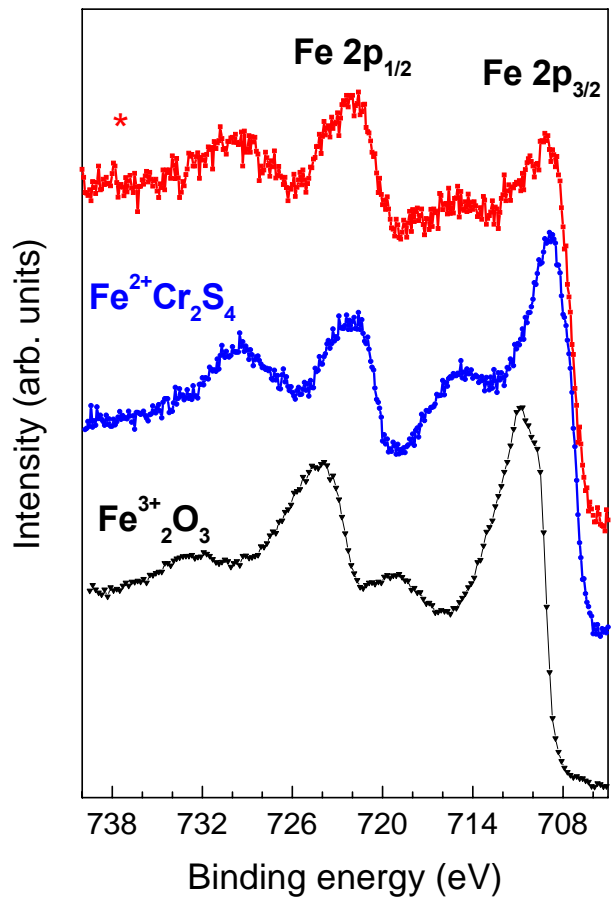


- no satellite in the Cu 2p spectra of $\text{Fe}_{0.5}\text{Cu}_{0.5}\text{Cr}_2\text{S}_4$
- no exchange splitting for the Cu 3s state



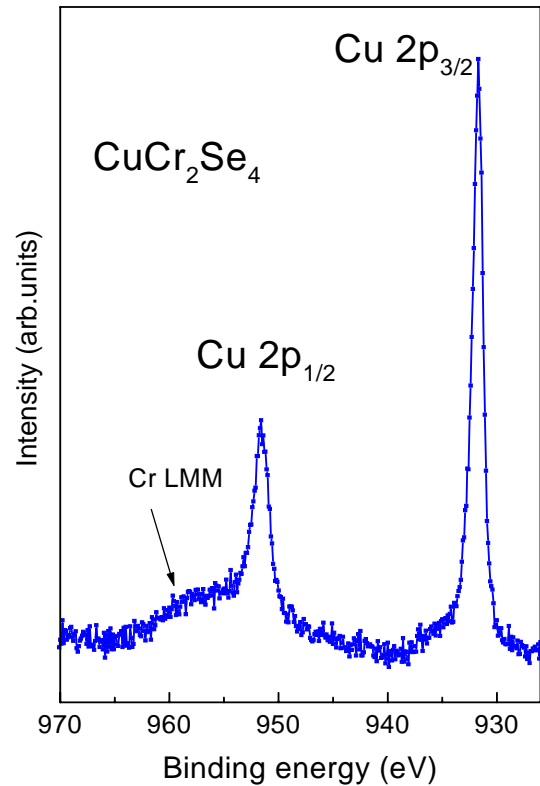
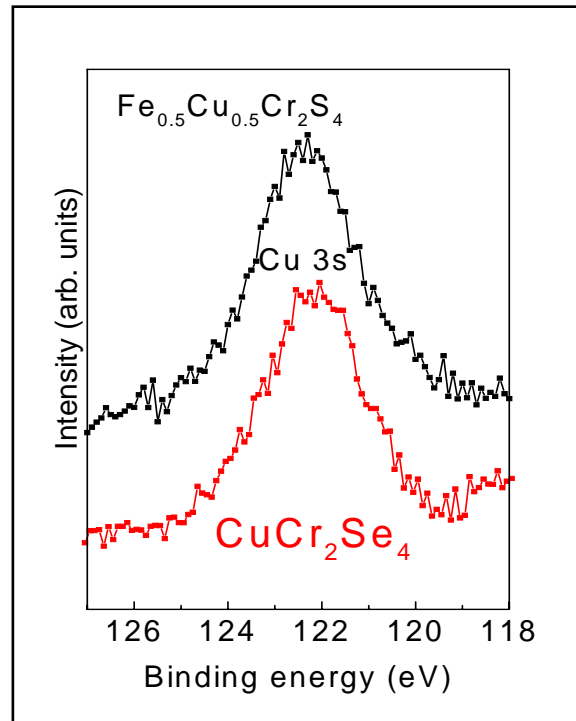
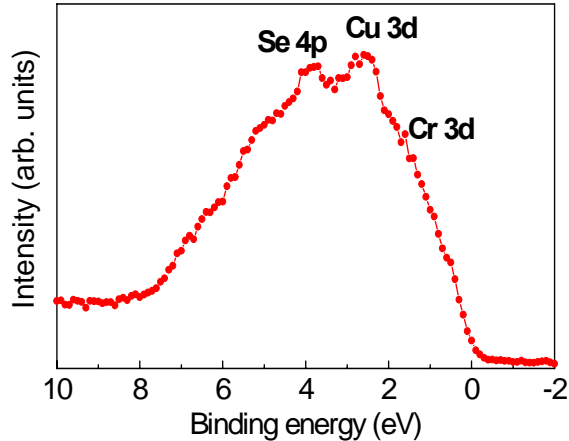
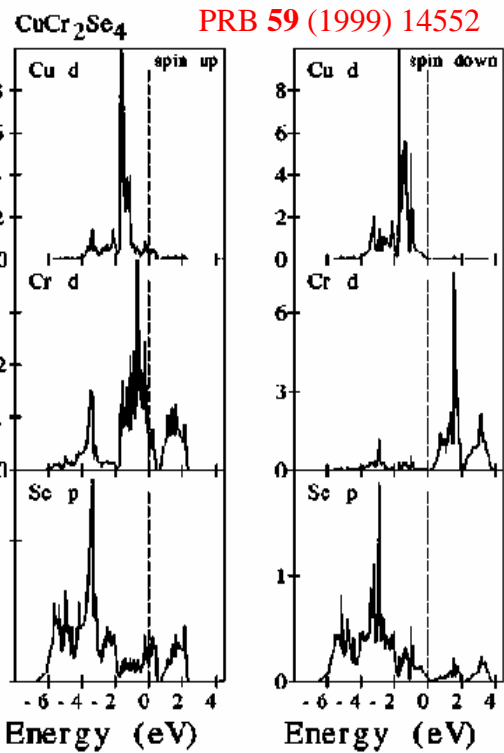
⇒ 3d¹⁰ configuration of the Cu⁺ ion

Fe 2p & S 2p XPS spectra



charge transfer from S²⁻ to Fe³⁺ : Fe²⁺

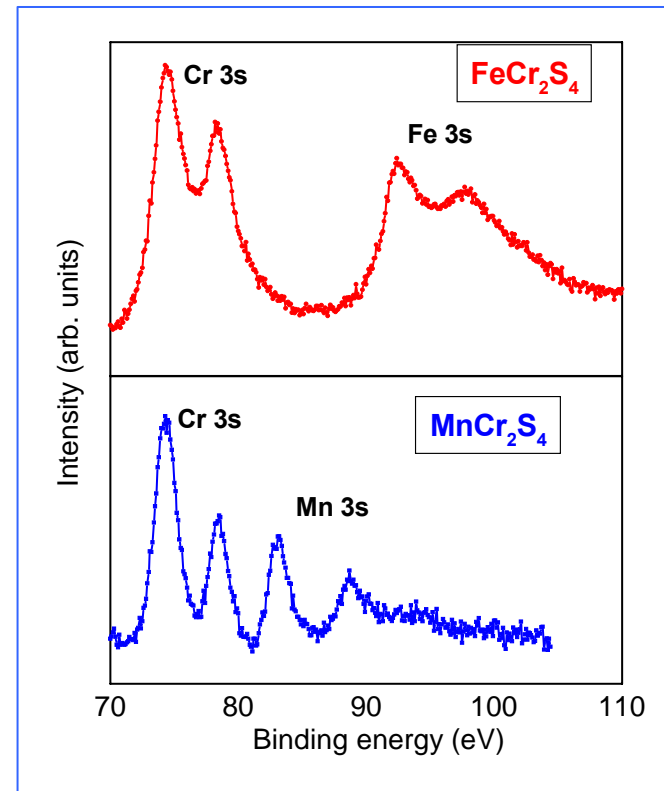
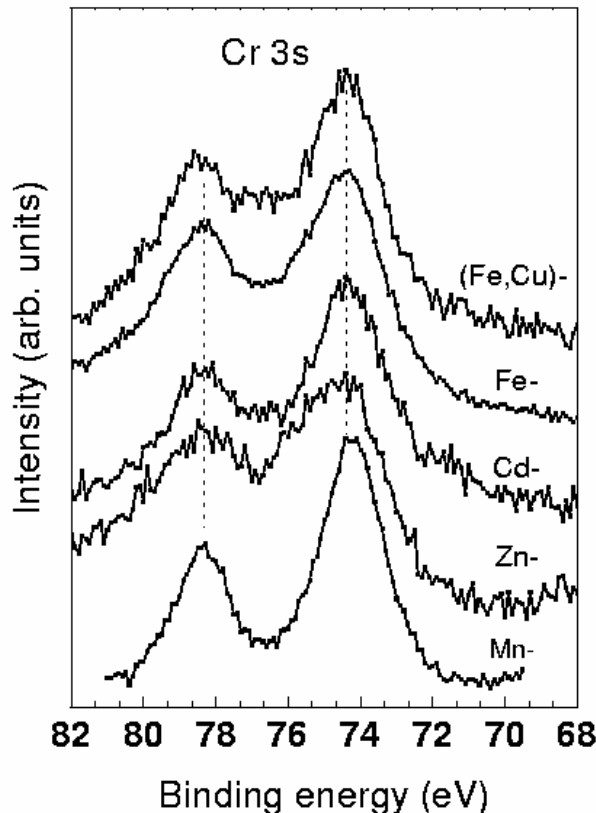
CuCr₂Se₄



No exchange splitting of Cu 3s
⇒ Cu⁺ character of the Cu ions

TM 3s splitting

Sol. St. Comm. **114** (2000) 149



$$\Delta E_{\text{ex}}^{(\text{Fe})} = 5.4 \text{ eV}$$

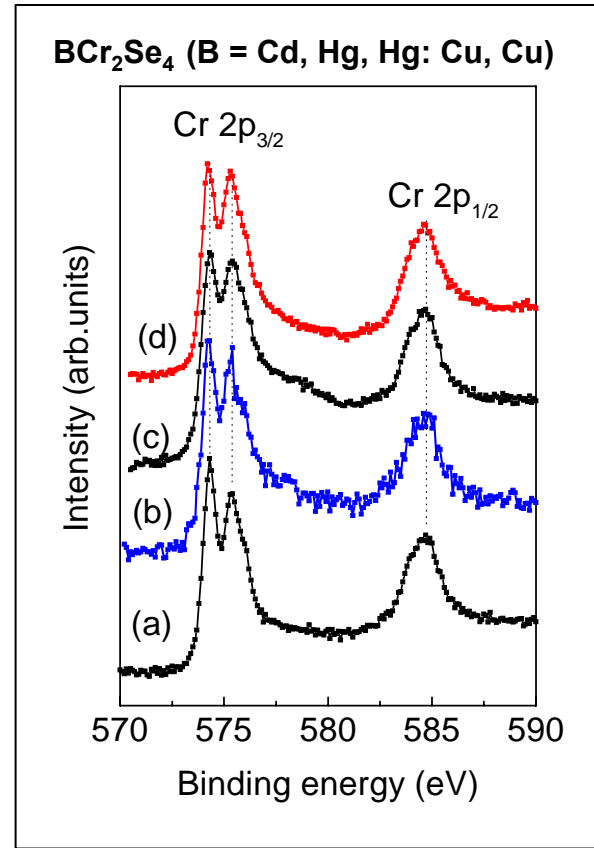
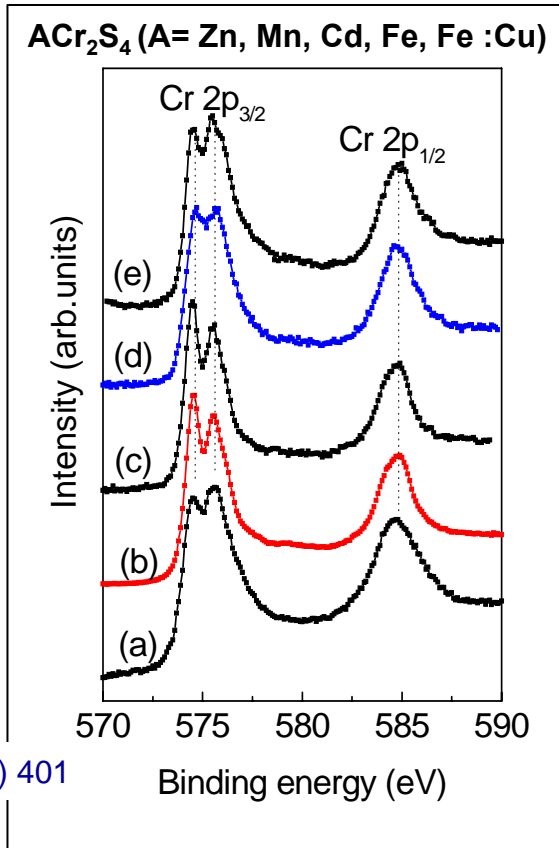
Fe^{2+}

$$\Delta E_{\text{ex}}^{(\text{Mn})} = 5.7 \text{ eV}$$

Mn^{2+}

- the same Cr 3s exchange splitting ΔE_{ex} (~ 4 eV) for all compounds
- similar values for the local magnetic moments of Cr ◆ Cr^{3+} ions

Cr 2p XPS spectra



Eur. J. B 15 (2000) 401

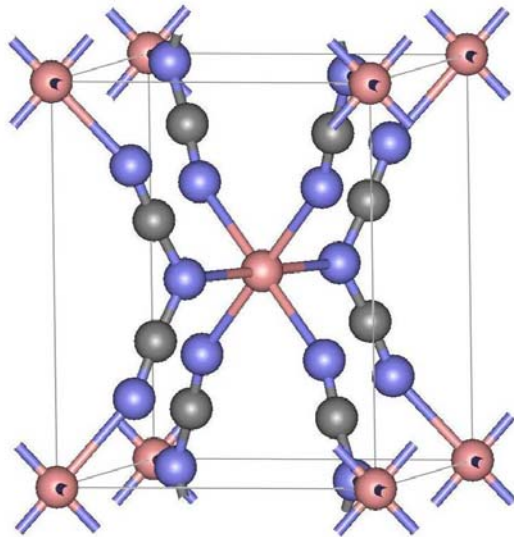
$\mu_{\text{loc}} (\text{Cr}) = 2.9 - 3.0 \mu_B \rightarrow \Delta E(\text{Cr } 2p) = 0.95 - 1.0 \text{ eV}$
→ localised character of the magnetic moments for Cr³⁺ in a 3d³ configuration.

Summary: chalcogenide spinels

- CuCr_2Se_4 : monovalent Cu ions = Lotgering model
- $\text{Fe}_{0.5}\text{Cu}_{0.5}\text{Cr}_2\text{S}_4$: Cu^{1+} mainly affects the Fe and S ions
- well-resolved Cr 2p splitting for Cr-chalcogenide spinels
- ACr_2X_4 : the same Cr 3s splitting \dagger $\text{Cr}^{3+}(3\text{d}^3)$
- XPS & XES data -- excellent agreement with band structure calculations

organometallic materials

XPS on organometallic materials



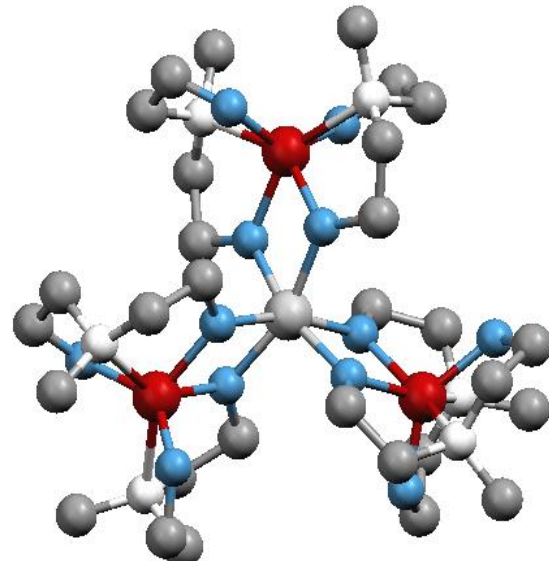
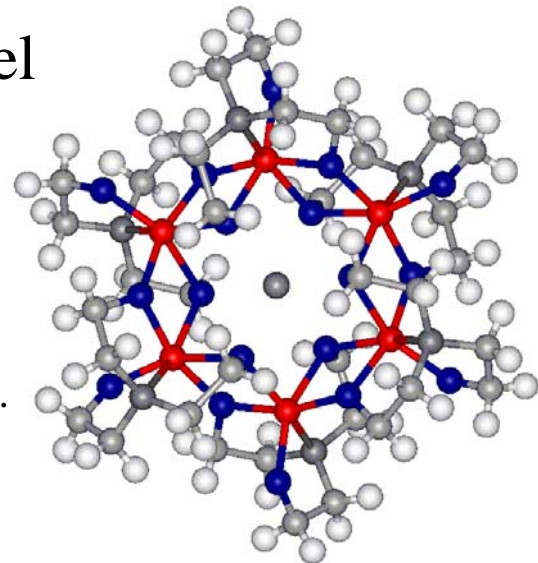
di-cyanamides

molecule based solids

ferric wheel

Magnetic molecules

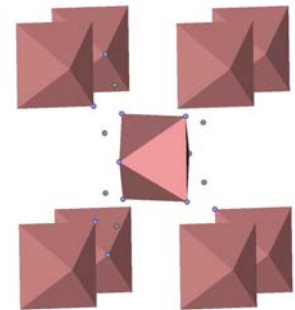
Synthesized by R.Saalfrank et al.
Erlangen



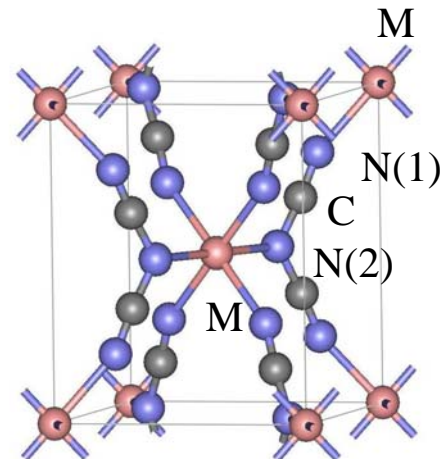
ferric star

Dicyanamide materials $M[N(CN)_2]_2$

$M = Mn, Fe, Ni, Cu$



- each metal ion is surrounded by six nitrogen atoms in a distorted (axially elongated) octahedral geometry
- the rutile-like structure consists of rhombus-shaped units which adopt a chain alignment parallel to the c axis
- tilting of the elongated octahedra in the crystallographic ab plane



$M =$ Mn, Fe, Co, Ni, Cu

↓ ↑
change over

Dicyanamide materials $M[N(CN)_2]_2$

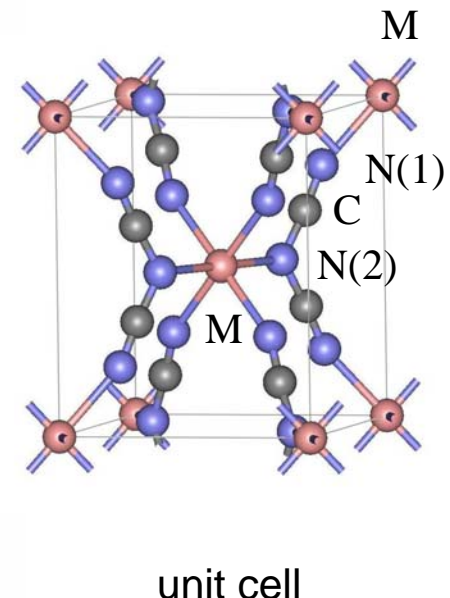
$M = Mn, Fe, Ni, Cu$

Crystallographic data - isostructural series

Compound	$Mn[N(CN)_2]_2$	$Fe[N(CN)_2]_2$	$Co[N(CN)_2]_2$	$Ni[N(CN)_2]_2$	$Cu[N(CN)_2]_2$
Space group	$Pnnm$	$Pnnm$	$Pnnm$	$Pnnm$	$Pnnm$
Interatomic distances and angles at:					
	4.6 K	1.6 K	1.6 K	1.6 K	—
M–M	6.0657(1)	5.9670(1)	5.9158(1)	5.8634(1)	—
M–N(2)–C	119.2(1)	119.6(1)	120.6(1)	121.0(1)	—
N(2)–C–N(1)	175.2(3)	175.5(2)	175.1(2)	174.6(2)	—
C(2)–N(1)–M	158.5(2)	158.9(1)	159.6(1)	159.5(1)	—
α	140.4(1)	141.7(1)	142.3(1)	142.6(1)	—
M–N(1)	2.189(1)	2.126(1)	2.093(1)	2.053(1)	—
M–N(2)	2.291(2)	2.206(1)	2.156(2)	2.129(2)	—
Δ	1.047	1.038	1.030	1.037	—
β	25.2(2)	26.4(2)	27.5(2)	27.6(2)	—
Magnetic ordering type	canted AFM ($2\phi \approx 10^\circ$)	canted AFM	collinear FM	collinear FM	para
Ordering temperature	16 K	—	9 K	21 K	—
Local magnetic moments of 3d–ions	$4.61 \mu_B$	$4.23 \mu_B$	$2.67 \mu_B$	$2.21 \mu_B$	$1.05 \mu_B$

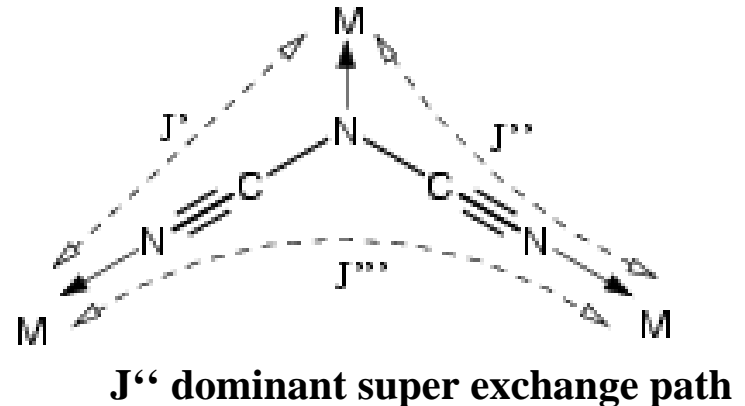
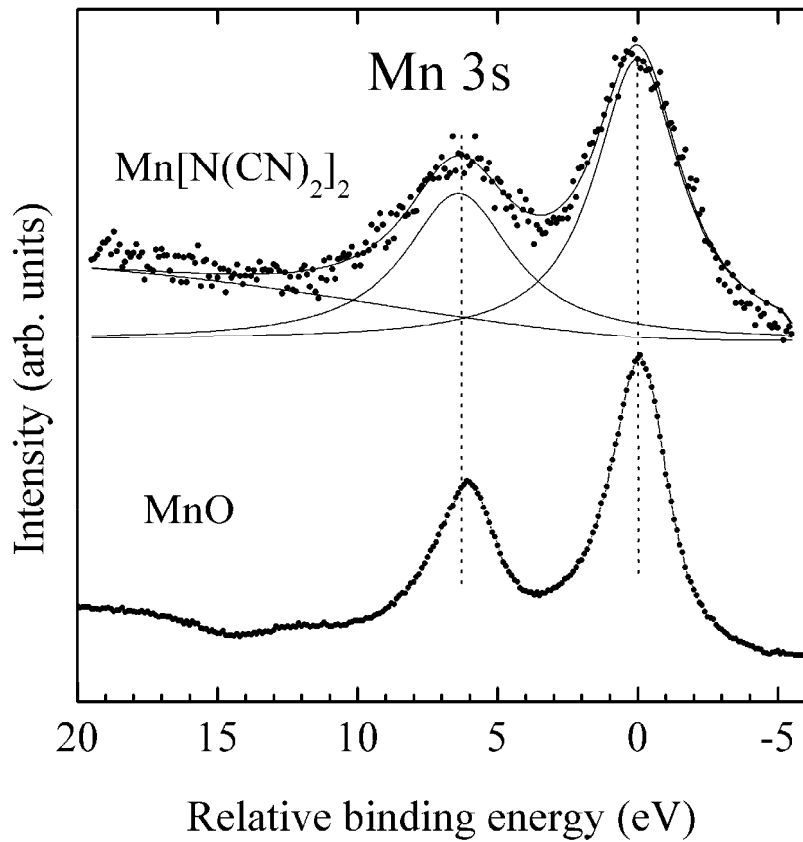
↓ ↑ change over ↑↑

C.R. Kmety *et al.*
Physical Review B, 62 5576-5588 (2000)



Dicyanamide $\text{Mn}[\text{N}(\text{CN})_2]_2$

3s splitting



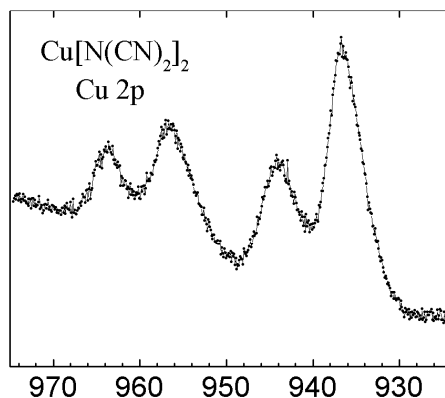
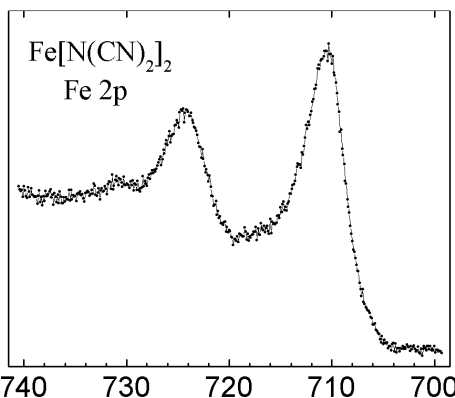
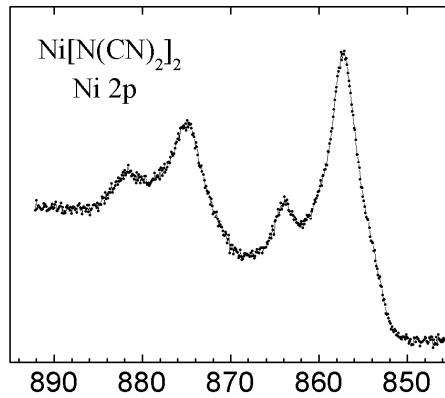
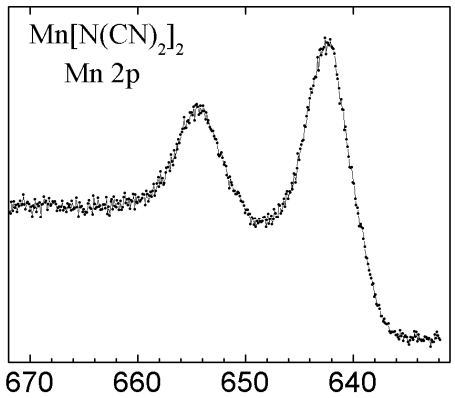
Magnetic moments on Mn:

$$4.65 \mu_B/\text{atom } \text{Mn}[\text{N}(\text{CN})_2]_2$$
$$4.45-4.79 \mu_B/\text{atom } \text{MnO}$$

- the magnetic moment per Mn atom is slightly reduced as expected from a Mn^{2+} ($3d^5$) ion due to a reduction in spin polarization driven by $\text{Mn}(3d) \leftrightarrow \text{N}(2sp)$ interaction.

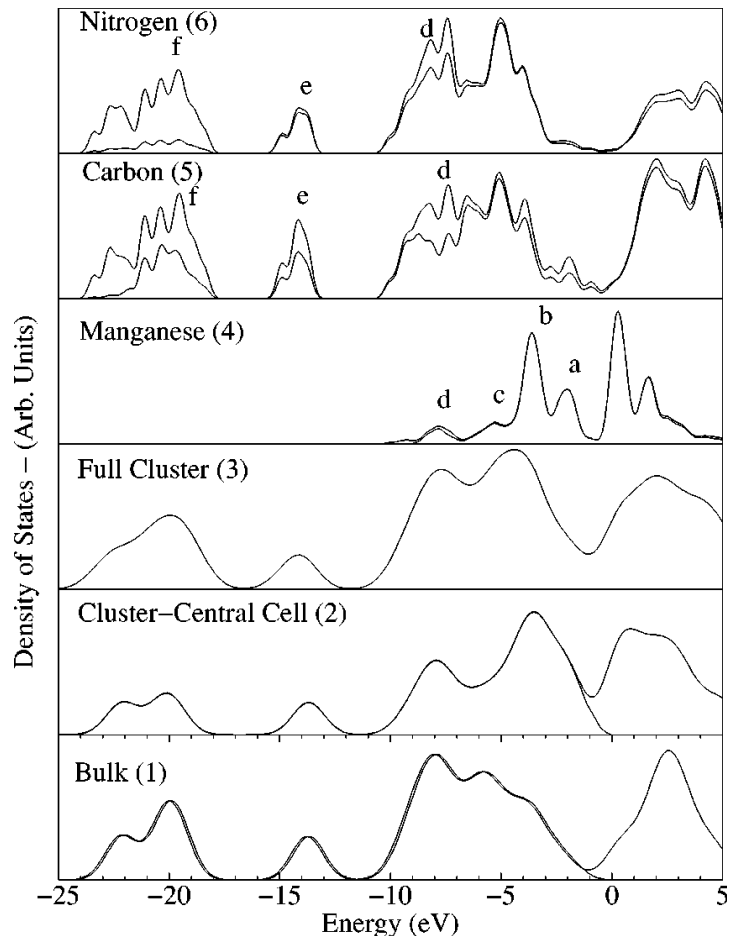
Dicyanamides transition metal 2p core level spectra

Intensity (arb. units)



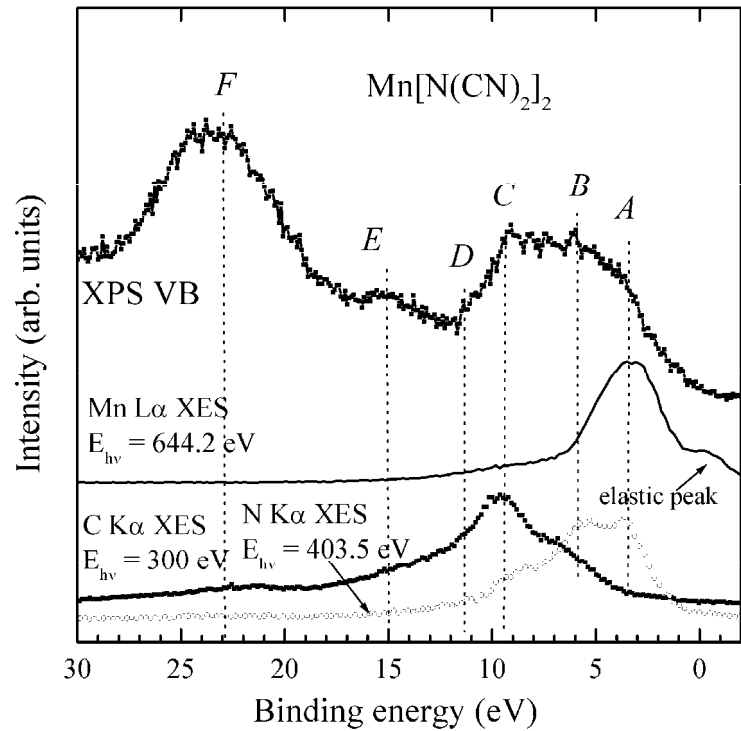
Screening effects:
low with Mn and Fe
pronounced with Ni and Cu
valencies confirmed
as before

Valence bands of $\text{Mn}[\text{N}(\text{CN})_2]_2$



HOMO: Mn : majority spin
LUMO : minority spin

N DOS
N 2p DOS
C DOS
C 2p DOS
Mn DOS
Mn 3d DOS

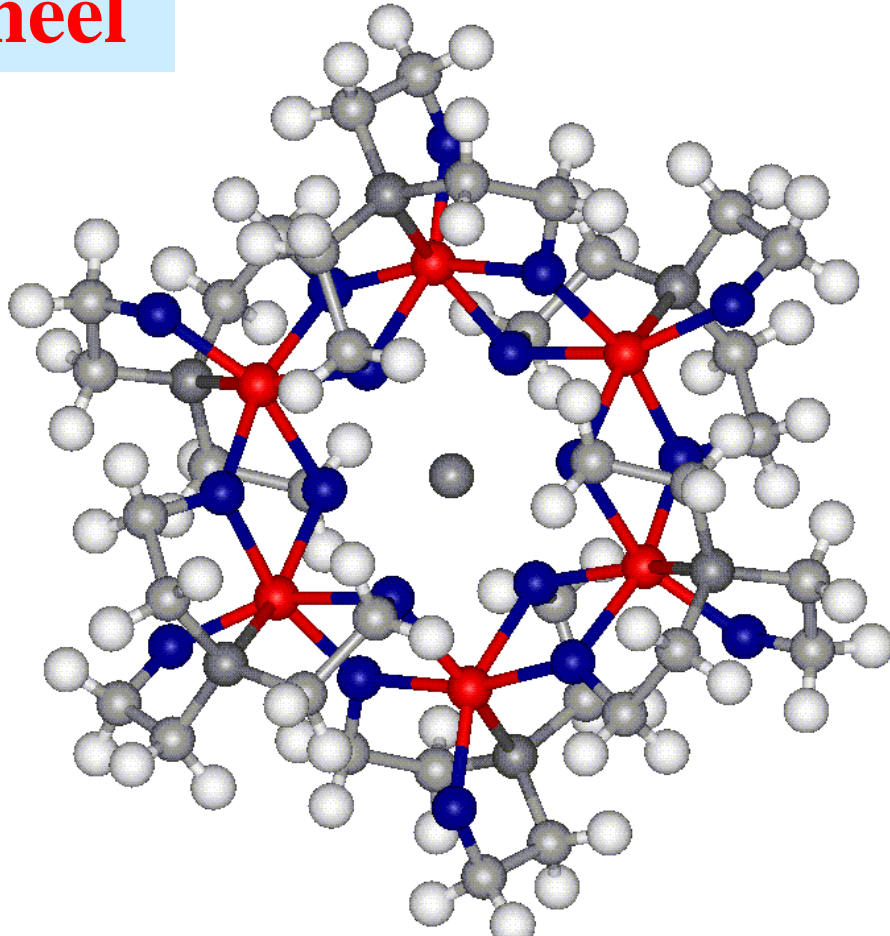


Phys. Rev. **B66**, 014446(8) (2002)

filling of e_g and t_{2g} levels is important for the super exchange interaction, and responsible for the change over AFM - FM

D.O.Demchenko et al. Phys. Rev. **B 69**, 205105(9) (2004)

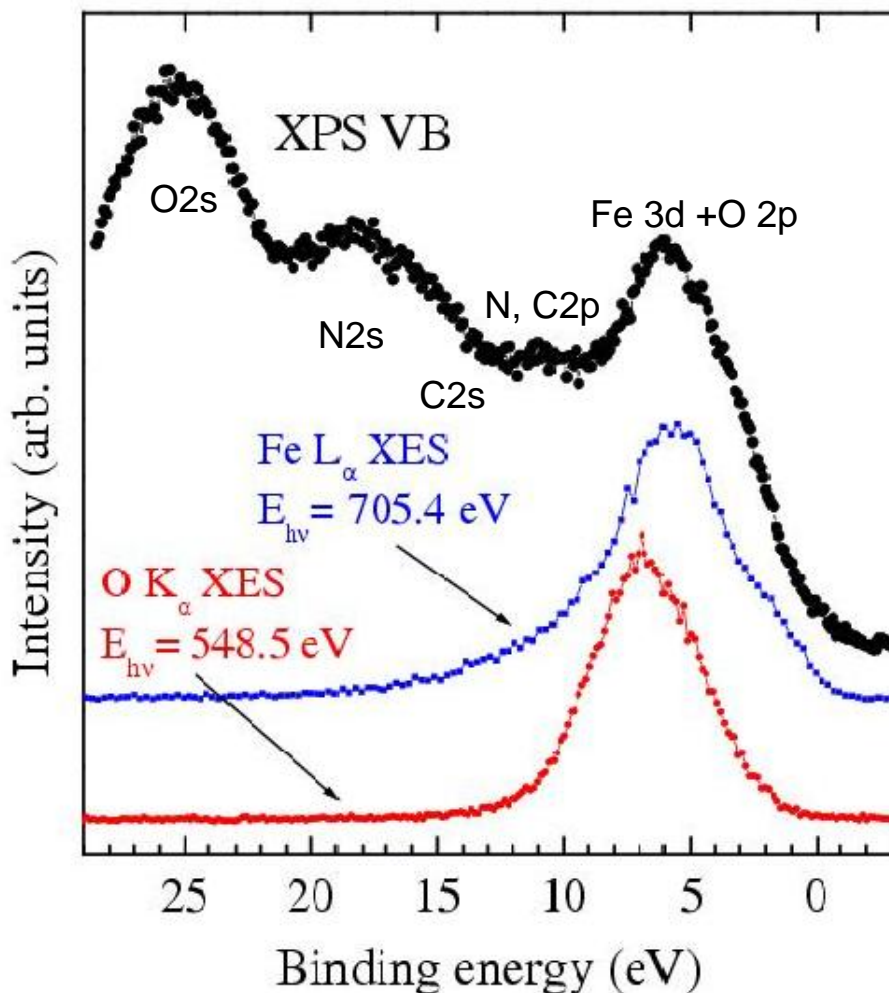
ferric wheel



[Li₂Fe₆L₆]Cl·6CHCl₃, L=N(CH₂CH₂O)₃

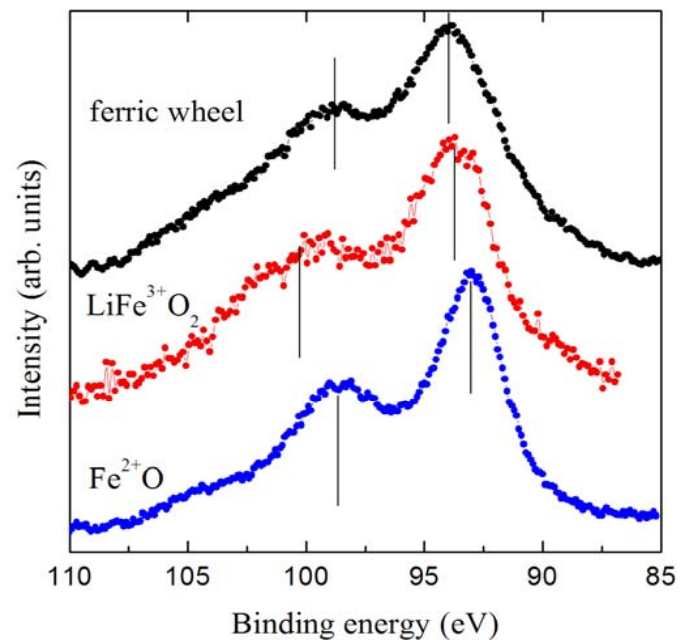
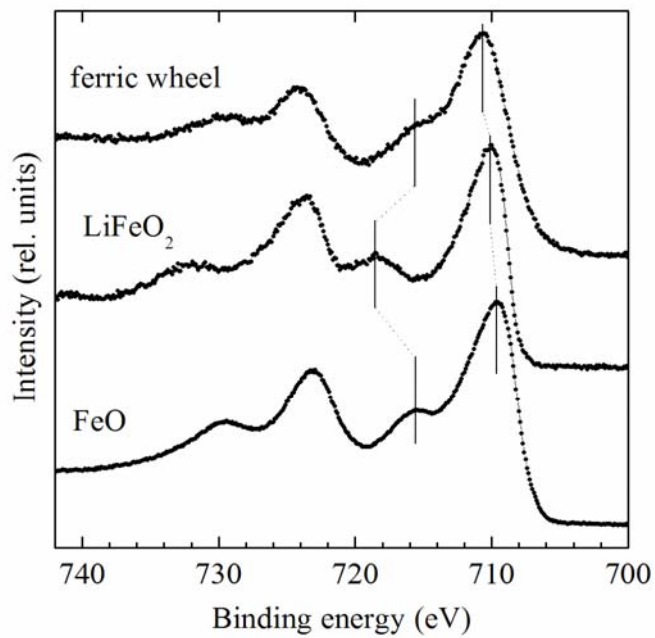
prepared by Saalfrank et al. Erlangen

Valence bands ferric wheel



[Li₂Fe₆L₆]Cl⁺·6CHCl₃, L=N(CH₂CH₂O)₃

Determination of the valency of Fe



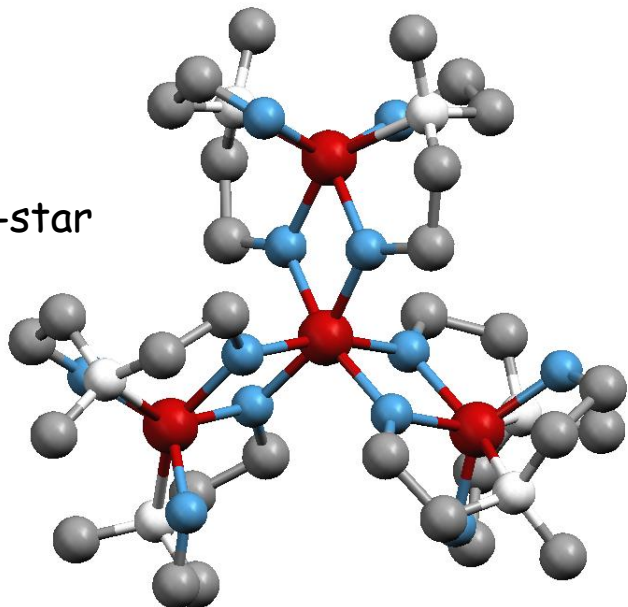
$\text{Fe}^{2+}\underline{\text{L}}$ and Fe^{3+}

S.G. Chiuzbaian et al. Surf. Sci. 482-485, 1272 – 1276 (2001)

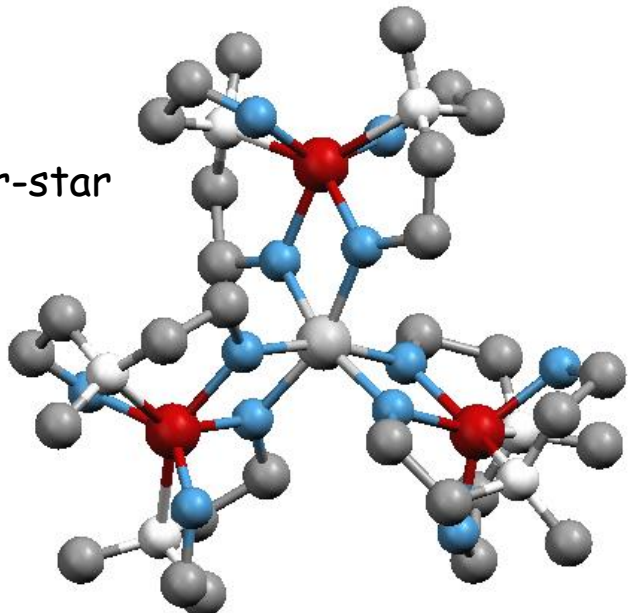
A.V. Postnikov et al. J. Phys. Chem. Solids **65/4**, 813-817 (2004)

ferric star molecules

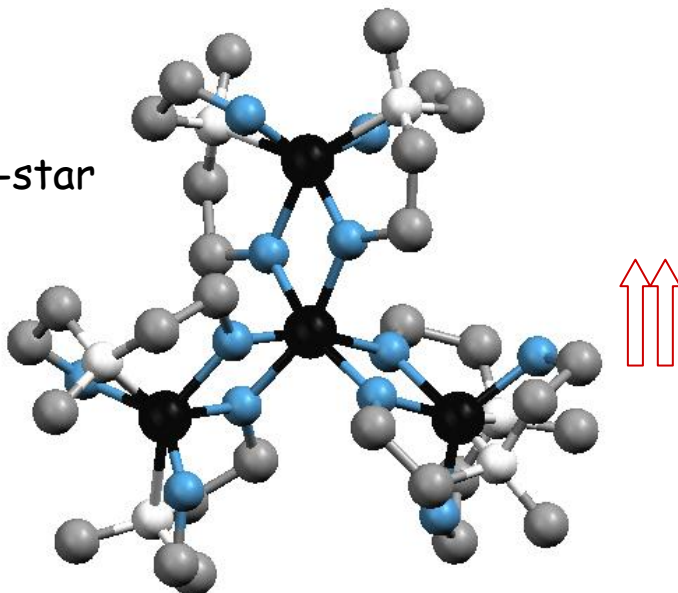
Fe-star

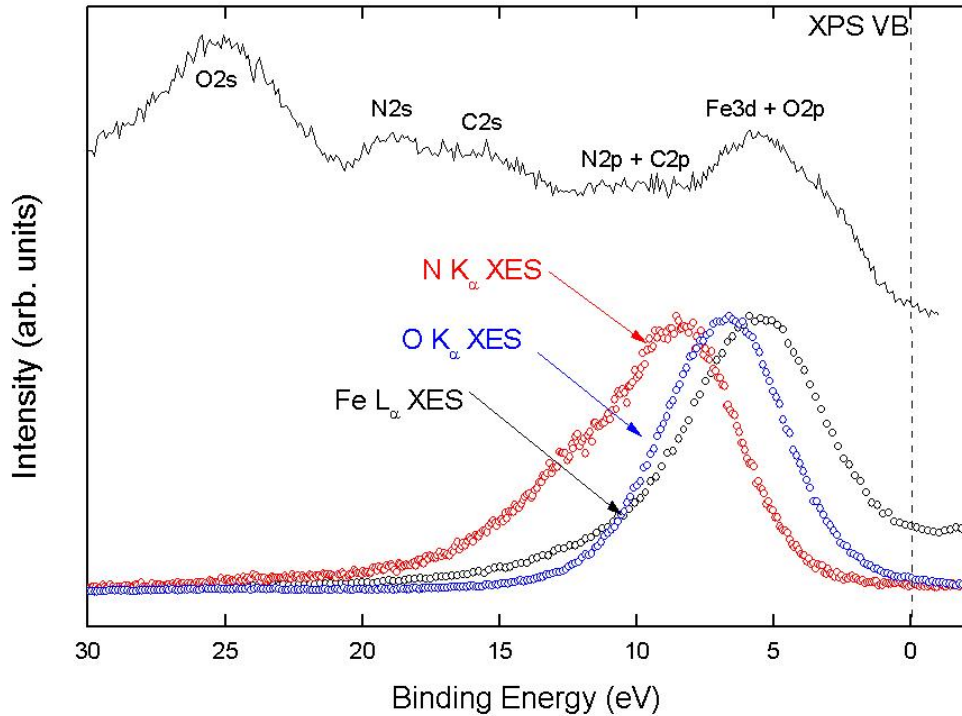


Fe₃Cr-star

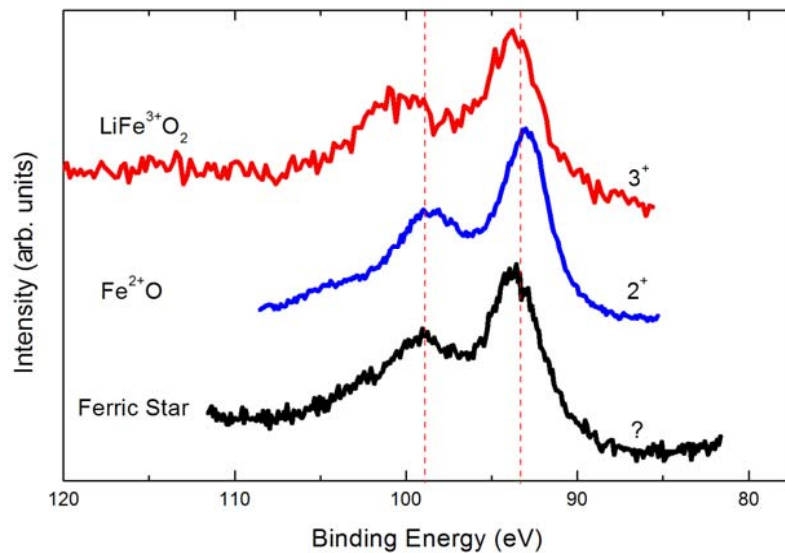
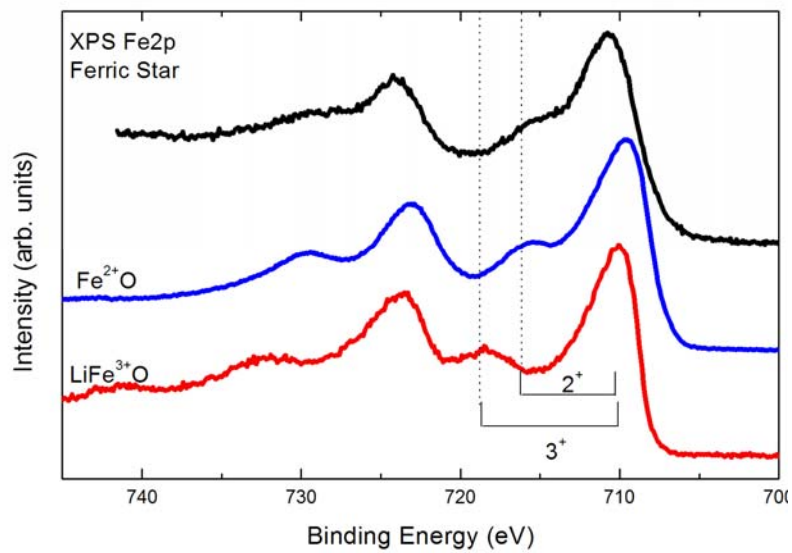


Mn-star





- the top of the valence band is primarily derived from Fe 3d and O 2p states
 - in the middle part the structures result from hybridization of the C 2p, N 2p, C 2s and N2s states
 - at the bottom of the valence band we have the O2s states



Colossal Magnetoresistance Materials Characterized by X-ray Spectroscopic Methods

**M. Neumann, K. Kuepper, H. Hesse,
E. Burzo¹, I. Balasz¹, V.R. Galakhov²**



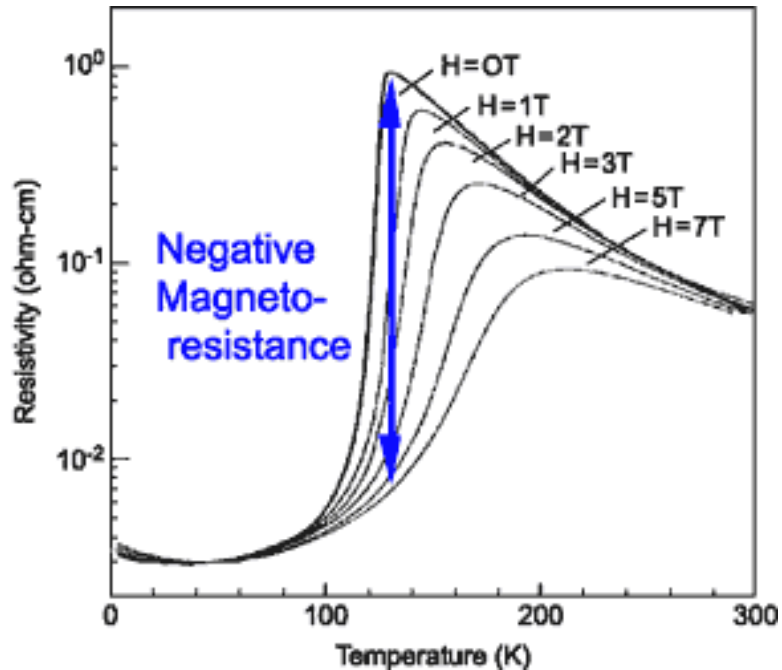
¹ Babes Bolyai University, Cluj-Napoca, Romania

² Russ. Acad. of Sciences, Yekaterinburg

Outline

- **Introduction**
- **Methods:** XPS, XES, XAS, XLD, XMCD, RIXS
- **CMR materials:** © $\text{La}_{1-x}\text{A}_x\text{Mn}_{1-y}\text{TM}_y\text{O}_3$
© $\text{Sr}_2\text{FeMoO}_6$
(© spinells ACr_2X_4)
- **Summary**

colossal magneto-resistance (CMR)



- The Magneto Resistance is defined as the change of the resistance by applying an external magnetic field
- changes of 100% to several 1000% have been reported
- different applications

Science 292, 1509 (2001)

CMR materials

Colossal magnetoresistance effect (CMR)

© $\text{La}_{1-x}\text{A}_x\text{MnO}_3$ † Science 264, 413 (1994)

Double exchange model (Mn^{3+} , Mn^{4+}) (Zener, PR 81, 440 (1955))

Electron- phonon interaction (Millis et al., PRL 74, 5144 (1995))

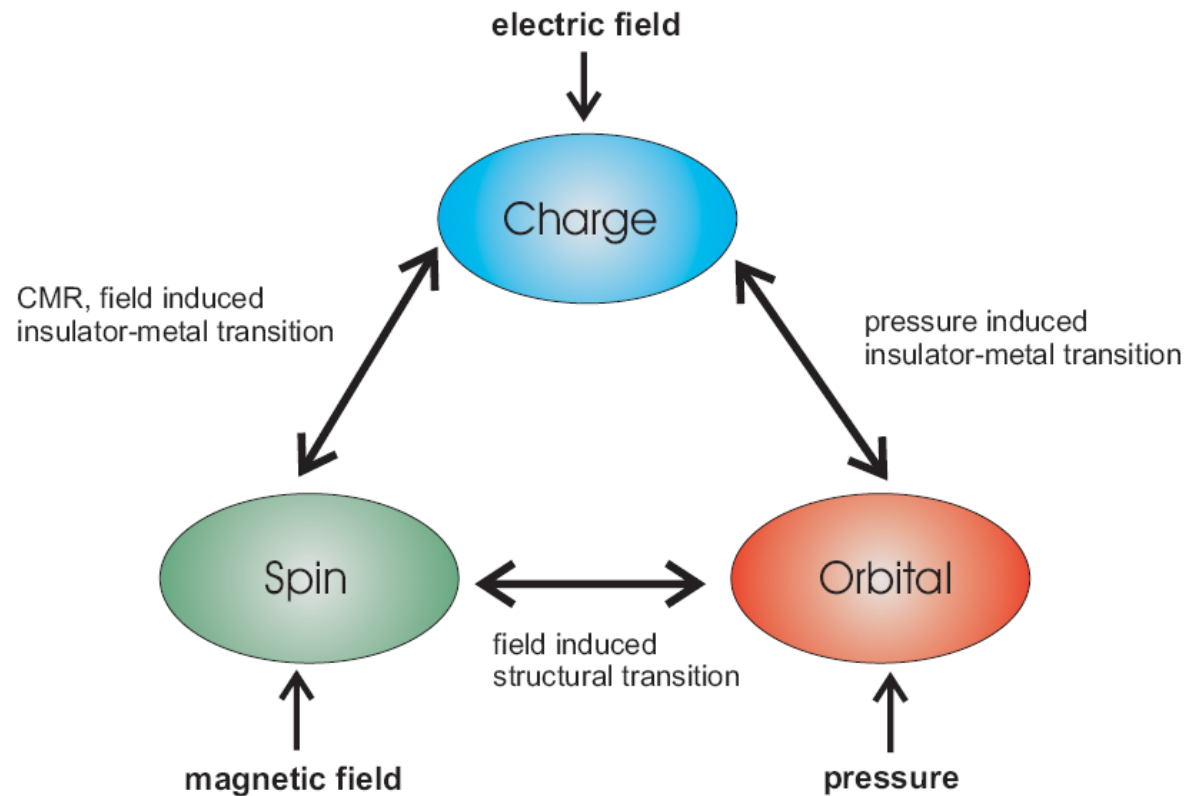
© $\text{Sr}_2\text{FeMoO}_6$ **high $T_c = 420\text{K}$**

low fields for CMR (Kobayashi et al., Nature 395, 677 (1998))

© $\text{Fe}_{1-x}\text{Cu}_x\text{Cr}_2\text{S}_4$; (ACr_2X_4) † Nature 387, 268 (1997)

$\text{La}_{2-2x}(\text{Sr, Ca, Sn})_{1+2x}\text{Mn}_2\text{O}_7$ (Nature 380, 141 (1996)); $\text{Sr}_{2-x}\text{Nd}_{1+x}\text{Mn}_2\text{O}_7$ (JPCM 8, L 427 (1996));
 $\text{Tl}_2\text{Mn}_2\text{O}_7$ (Nature 379, 53 (1996), Science 273, 81 (1996)); $\text{Eu}_{14}\text{MnBi}_{11}$ (PRB 57, R 8103 (1998));

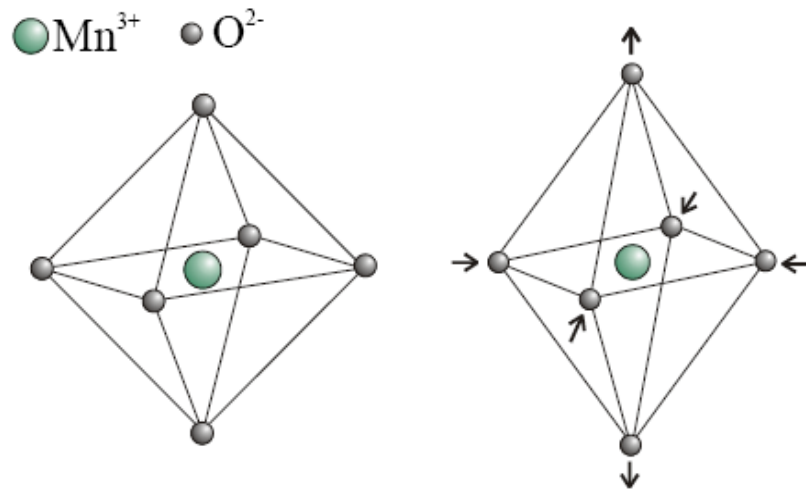
Introduction



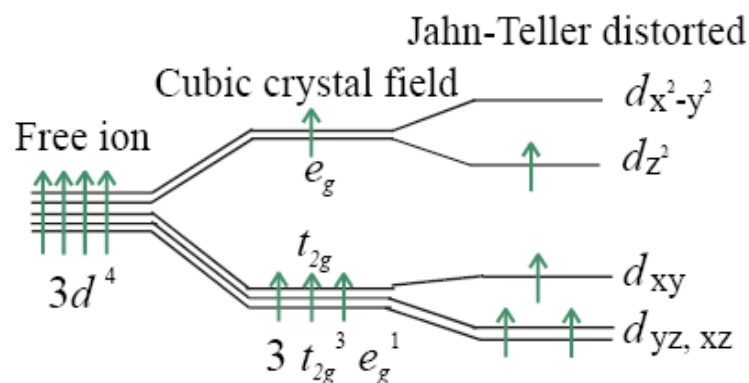
➤ The 3d transition metal oxides exhibit a rich variety of electronic and magnetic properties

➤ This is due to the intricate interplay between the charge, magnetic and orbital degrees of freedom

Manganese perovskites: $\text{La}_{1-x}\text{A}_x\text{MnO}_3$



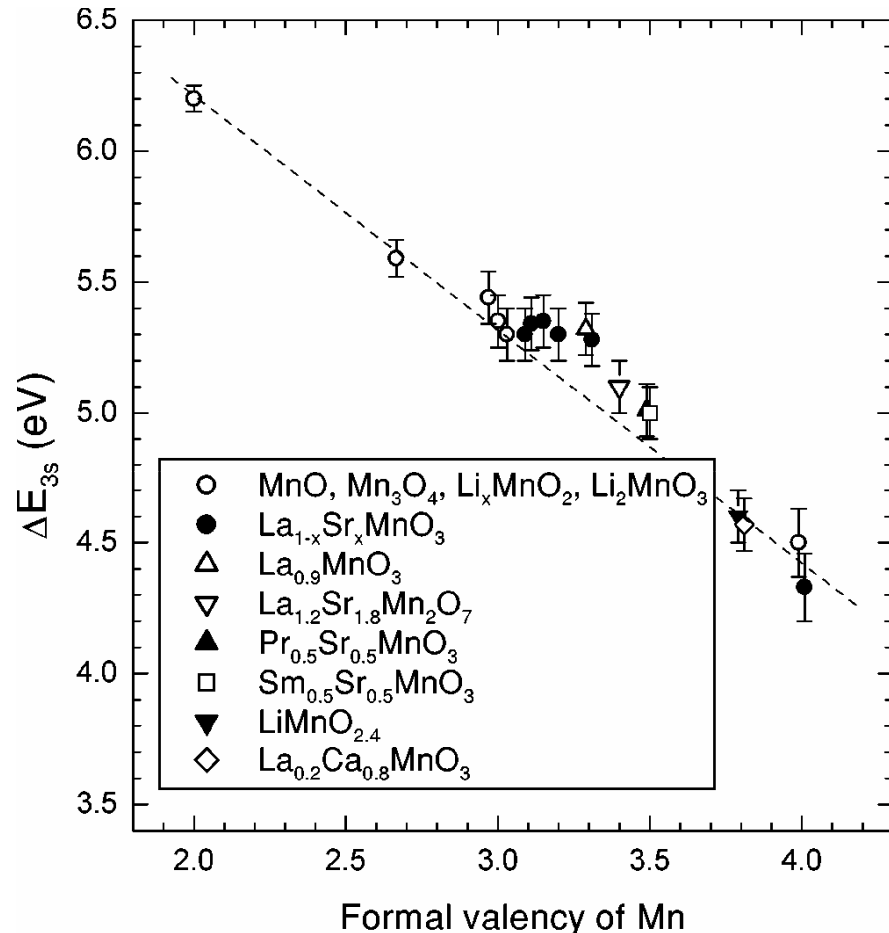
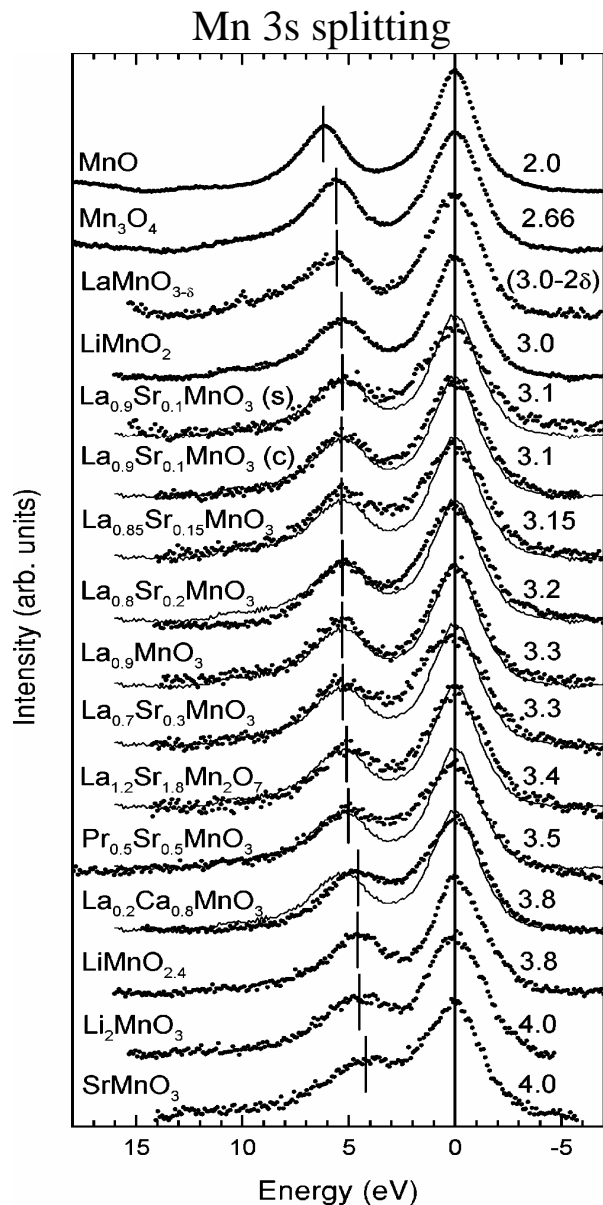
➤ In perovskites like LaMnO_3 a cooperative Jahn-Teller distortion, i. e. a collective elongation (compression) of one crystal axis may lead to a preferential occupation of a certain type of $3d$ orbital -> **orbital ordering**



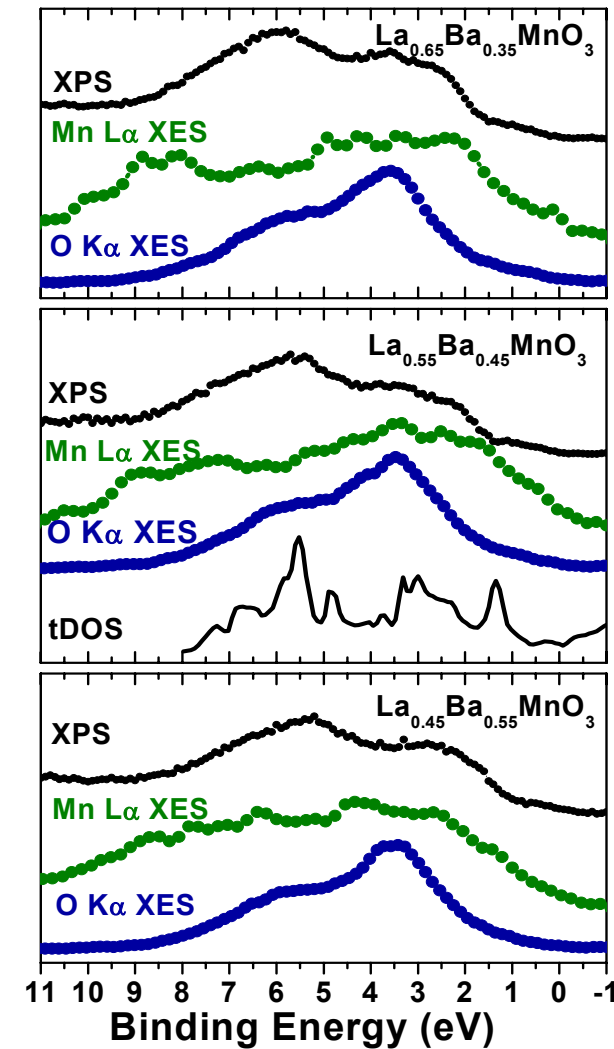
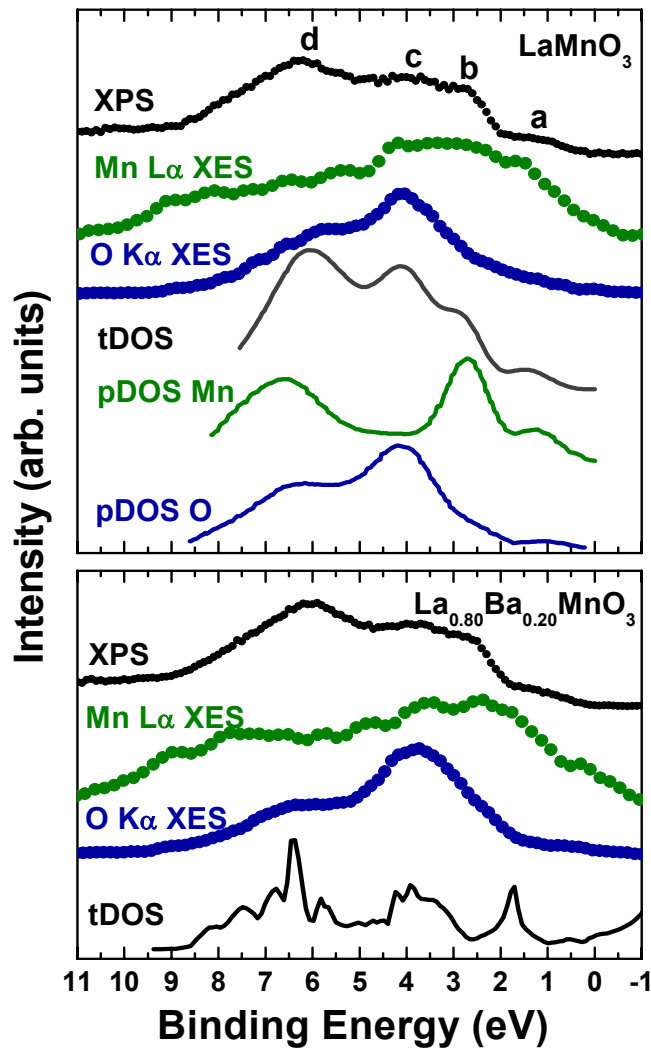
Methods

- X-ray Photoelectron Spectroscopy (XPS) ⇒ Osnabrück
- X-ray Emission Spectroscopy (XES),
X-ray Absorption Spectroscopy (XAS)
Resonant Inelastic X-ray Scattering (RIXS)
X-ray linear dichroism (XLD)
X-ray magnetic circular dichroism (XMCD)
⇒ ALS, Beamline 8.0.1, SXF and 4.0.2 (XMCD)
- ⇒ ELETTRA , Beamline BACH, COMIXS (CCD detector)
- ⇒ BESSY II, Beamline U-41 PGM, ROSA

Mn 3s XPS spectra of Mn oxides

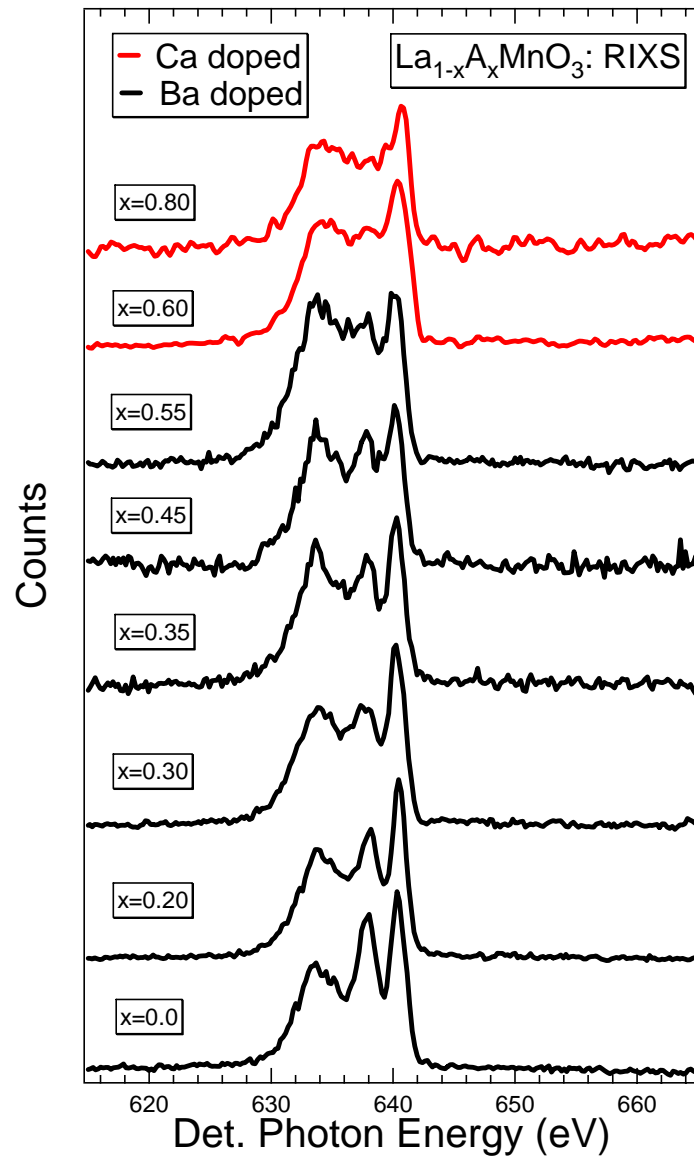
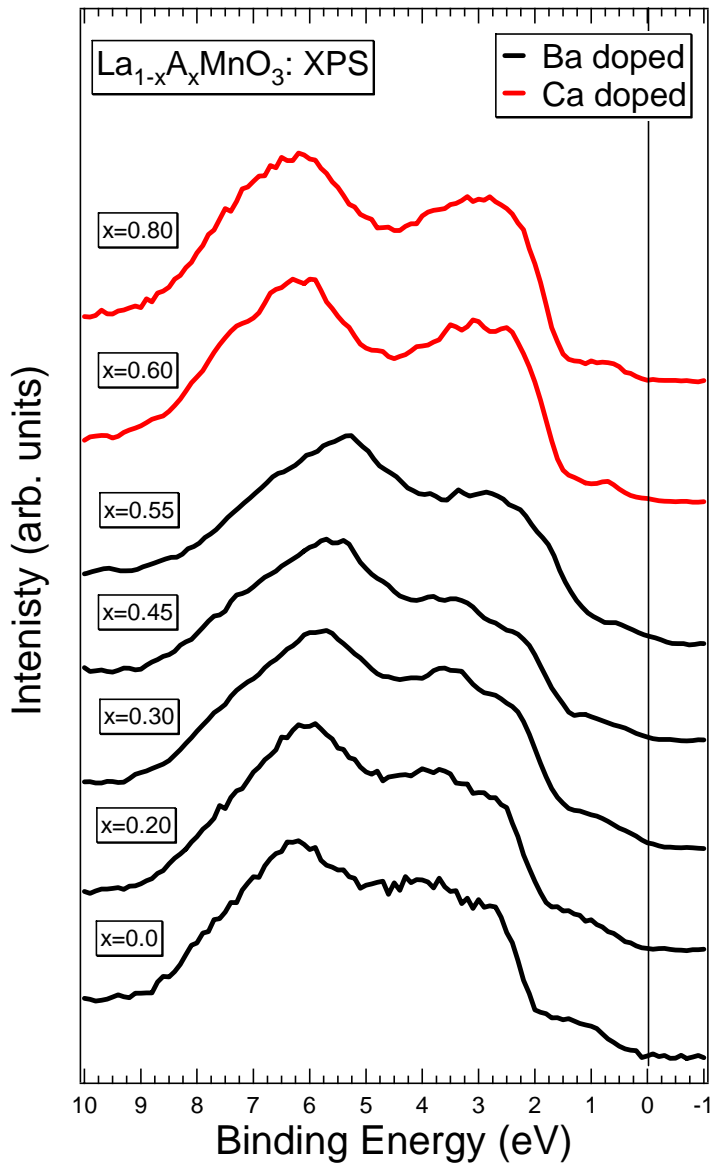


$\text{La}_{1-x}\text{Ba}_x\text{MnO}_3$: XPS VB & XES



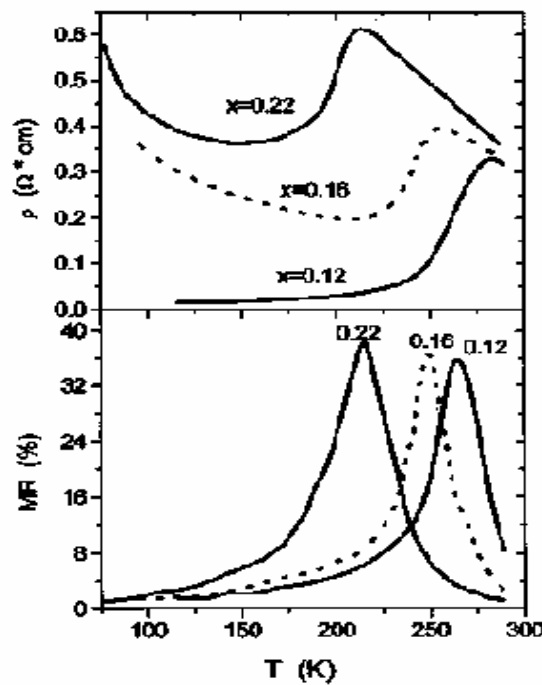
- Strong hybridization of the Mn 3d and O 2p states

$\text{La}_{1-x}\text{A}_x\text{MnO}_3$ (A=Ba,Ca): metal to insulator transition: XPS and RIXS

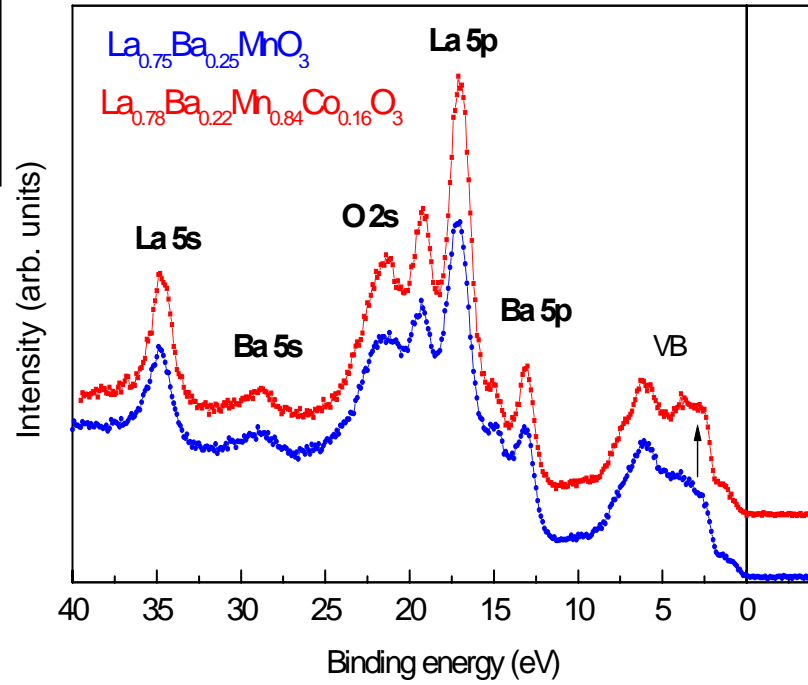


(La,Ba)Mn_{1-x}Co_xO₃

- LaCoO₃ : Co³⁺ (3d⁶) LS state
(no magnetic moment)
- LaMn_{1-x}Co_xO₃: (RPES, XAS) Co²⁺

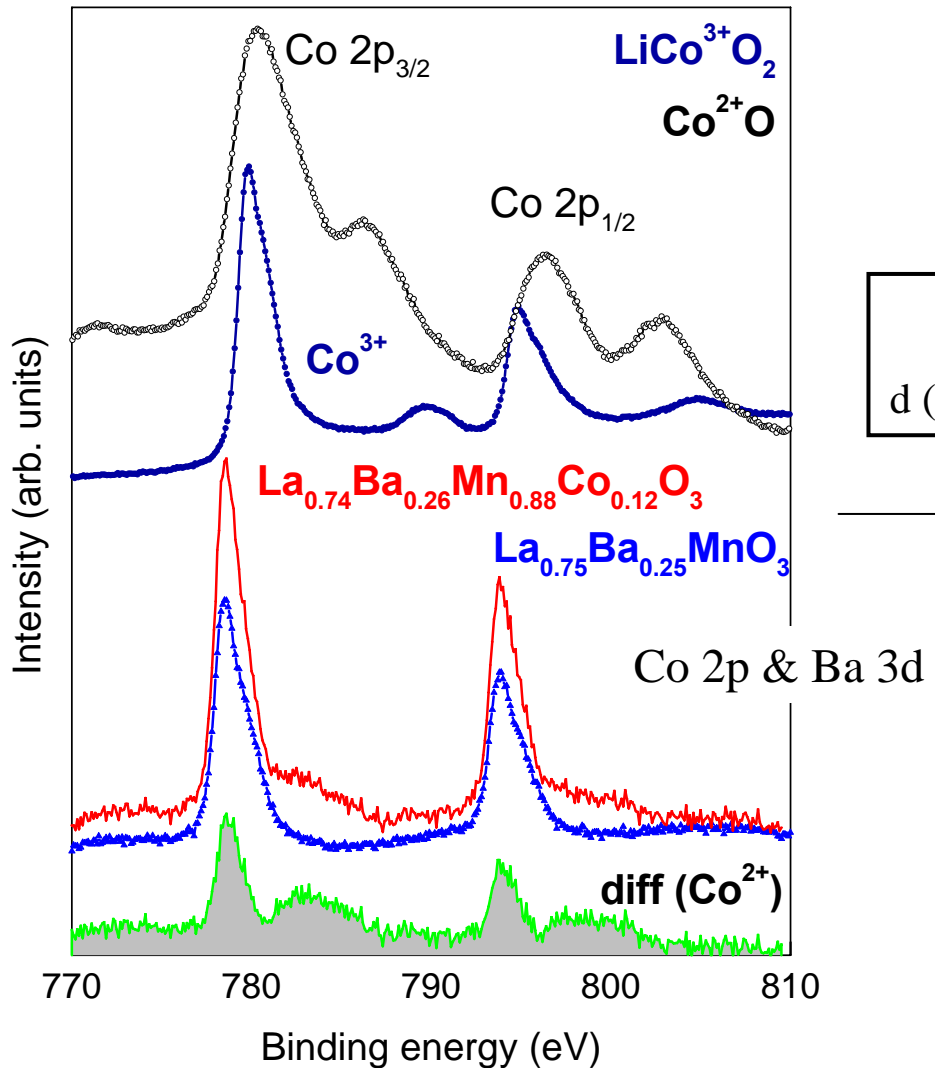


Jmmm 210 (2000) 63



- increase of the intensity of the VB spectrum of the Co-doped (La,Ba)MnO₃ at $\sim 2.5 \div 4$ eV
- slight changes in the small peak below E_F (e_g states) suggest Co bivalent character, as for La(Mn:Co)O₃

$\text{La}_{1-x}\text{Ba}_x\text{Mn}_{1-y}\text{Co}_y\text{O}_3$



$$\begin{aligned}(I_{\text{ML}}/I_{\text{sat}})_{\text{LiCoO}_2} &> (I_{\text{ML}}/I_{\text{sat}})_{\text{CoO}} \\ d_{(\text{ML-sat})_{\text{LiCoO}_2}} &> d_{(\text{ML-sat})_{\text{CoO}}}\end{aligned}$$

Co 2p spectra analysis:

Co^{2+}

$\text{La}_{7/8}\text{Sr}_{1/8}\text{MnO}_3$: X-ray Linear Dichroism and Orbital Ordering

VOLUME 92, NUMBER 8

PHYSICAL REVIEW LETTERS

week ending
27 FEBRUARY

Orbital Ordering in $\text{La}_{0.5}\text{Sr}_{1.5}\text{MnO}_4$ Studied by Soft X-Ray Linear Dichroism

D. J. Huang,^{1,2} W. B. Wu,^{2,1} G. Y. Guo,^{3,1} H.-J. Lin,¹ T. Y. Hou,¹ C. F. Chang,¹ C. T. Chen,^{1,3} A. Fujimori,⁴ T. Kimura,⁵ H. B. Huang,⁶ A. Tanaka,⁶ and T. Jo⁶

¹National Synchrotron Radiation Research Center, Hsinchu 30077, Taiwan

²Department of Electrophysics, National Chiao-Tung University, Hsinchu 300, Taiwan

³Department of Physics, National Taiwan University, Taipei 106, Taiwan

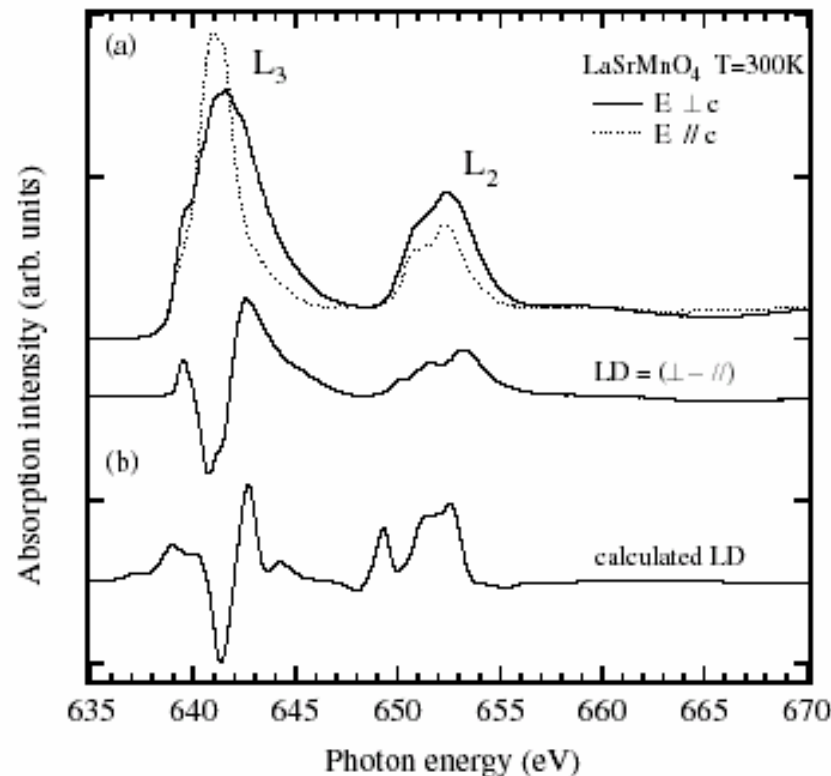
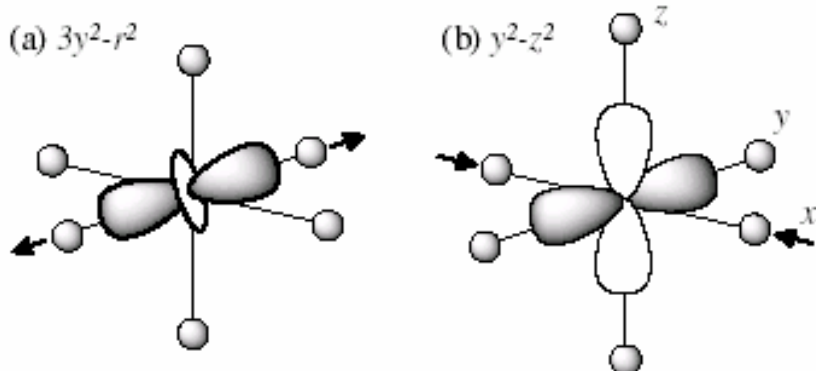
⁴Department of Physics and Department of Complexity Science and Engineering, University of Tokyo, Tokyo 113-0033, Japan

⁵Department of Applied Physics, University of Tokyo, Tokyo 113-8656, Japan

⁶Department of Quantum Matters, ADSM, Hiroshima University, Higashi-Hiroshima 739-8530, Japan

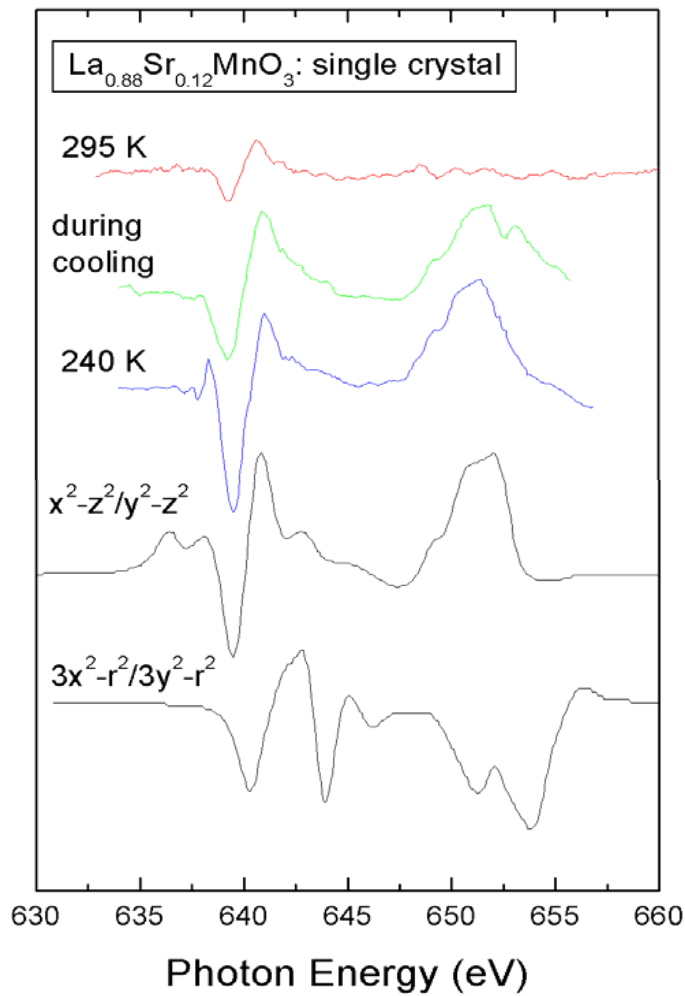
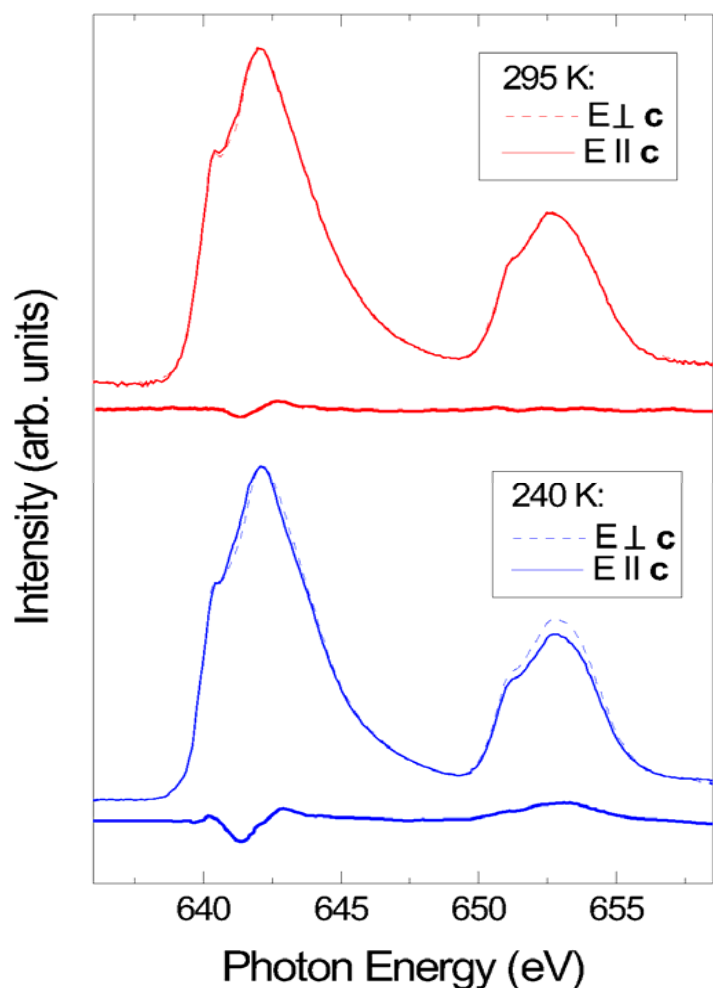
(Received 8 May 2003; revised manuscript received 17 November 2003; published 26 February 2004)

We found that the conventional model of orbital-ordering of $3x^2 - r^2/3y^2 - r^2$ type in the e_g states of $\text{La}_{0.5}\text{Sr}_{1.5}\text{MnO}_4$ is incompatible with measurements of linear dichroism in the Mn 2p-edge x-ray absorption, whereas these e_g states exhibit predominantly cross-type orbital ordering of $x^2 - z^2/y^2 - z^2$. LDA + U band-structure calculations reveal that such a cross-type orbital-ordering results from a combined effect of antiferromagnetic structure, Jahn-Teller distortion, and on-site Coulomb interactions.

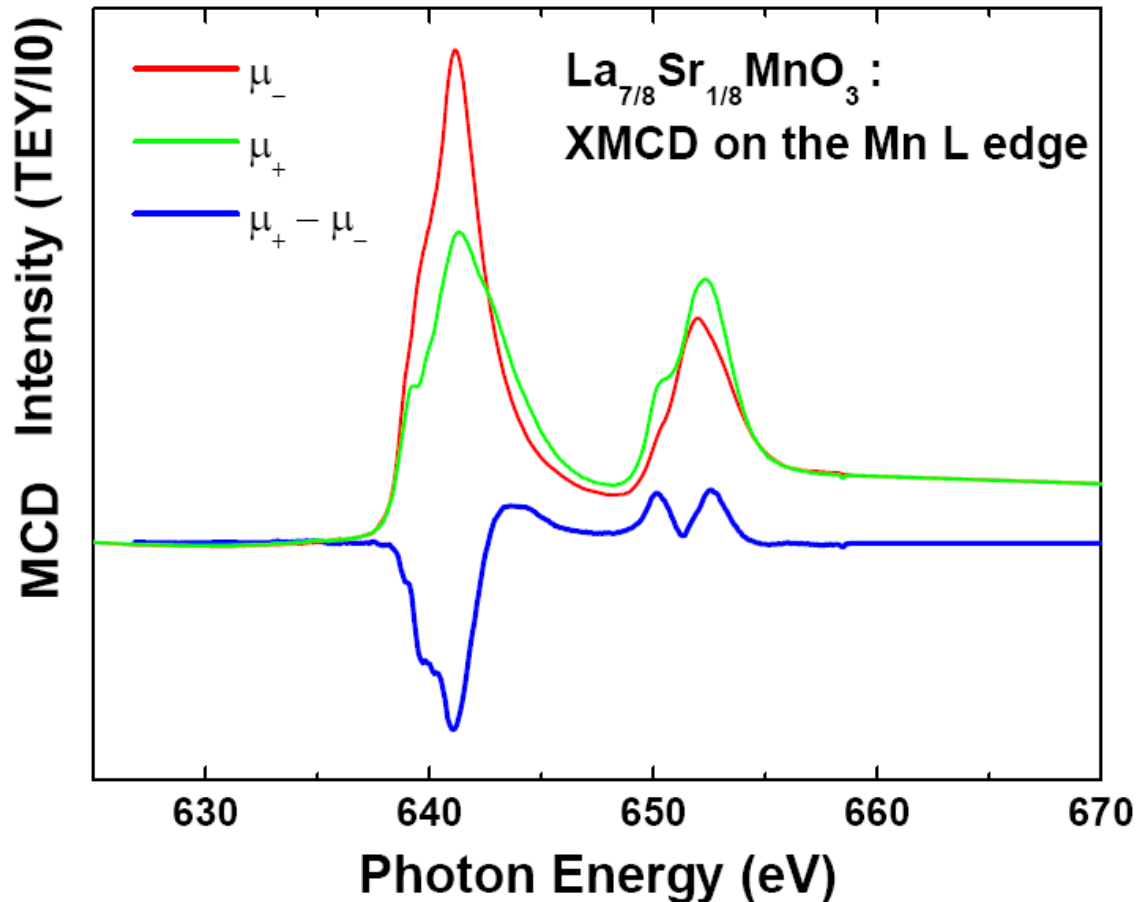


Layered manganite LaSrMnO_4 :
 $(3z^2-r^2)$ - orbital ordering
(PRL 92, 087202)

$\text{La}_{7/8}\text{Sr}_{1/8}\text{MnO}_3$: X-ray Linear Dichroism and Orbital Ordering

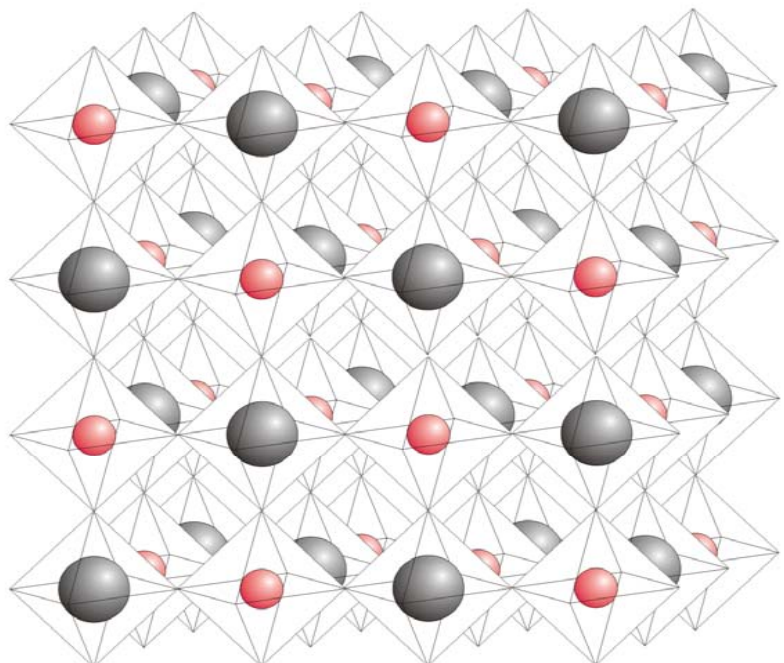


$\text{La}_{7/8}\text{Sr}_{1/8}\text{MnO}_3$: XMCD

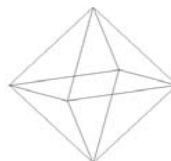


Applying the sum rules reveals
a spin moment of $+3.8 \mu_B$ and an orbital moment of approx. $-0.3 \mu_B$
→ total moment $3.5 \mu_B$.

$\text{Sr}_2\text{FeMoO}_6$



Mo

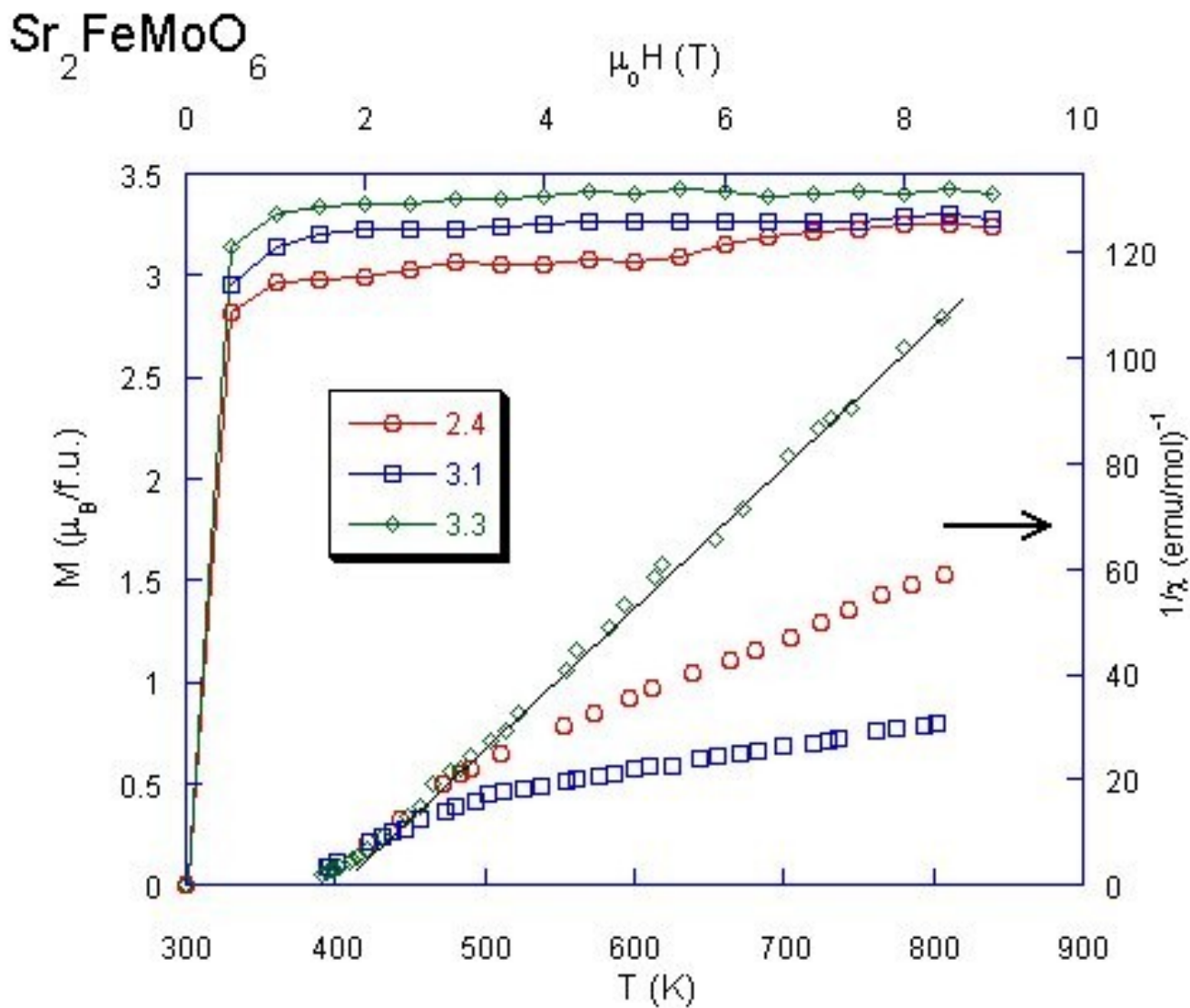


Oxygen-octahedron

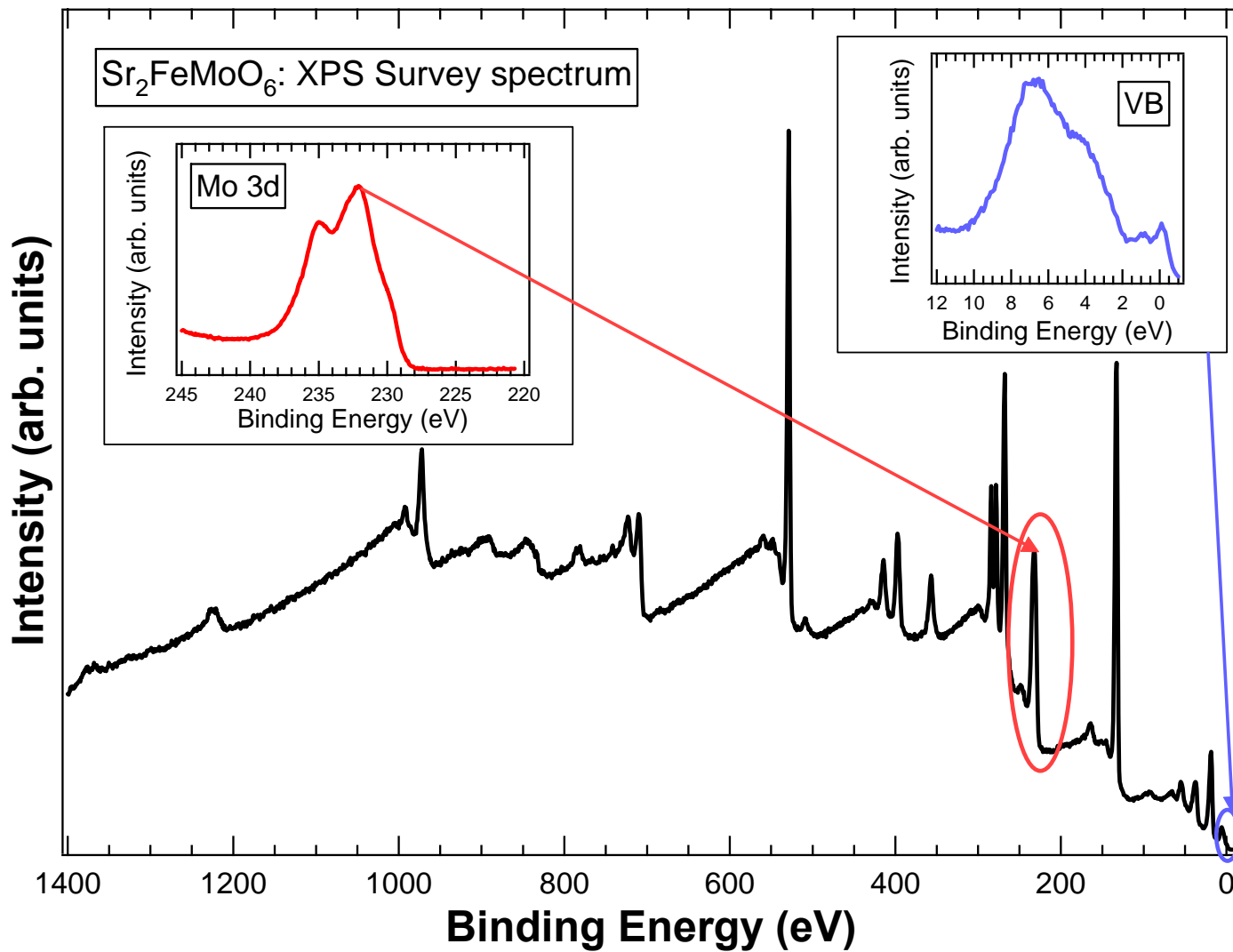
Y. Tomioka *et. al.* Phys. Rev. B 61, 422 (2000)

- Ⓐ ordered double perovskite
- Ⓑ poly crystal
- Ⓒ Fe^{3+} and Mo^{5+} build up antiferromagnetic coupling
- Ⓓ shows colossal magneto-resistance (CMR) at room temperature
- Ⓔ T_c : 410-450 K
- Ⓕ halfmetallic: Up-Spin band shows band gap, Down-Spin band is metallic (Nature 395, p. 677, 1998)
- Ⓖ possible application as magnetic storage
- Ⓗ different theoretical approaches lead to different interpretation about the correlation / hybridization mechanism (Phys. Rev. B 66, 035112 (2002), Phys. Rev. B 67, 085109 (2003))

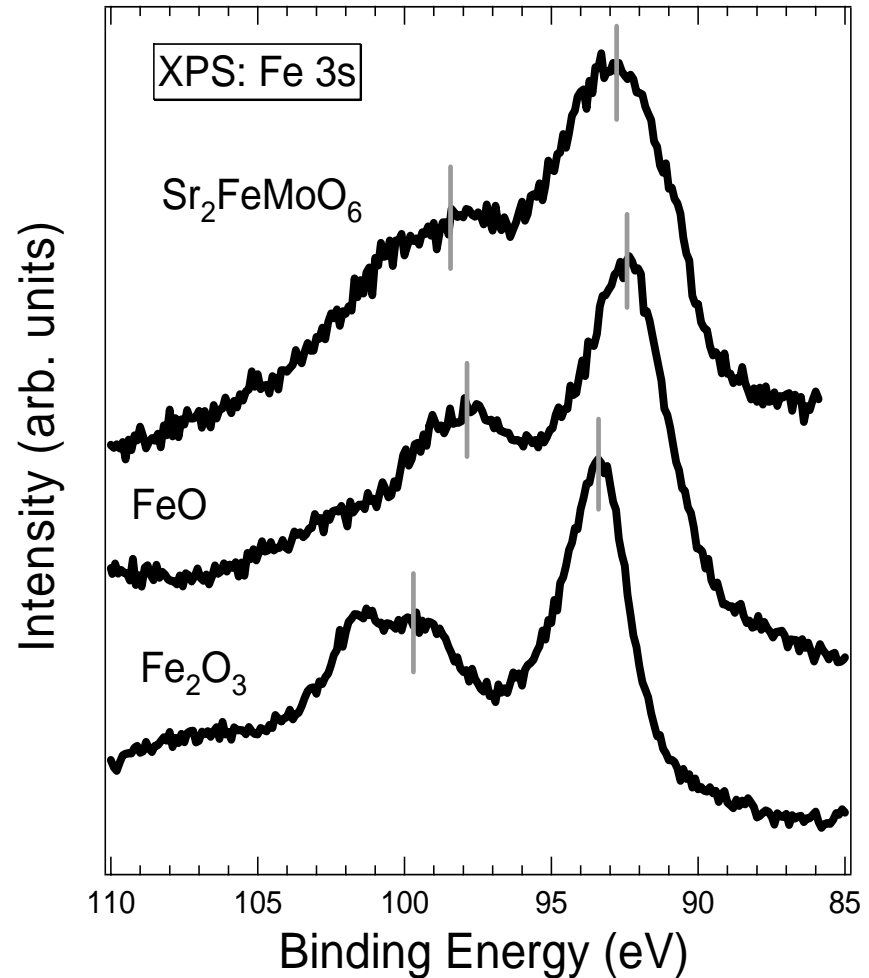
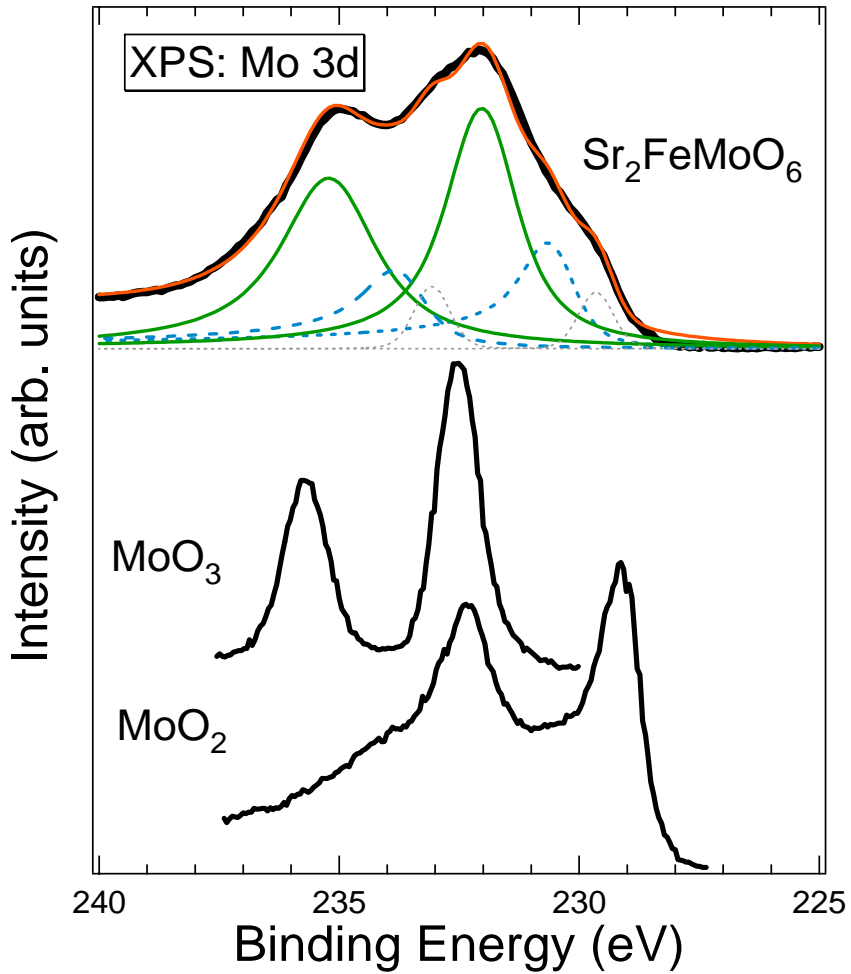
$\text{Sr}_2\text{FeMoO}_6$: magnetic measurements



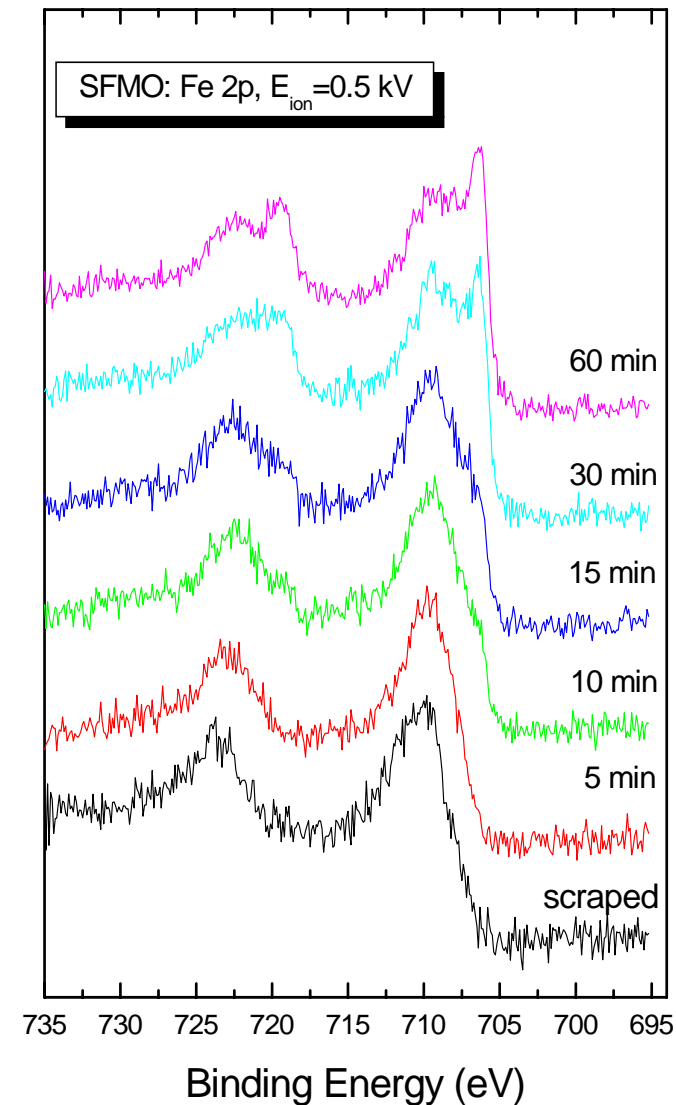
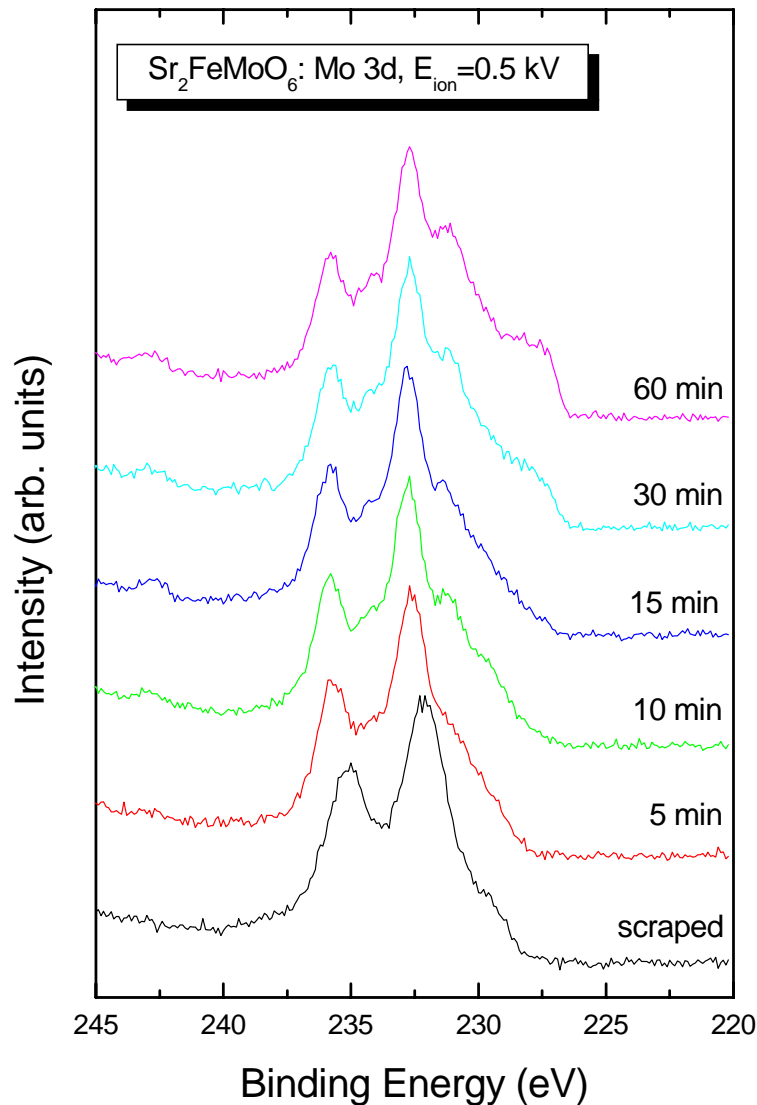
XPS survey spectrum of $\text{Sr}_2\text{FeMoO}_6$



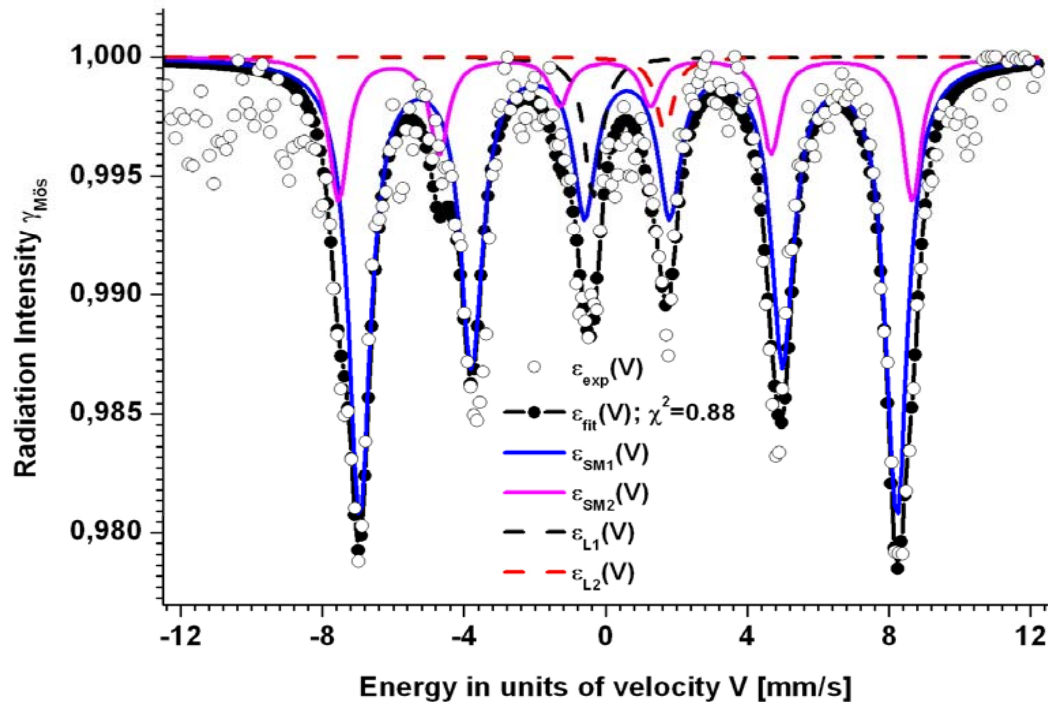
$\text{Sr}_2\text{FeMoO}_6$: XPS core levels



$\text{Sr}_2\text{FeMoO}_6$: XPS, influence of sputtering



Sr₂FeMoO₆: Mößbauer data



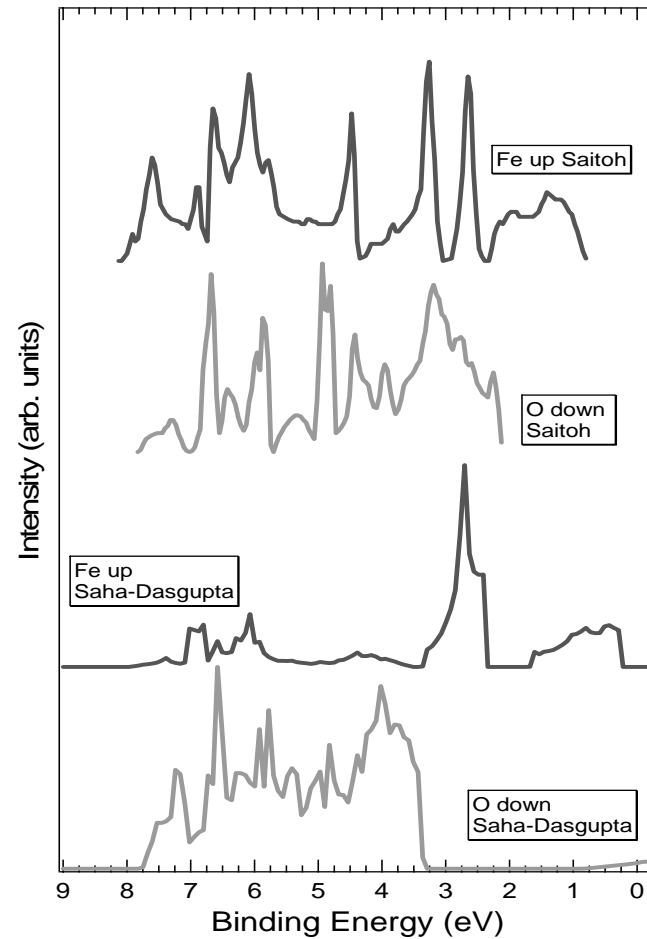
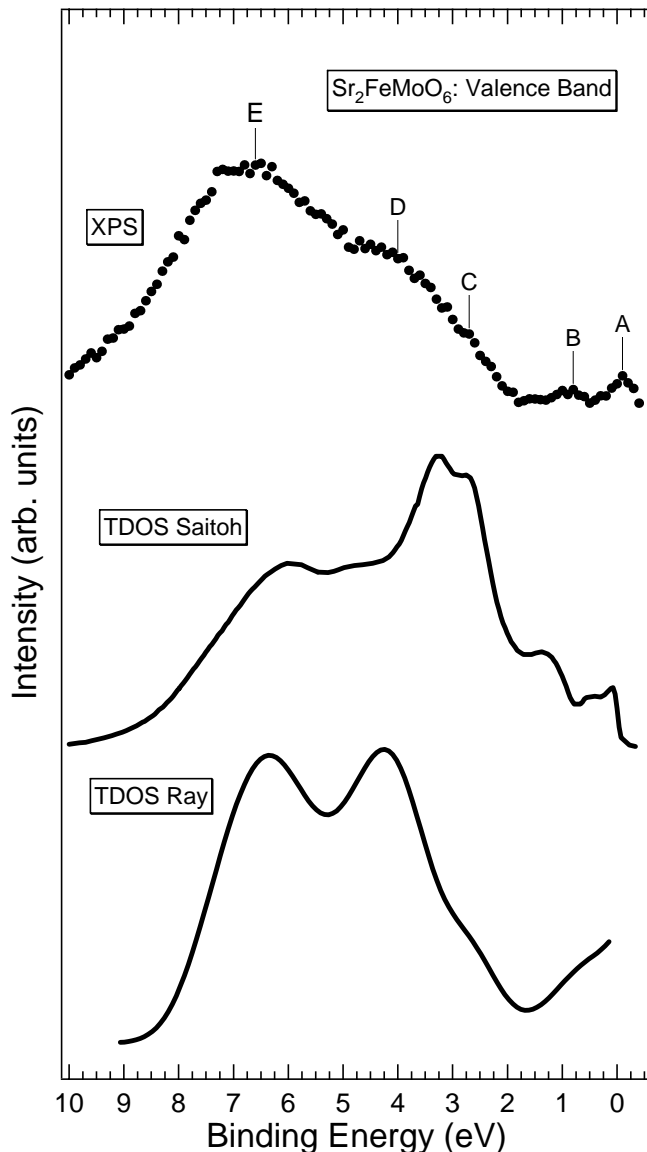
- Mößbauer data fitted with two sextets and two singlets
- ϵ_{SM1} : 73.6 % bulk
 $B_{\text{hf}}=47.1\text{T}$ → close to Fe 2+
- ϵ_{SM2} : 19.5 % grain boundaries
 $B_{\text{hf}}=50.3\text{T}$ → close to Fe 3+
- ϵ_{L1} and ϵ_{L2} : antisite defects
- Electron hopping Fe - Mo valence fluctuations $\text{Fe}^{2+}/\text{Fe}^{3+}$

variance	lattice	δ_{Rh} in mm/s	$eQV_{ZZ}/8$ in mm/s	Θ in °	Γ in mm/s	B in 10^{-1}T	P in %
$\chi^2 = 0.88$	SM1	0.62	-0.012	125	0.38	471	73.61
	SM2	0.27	-0.063	67	0.31	503	19.52
	L1	-0.35	-	-	0.29	-	4.47
	L2	1.66	-	-	0.30	-	2.40

ME gives averaged B_{hf}
XPS gives a snap shot:

70 % Fe 2+ and 30 % Fe 3+

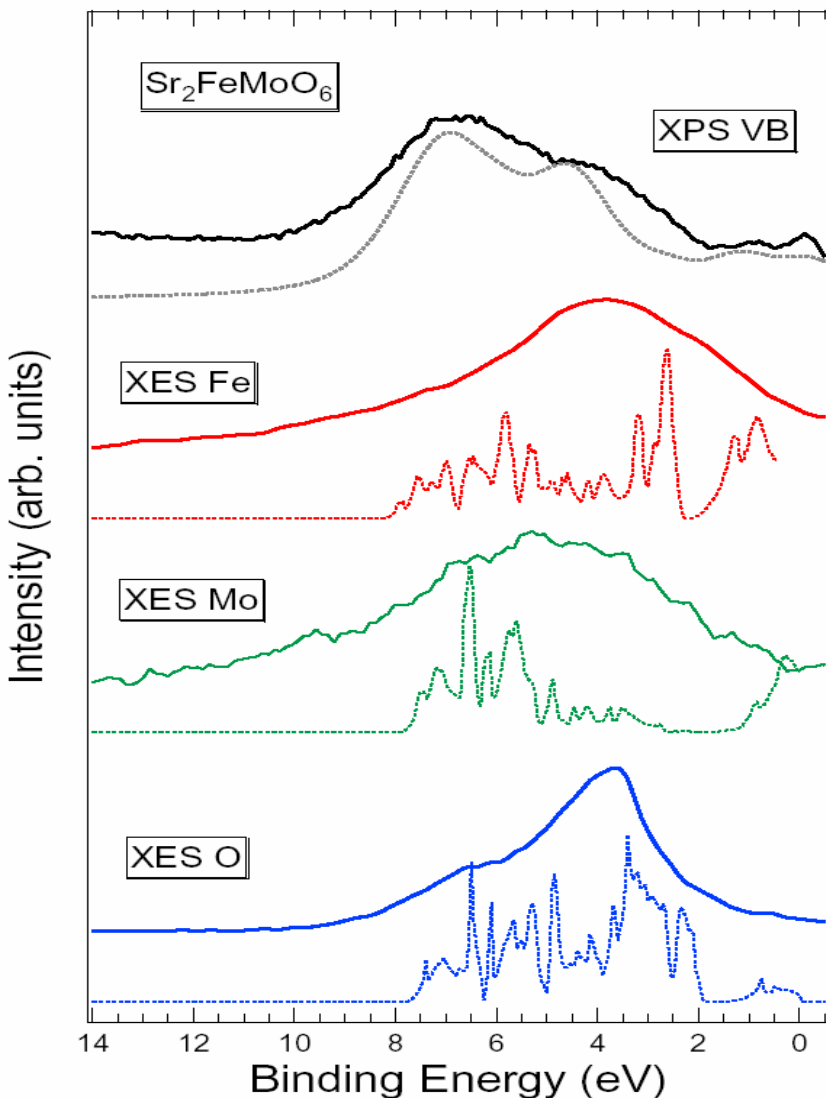
$\text{Sr}_2\text{FeMoO}_6$: XPS valence band and calculations



Saitoh et al. (Phys. Rev. B 66, 035112 (2002)),
→ strong hybridization

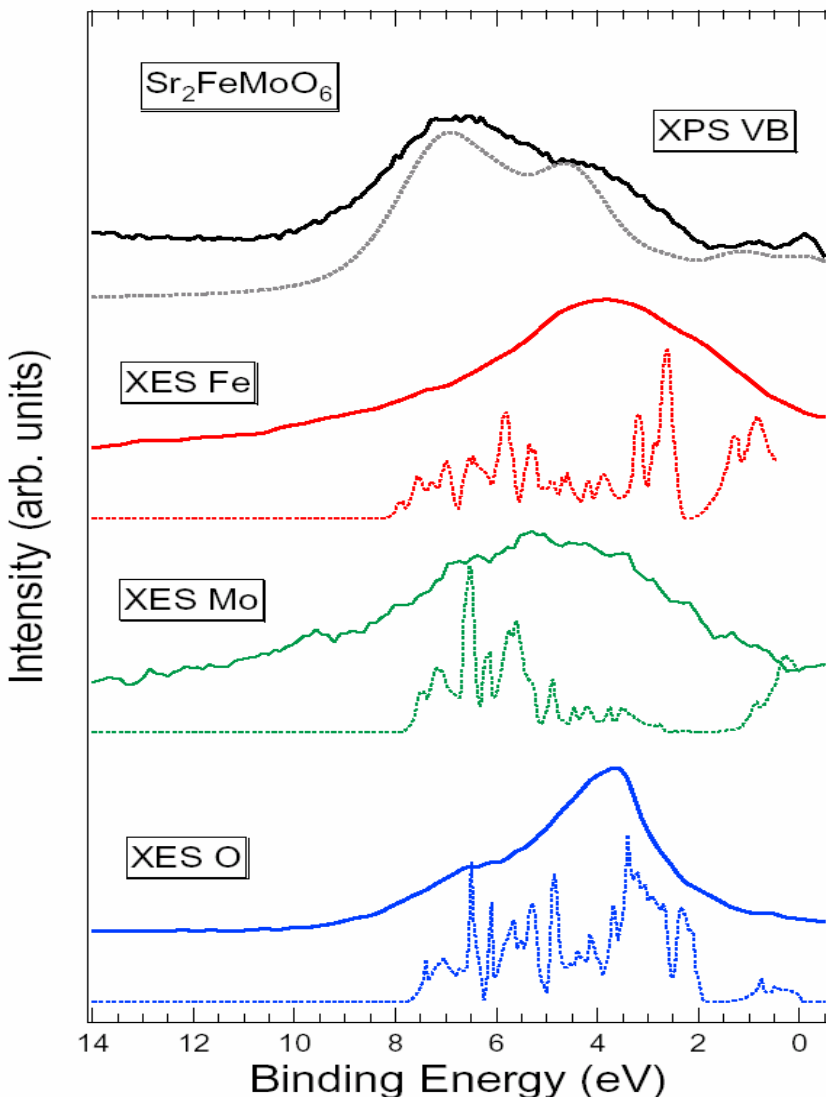
Saha-Dasgupta et al. (Phys. Rev. B 64, 064408 (2001)),
→ strong correlation

$\text{Sr}_2\text{FeMoO}_6$: XPS, XES, band structure



- comparison of the XPS and XES spectra with new band structure calculations, use of the lattice parameters of the best sample as input parameter!
- Perdew Wang GGA approximation (calculations performed by M. Kadiroglu and A. V. Postnikov)
- good agreement between the experimental and the calculated partial densities of states
- the total density of states have been derived by weighting the partial densities of states with help of the cross sections, good agreement with the experiment is achieved

$\text{Sr}_2\text{FeMoO}_6$: XPS, XES, band structure



- comparison of the XPS and XES spectra with new band structure calculations,
Perdew Wang GGA approximation
- good agreement between the experimental and the calculated partial densities of states
- the total density of states have been derived by weighting the partial densities of states with help of the cross sections, good agreement with the experiment is achieved

K. Kuepper et al. J. Phys.: Condens. Matter **17**, 4309 -4317 (2005)

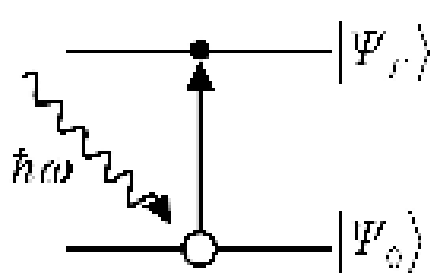
CMR compounds Summary

- **La_{1-x}Sr_xMnO₃:** $x < 0.3$, the doping holes have mainly O 2p character
 - high value of the Mn 3s splitting (5.3 eV) : the HS state
- **La_{1-x}(Sr,Ba)_xMnO₃:** strong hybridization of the TM 3d and O 2p states
- **La_{7/8}Sr_{1/8}MnO₃:** strong indications for a cross type (x^2-z^2)/ (y^2-z^2) orbital ordering in the cooperative Jahn Teller distorted phase
- **XMCD reveals a total magnetic moment of 3.5 μ_B**
- **Sr₂FeMoO₆, around 65% Fe²⁺ and Mo⁶⁺, 35% Fe³⁺, Mo⁵⁺ contributions**
- **Sr₂FeMoO₆, evidence for moderate correlation**
- **Mößbauer reveals about 20% grain boundaries, 4% anti-sites from XRD**

Acknowledgements

- G. Borstel, A.V. Postnikov, Univ. Osnabrück
- K.C. Prince, M. Matteucci ELETTRA, Italy
- the group of Prof. F. Parmigiani, Trieste
- Ya.M. Mukovskii, Moscow, Russia
- A. Winiarski, Univ. Katowice, Poland
- helpful assistance at ALS, BESSY and ELETTRA

photo electron emission process (I)



Perturbation theory

Transition probability:

$$W = \frac{2\pi}{\hbar} |\langle \Psi_F | \Delta | \Psi_0 \rangle|^2 \delta(E_F - E_0 - \hbar\omega)$$

$$\Delta = \frac{e}{2mc} (A \cdot p + p \cdot A) - e\phi + \frac{e^2}{2mc^2} A \cdot A$$

A : vector potential of the incoming light

ϕ : scalar potential

$A \cdot A$ to be neglected for one photon processes

$\nabla A = 0 \rightarrow$ no nonlocal field effects

ϕ vanishes with Coulomb gauge

$\lambda \gg$ atomic distances (UV-range)

$\rightarrow A = A_0 e^{i\vec{q}\vec{r}} \approx A_0$ (dipole approximation)

(Fresnel-equations generally well applicable)

Final state $|\Psi_F|$ consists of ion + electron!

photo electron emission process (II)

Intensity:

$$I \propto \left| \sum_{k,e} \langle \Phi_e | \Delta | \Phi_k \rangle \langle {}^{N-1}\Psi_e | a_k | \Psi_i \rangle \right|^2$$

appearance of
satellites one electron
matrix element
→ symmetry
→ angle dependent line width
 peak position (energy)

$\sum_{k,e}$ Summations on all possible ion states

Φ_e Wave function of the emitted electron (totally symm.) (LEED)

Δ one electron dipole operator $\sim A_0 \cdot p$

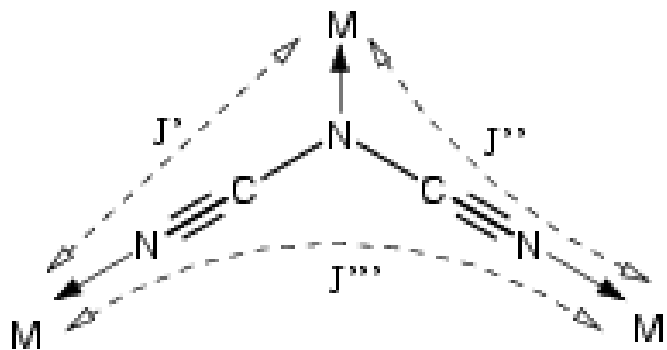
Φ_e, Φ_k one electron wave functions

${}^{N-1}\Psi_e$ ion state

a_k annihilation operator

Ψ_i neutral groundstate

Magnetic interactions



J' direct metal to metal exchange

$d(M-M) = 5.9\text{-}6.3 \text{ \AA}$ $\Rightarrow J'$ utterly negligible

J'' superexchange path **M-N-C-N-M**

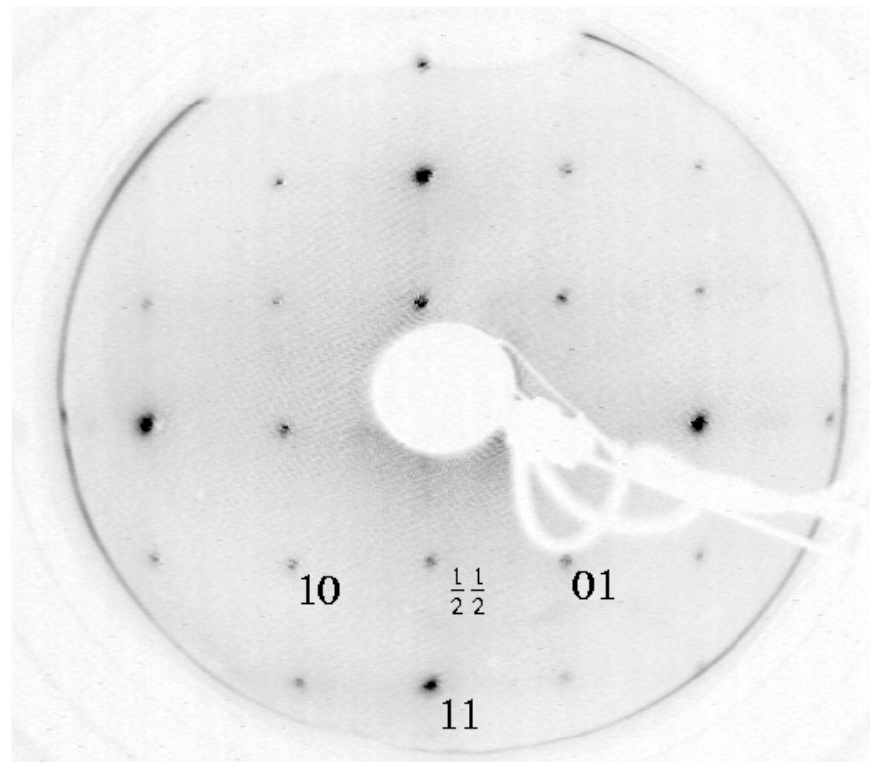
J''' superexchange path **M-N-C-N-C-N-M**

about $0.3\text{-}0.4 \text{ cm}^{-1}$

A. Escuer *et al.*, Inorganic Chemistry **39** 1668-1673 (2002)

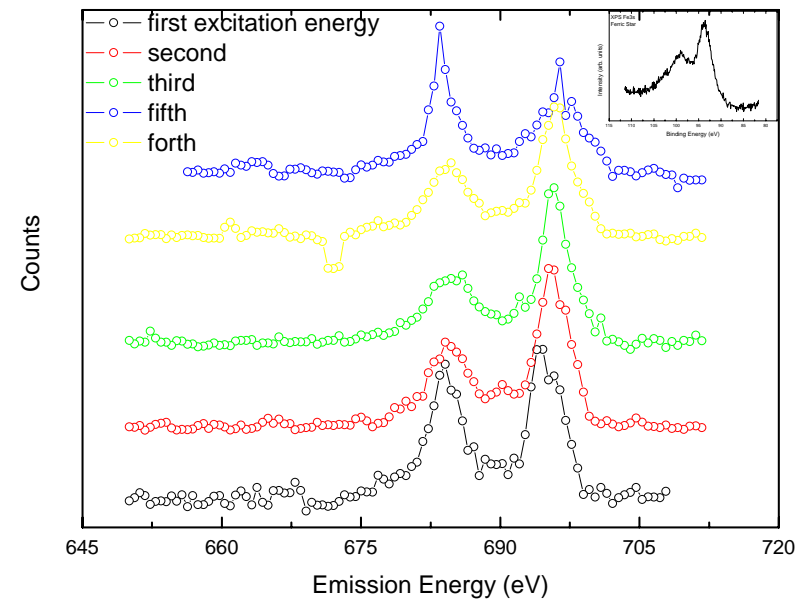
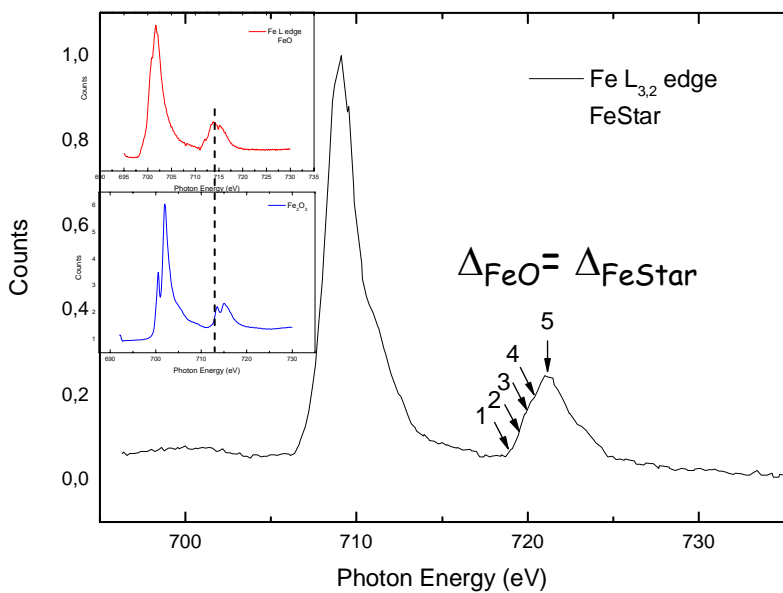
→ J'' dominant

semi-Heusler NiMnSb



core level studies

FeStar



The absorption measurements on the FeStar molecule gives us also Fe²⁺ which is in a good agreement with the XPS data.

core level studies

CrStar

